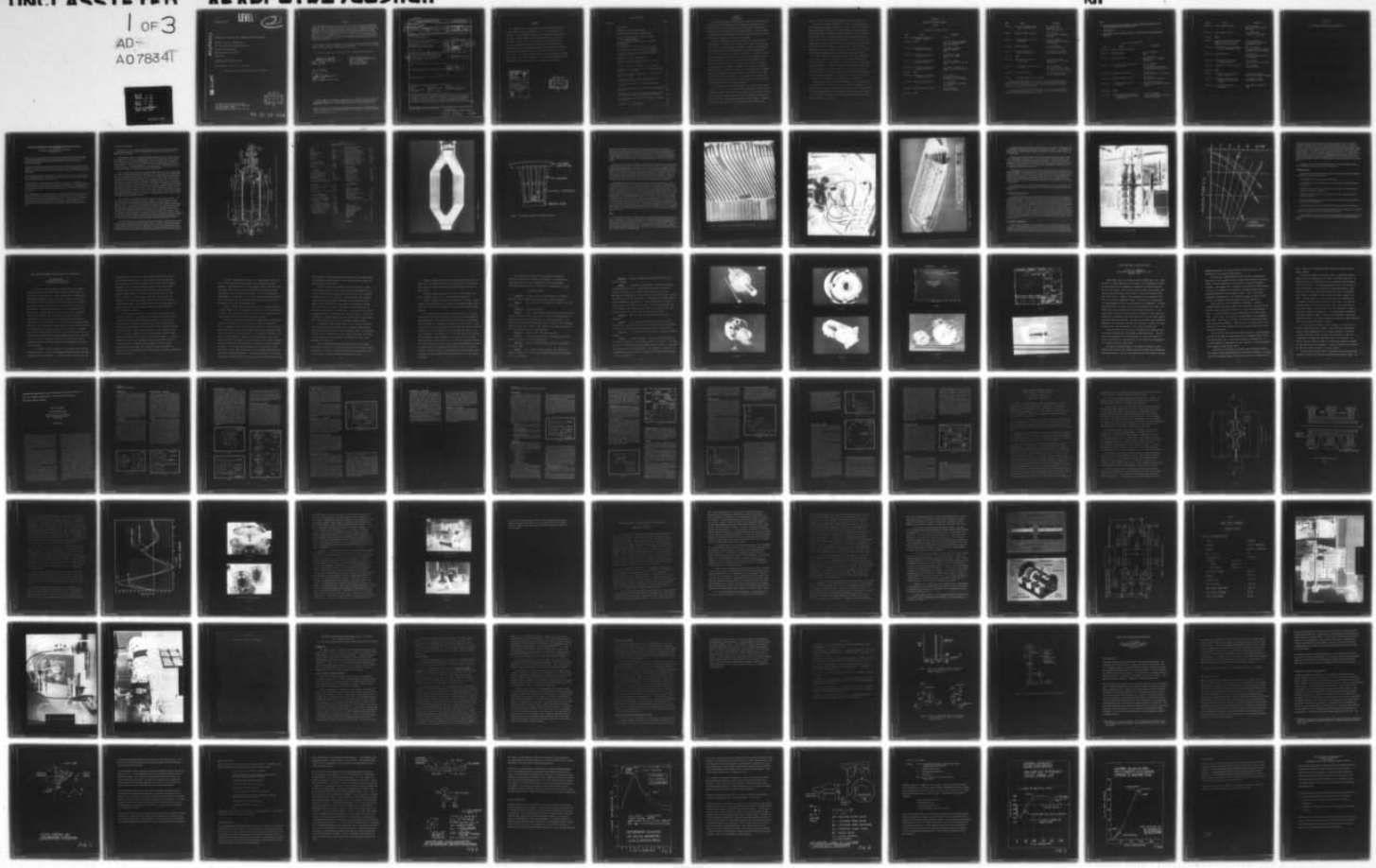
AD-A078 341 AIR FORCE AERO PROPULSION LAB WRIGHT-PATTERSON AFB OH F/G 10/2
PROCEEDINGS OF THE AFAPL GENERATOR AND MOTORS SEMINAR (1ST), HE--ETC(U)
AUG 79 H L SOUTHALL , J L MCCABRIA

UNCLASSIFIED AFAPL-TR-79-2090 NL

1 OF 3
AD-
A078341



AFAPL-TR-79-2090

LEVEL II



AD A078341

PROCEEDINGS OF THE FIRST AFAPL GENERATORS AND MOTORS SEMINAR

AUTHORS: CAPT. H.L. SOUTHALL, et. al.

U.S. Air Force Aero Propulsion Laboratory

Air Force Systems Command

Wright-Patterson AFB, OH 45433

August 1979

TECHNICAL REPORT AFAPL-TR-79-2090

Interim Report 1 Oct 1977 to 1 Jul 1979

Approved for public release; distribution unlimited

DDC FILE COPY

DDC
RECEIVED
DEC 14 1979
D

AIR FORCE AERO PROPULSION LABORATORY
AIR FORCE WRIGHT AERONAUTICAL LABORATORIES
AIR FORCE SYSTEMS COMMAND
WRIGHT-PATTERSON AIR FORCE BASE, OH 45433

79 12 12 044

NOTICE

When Government drawings, specifications, or other data are used for any purpose other than in connection with a definitely related Government procurement operation, the United States Government thereby incurs no responsibility nor any obligation whatsoever; and the fact that the government may have formulated, furnished, or in any way supplied the said drawings, specifications, or other data, is not to be regarded by implication or otherwise as in any manner licensing the holder or any other person or corporation, or conveying any rights or permission to manufacture, use, or sell any patented invention that may in any way be related thereto.

This report has been reviewed by the Information Office (OI) and is releasable to the National Technical Information Service (NTIS). At NTIS, it will be available to the general public, including foreign nations.

This technical report has been reviewed and is approved for publication.

Hugh L. Southall

HUGH L. SOUTHALL, Capt, USAF
Project Engineer

Paul R. Bertheaud

PAUL R. BERTHEAUD
Technical Area Manager
Power Systems Branch

FOR THE COMMANDER

JAMES D. REAMS
Chief, Aerospace Power Division

"If your address has changed, if you wish to be removed from our mailing list, or if the addressee is no longer employed by your organization please notify AFAPL/POP-2, *W-PAFB, OH 45433 to help us maintain a current mailing list".*

Copies of this report should not be returned unless return is required by security considerations, contractual obligations, or notice on a specific document.

AIR FORCE/56780/19 November 1979 — 140

UNCLASSIFIED

SECURITY CLASSIFICATION OF THIS PAGE (When Data Entered)

REPORT DOCUMENTATION PAGE

READ INSTRUCTIONS BEFORE COMPLETING FORM

1. REPORT NUMBER: AFAPL-TR-79-2090	2. GOVT ACCESSION NO.
3. RECIPIENT'S CATALOG NUMBER	
4. TITLE (and Subtitle): Proceedings of the First AFAPL Generator and Motors Seminar (1st) Held at Wright-Patterson AFB, Ohio in October 1977.	5. TYPE OF REPORT & PERIOD COVERED: Interim Report, 1 Oct 77 - 1 Jul 79
6. PERFORMING ORG. REPORT NUMBER	
7. AUTHOR(s): Capt H.L. Southall, et. al. (See Table of Contents)	8. CONTRACT OR GRANT NUMBER(s): In-House
9. PERFORMING ORGANIZATION NAME AND ADDRESS: U.S. Air Force Aero Propulsion Laboratory, AFAPL/POP-2, Wright-Patterson AFB, OH 45433	10. PROGRAM ELEMENT, PROJECT, TASK AREA & WORK UNIT NUMBERS: 3145-32-21
11. CONTROLLING OFFICE NAME AND ADDRESS: Same as block 9	12. REPORT DATE: Aug 79
	13. NUMBER OF PAGES: 206
14. MONITORING AGENCY NAME & ADDRESS (if different from Controlling Office)	15. SECURITY CLASS. (of this report): UNCLASSIFIED
	15a. DECLASSIFICATION/DOWNGRADING SCHEDULE

16. Hugh L./Southall, J.L./McCabria, Sam/Noodleman, M. S./Isaacson, W. F./Weldon

Approved for public release; distribution unlimited.

17. DISTRIBUTION STATEMENT (of the abstract entered in Block 20, if different from Report)

62203F

18. SUPPLEMENTARY NOTES

19. KEY WORDS (Continue on reverse side if necessary and identify by block number)

Generators	Pulsed power	High power
Motors	Synchronous machines	Permanent magnet generators
Rotating machinery	DC motors	Mathematical modeling
Alternators	Generator modeling	

20. ABSTRACT (Continue on reverse side if necessary and identify by block number)

A seminar was held at Wright-Patterson AFB in October 1977 to provide for government, industry, and university presentations on the latest developments in generator and motor technology. In addition, the mathematical modeling of generator and motors was the subject of other presentations at the meeting. This Technical Report organizes and publishes presentations made at the seminar.

DD FORM 1 JAN 73 1473 EDITION OF 1 NOV 65 IS OBSOLETE

UNCLASSIFIED

SECURITY CLASSIFICATION OF THIS PAGE (When Data Entered)

011570

FOREWORD

This Technical Report was prepared by the Power Systems Branch of the Aerospace Power Division (AFAPL/POP-2), U.S. Air Force Aero Propulsion Laboratory. The presentations published in this report were given at the "Generators and Motors Seminar" held at Wright-Patterson AFB, OH, Bldg 450, Area B, in October 1977. The seminar was co-sponsored by the U.S. Air Force Aero Propulsion Laboratory and the Power Information Center, Philadelphia, PA. The seminar was organized and the proceedings published under Project 3145, Task 32, Work Unit 21 and took place from 1 Oct 1977 to 1 Jul 1979. The help of Mr William Duffy of the Power Information Center (PIC) and Mr Pierre Thollot, Chairman of the Electrical Working Group of the Inter Agency Advanced Power Group (PIC) is gratefully acknowledged.

Accession For
NTIS GRA&I
DDC TAB
Unannounced
Justification
By
Distribution/
Availability Codes
Dist | Avail and/or special
A

DDC
RECEIVED
DEC 14 1979
D

TABLE OF CONTENTS

SECTION		PAGE
I	INTRODUCTION	1
II	GENERATORS AND MOTORS SEMINAR AGENDA	3
III	NEW GENERATOR DESIGN CONCEPTS PRESENTATIONS	7
	Air Force Superconducting Generator Development Program - J.L. McCabria	8
	Rare Earth Permanent Magnet Motors and Generators - Sam Noodleman	22
	A New Brushless DC Motor Concept - M.S. Isaacson	33
	Pulsed Homopolar Generator Research - W.F. Weldon	46
	The Segmented Magnet (SEGMAG) Machine Development Program - D.L. Greene	56
IV	MATHEMATICAL MODELING PRESENTATIONS	66
	High Power, Airborne Generator Modeling in the U.S. Air Force - Capt. H.L. Southall	67
	Evolution of Machine Design Models - W.J. Shilling	75
	Mechanical Forces in Damper Shields for Superconducting Generators - J.L. McCabria	91
	Modeling of Superconducting Generators with Rectified Output - T.A. Stuart	114
	Computer Simulation of a 6-KVA Aircraft Alternator and Comparison of Test Results - C.H. Lee	137
	Parameter Identification of a Synchronous Machine - O.T. Tan	153
	Higher Order Modelling of Solid Iron Rotor Turbogenerators - D.R. Brown	158
	Mathematical Model of Direct Current Machines Including of the Effects of Magnetic Saturation - D.D. Wier	168
	Power Research at the University of Missouri - Columbia - C. Slivinsky	188
	APPENDIX A - List of Attendees	192

SECTION I

INTRODUCTION

The initial planning for this seminar took place at a previous meeting of The Electrical Working Group of The Interagency Advanced Power Group. That planning consisted of the Aero Propulsion Laboratory representative stating "we'll have the meeting at Wright-Patterson AFB". He then returned to Wright-Patterson and informed the suddenly responsible people that "we're going to have a meeting". That was our total guidance.

We began our preparation by assessing the goals of our rotating machinery programs. Two distinct facts became vividly clear: we were not very aware of recent rotating machinery developments outside our own laboratory, and rotating machinery development programs have become prohibitively expensive. The first fact set the tone for the meeting, it would be a seminar on motors and generators. The second fact started us thinking about computer-aided-design, and the associated mathematical developments. Combining the two topics resulted in a seminar with the purpose of bringing together personnel from industry, government, and academia to informally discuss the latest technological advances in rotating machinery and computer-aided-design techniques for rotating machinery. Presentations were made, and a lot of discussion generated, in the following areas: generator and motor manufacturing technology, new concepts in generator and motor design, and mathematical modeling of rotating machinery.

It was hoped that a significant amount of "cross fertilization" would take place. There is a lot of rotating machinery modeling being pursued in academia, however, it often suffers from a lack of the fine touch of reality. On the other hand, there are many industrial and government personnel that are not fully aware of the resources available within academia. Therefore, a purpose of this seminar was to stimulate discussions among the three

entities. We feel that the seminar successfully fulfilled that purpose.

This report is divided into two main sections containing presentations made during the two separate sessions of the seminar. Section III contains presentations given on the first day of the seminar. These presentations covered new concepts in generator and motor manufacture. Several advanced design concepts such as superconducting windings and permanent magnet excitation were covered. Section IV contains a collection of presentations on mathematical modeling of rotating machinery. There presentations were made on the second day of the seminar, and covered topics such as generator modeling, prediction of mechanical stresses, and the important area of predicting machine performance based upon postulated mathematical models.

A cursory comparison of the seminar agenda with the Table of Contents shows that this report does not contain all the presentations that were made at the seminar. A formal paper was not required for this seminar since each presentation was recorded. A transcript of the presentation was sent to each presentor, and an edited version of the transcript with figures requested in return. For various reasons, over 50 percent of the presenters never returned the transcripts. This approach was subject to speculation at the time it was conceived. The speculation has been justified.

Regardless of the response to the proceedings, we feel that the seminar was a smashing success. It's purpose was to stimulate discussion on an informal basis, and it succeeded beyond our expectations. We sincerely thank each participant and hope that the comaraderie, mutual respect, and communication exhibited by the members of the rotating machinery community at this seminar continues in the future.

SECTION II

GENERATORS AND MOTORS SEMINAR

AGENDA

Wednesday (19 October 1977)

Time	Topic	Presenter
8:00 a.m.	Registration and Meeting of Today's Presenters	(none)
9:00 a.m.	Welcome	Col. P.O. Bouchard, Commander Air Force Aero Propulsion Laboratory (AFAPL)
9:15 a.m.	Seminar Objectives and Introductory Remarks	Capt. Hugh L. Southall Electrical Engineer AFAPL
9:30 a.m.	Overview of Air Force High Power R&D Efforts	Mr. Richard L. Verga Technical Area Manager AFAPL
9:50 a.m.	Navy High Power R&D Efforts: Program Objectives	Mr. John H. Harrison David W. Taylor Naval Ship R&D Center
10:10 a.m.	Navy High Power R&D Efforts: Hardware Development	Mr. Howard O. Stevens, Jr. David W. Taylor Naval Ship R&D Center
10:30 a.m.	BREAK	
10:45 a.m.	Status Report, 2.5 Megawatt (AMMS) Generator	Mr. A.E. King Westinghouse Electric Corp. Aerospace Electrical Division
11:05 a.m.	Army Generator R&D Efforts	Dr. A.L. Jokl U.S. Army Mobility Equipment R&D Command
11:25 a.m.	Pulsed Homopolar Generators	Mr. Bill Weldon University of Texas
11:45 a.m.	LUNCH	

Time	Topic	Presenter
1:00 p.m.	Rare Earth Permanent Magnet Motors and Generators	Mr. Sam Noodleman Kollmorgan Corp. Inland Motor Division
1:20 p.m.	Permanent Magnet Generators	Dr. Eike Richter General Electric Corporate R&D Center
1:40 p.m.	Permanent Magnet Motors and Generators	Mr. E. F. Echolds AiResearch Manufacturing Co. of California
2:00 p.m.	SEGMAG Generator	Dr. David Greene Westinghouse R&D Center
2:20 p.m.	Battery Driven Motors for Undersea Propulsion	Mr. Leopold J. Johnson Naval Ocean Systems Center
2:40 p.m.	BREAK	
3:00 p.m.	Superconducting Generator Development	Mr. Bruce B. Gamble General Electric Corporate R&D Center
3:20 p.m.	Status Report, Superconducting Generator	Mr. J.L. McCabria Westinghouse Electric Corp. Aerospace Electrical Division
3:40 p.m.	Brushless DC Motors	Mr. Milton S. Isaackson Nu-Tech Industries, Inc.
4:00 p.m.	GOVERNMENT AGENCIES CLOSED SESSION	

All university and industrial participants are invited to make short (10 minutes maximum) presentations of new, proprietary R&D work to representatives of only the Government agencies. Actual scheduling will be accomplished on the first day of the meeting.

At the conclusion of these presentations, the Electrical Working Group of the Interagency Advanced Power Group (IAPG) will hold a brief business meeting covering the following three items:

ITEMS

1. Review and Approval of the Minutes of the 24 March 1977 Meeting of the Electrical Working Group (PIC-ELE 3/15).

2. Other Business.

3. Date, Place, Time and Agenda Items for the Next Electrical Working Group Meeting.

Thursday (20 October 1977)

Time	Topic	Presenter
8:15 a.m.	Meeting of Today's Presenters	
8:40 a.m.	Opening Remarks	Capt F. Brockhurst AFAPL
8:50 a.m.	Modeling in Design	Dr. Eike Richter General Electric Corporate R&D Center
9:10 a.m.	Evolution of Electrical Machine Design Models	Mr. W.J. Shilling Mr. H.J. Braun Westinghouse Electric Corp. Aerospace Electrical Division
9:30 a.m.	Parameter Identification	Dr. Atif Debs Georgia Institute of Technology
9:50 a.m.	Parameter Identification	Dr. Owen Tan Louisiana State University
10:10 a.m.	Projecting Future Uses of Modeling	Mr. Timothy J. Doyle David W. Taylor Naval Ship R&D Center
10:30 a.m.	BREAK	
10:45 a.m.	Dynamic Analysis of Electrical Machines Including Magnetic Nonlinearities	Dr. N.A. Demerdash Virginia Polytechnic Institute and State University

Time	Topic	Presenter
11:05 a.m.	Finite Element Modeling	Dr. M.V.K. Chari General Electric Corporate R&D Center
11:25 a.m.	Finite Element Analysis	Dr. William Lord Colorado State University
11:45 a.m.	LUNCH	
1:00 p.m.	Superconducting Generator Damper Shields - Modeling of Flux Diffusion and Time Constants	Dr. J.H. Parker, Jr. Westinghouse Research and Development Center
1:20 p.m.	Superconducting Generator Damper Shields - Mechanical Forces	Mr. J.L. McCabria Westinghouse Electric Corp. Aerospace Electrical Division
1:40 p.m.	Computer Simulation	Dr. C.H. Lee AiResearch Manufacturing Co. of California
2:00 p.m.	State Variable Modeling and Transient Behaviour	Dr. D.P. Weir Mississippi State University
2:20 p.m.	A Comparison of Generator Models	Mr. Dave Brown Purdue University
2:40 p.m.	BREAK	
2:50 p.m.	Solid State Device Models and Hybrid Simulation	Dr. Charles Slivinsky University of Missouri-Columbia
3:10 p.m.	Modeling of Superconducting Generators with Rectified Output	Dr. Thomas A. Stuart University of Toledo
3:30 p.m.	U.S. Air Force Modeling Requirements	Capt. Hugh L. Southall AFAPL

SECTION III

NEW GENERATOR DESIGN CONCEPTS PRESENTATIONS

AIR FORCE SUPERCONDUCTING GENERATOR DEVELOPMENT PROGRAM

J.L. McCABRIA
WESTINGHOUSE ELECTRIC CORPORATION
OCTOBER, 1977

In 1971, the U.S. Air Force initiated a program directed toward the development of a high-speed generator with a superconducting rotating field winding. This new class of generator offers outstanding features for special high power, airborne applications.

Firstly, the machine is small and can be directly coupled to a high speed turbine. Secondly, it can be designed for a large rating and a high voltage without becoming excessively heavy. Also, the need for an equally heavy high power transformer is eliminated.

The first phase effort was successfully concluded in January, 1974, with the testing of a prototype rotor. This rotor was cooled down to a superconducting state and tests were conducted up to 13,200 rpm.

The second phase of the program was completed in April, 1977. An 1100 pound, 5000 kVA prototype generator was designed and constructed. Static tests performed on the stator and superconducting field winding have fulfilled our expectations and indicate the machine will be capable of generating 7700 kVA at 3800 volts and 12,000 rpm.

Room temperature spin-ups to 12,000 rpm. were completed and cool-down to liquid helium temperature (4.2 degrees Kelvin) was initiated in June. This test was terminated due to a loss of vacuum within the rotor. Subsequently, a small cold-leak within the rotor internal structure was found. A repair procedure was approved by the Air Force and this work is underway at the present time. It is anticipated that the superconducting rotational tests will be completed early in 1978.

PROTOTYPE GENERATOR

Figure (1) is a cross-section of the generator under construction and Table I presents the dimensions of this generator and the electrical parameters for a 5 MVA, 5000 volt rating.

The armature winding is composed of twelve identical coils. Each coil contains twenty-four, series connected turns which form a phase group for one pole. The winding has two parallel circuits; thus, each conductor carries one-half of the phase current and each phase group for one pole generates one-half of the phase voltage. A conductor consists of a 3 x 6 array of rectangular strands. The rectangular strands were formed from 16 gauge round wire. PYPE ML with a polysulfone overcoating was used for insulation on the strands.

The coils were made by winding simultaneously three strands in a fixture that contained eight slots for the upper side of the coil, eight slots for the lower side, and pins to form the hair pin turns. This step was repeated until eighteen layers (three conductors) were placed in the slots. A .25 x 4.5 mm ribbon of insulation was placed between the 6th and 7th layers and between the 12th and 13th layers of strands to separate adjacent conductors. After the strands were clamped in the winding fixture, the coil was spread to 17/24 coil pitch. Subsequently, the fixture and coil were placed in an oven and heated to a sufficient temperature to melt the polysulfone overcoating on the strands and the ribbon separators. After removal from the fixture, the conductors in the coil were in a rigid, bonded state as shown in Figure (2) and the coil as a unit could be handled easily. A 2000 volt conductor-to-conductor dielectric test was performed on the coils before the 3 groups of 16 conductors were connected in series.

The armature was assembled by laying the coils around the bore seal. "U" channels and wedge shaped sections of insulation, shown in Figure (3), were placed between the conductors to provide mechanical support against machine torque. The "U" channels kept the epoxy paste, which was applied to the surfaces of the bore seal and wedges, away from the conductors to insure oil flow through this monolithic structure. After the coils were placed, temporary bands were located around the structure and it was heated to cure the epoxy cement. Later, the exterior portion of the coil and wedges was wound with a glass-epoxy roving and then the entire structure was cured to form a rigid structure which was machined to mate with the iron shield. Phase-to-phase dielectric tests were performed at 11 kV (60 Hz) for 30 seconds with the armature submerged in transformer oil.

The ends of the coils, which produce the cross-overs to adjacent poles, were formed without curvature between the bend lines. Therefore, the knuckles at the ends of the conductors had a much greater envelope (39.6 cm diameter) than the center portion (35.9 cm diameter) of the coils. An extra large bore for the shield would have been required if the shield were installed over one end of the winding.

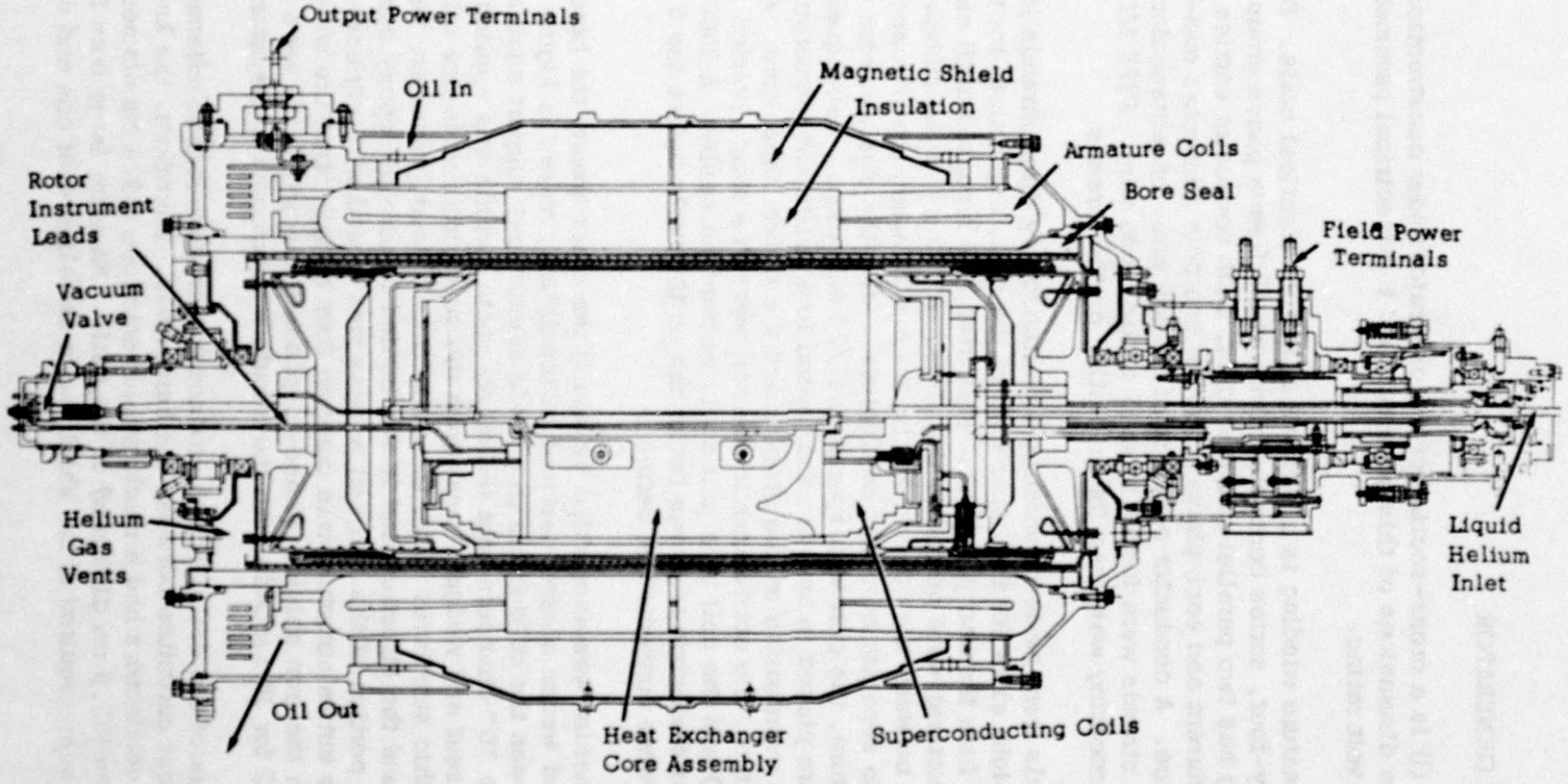


FIGURE 1 U.S. AIR FORCE SUPERCONDUCTING GENERATOR (10 MVA, 12000 RPM, 5000 VOLTS LINE-TO-LINE, 400 Hz)

TABLE I

DIMENSIONS AND DATA FOR GENERATOR

Rating	
Output	5 MVA
Voltage	5 kV
Voltage Regulation	9.27%
Power Factor	.95
Frequency	400 Hz
Phases	3 (Y)
Speed, r/min.	12,000
Reactances (Per Unit)	
Synchronous (Full Load)	.208
Transient	.228
Subtransient	.098
A. C. Winding	
Number Turns/Phase	48
Number of Parallel Paths	2
Number of Conductors	576
Strands per Conductor	18
Strand Size, mm	.111 x .155
Size of Conductors, cm	.685 x .500
Copper Current Density, A/in^2	16,210
Losses, kW	
Armature I^2R	29.4
Eddy-Currents, Armature	63.0
Iron Shield	8.1
Total	100.5
Percent of Output	2.0
Dimensions of Stator, cm	
Bore Seal Inner Diameter	25.20
Inner Diameter of Conductors	26.21
Outer Diameter of Conductors	
End Turns	39.58
Center of Machine	35.27
Inner Diameter of Iron Shield	36.30
Outer Diameter of Iron Shield	45.36
Outer Diameter of Frame (Max)	48.26
Length of Iron Shield	39.11
Length of Cylindrical Frame	67.92
Length of Bore Seal	72.39
Overall Length of Stator	74.68

Dimensions of Rotor (cm)	
Rotor Outer Diameter	24.69
Inner Diameter of Outer Shell	24.23
Outer Diameter of Wrapping on Copper in E/T Shield	24.03
Thickness of Copper in Shield	.15
Inner Diameter of Shield	23.06
Containment Vessel O.D.	22.86
Outer Diameter of Field Winding	20.32
Straight Length of Winding	24.64
Overall Length of Winding	37.59
Bearing to Bearing Length	75.69
Superconductor	
Conductor Size, cm	.094 x .14
Number of Filaments	500
Filament Diameter, μm	.36
Twist Pitch, cm	.84
Cu : Sc	2 : 1
Critical Current	830A
Field Self Inductance	1.22H
Field Current	228
Number Field Turns/Pole	1,220
Weights (Pounds)	
Stator	
Copper in Windings	166
Electrical Connections	8
Insulation	102
Stator Shield (Silicon Steel)	325
Frame Cylindrical	30
Main Bearings	12
Bearing Support End Plates	22
Housing, Seals, and Brushes	30
Total	695
Rotor	
Superconductor	75
Field Winding Supports	30
Auxiliary Heat Exchanger	10
Rotor Containment	67
Damper Shield	48
Torque Tubes	6
Ambient Shell	22
Shafts	62
Total	320
Generator	1015

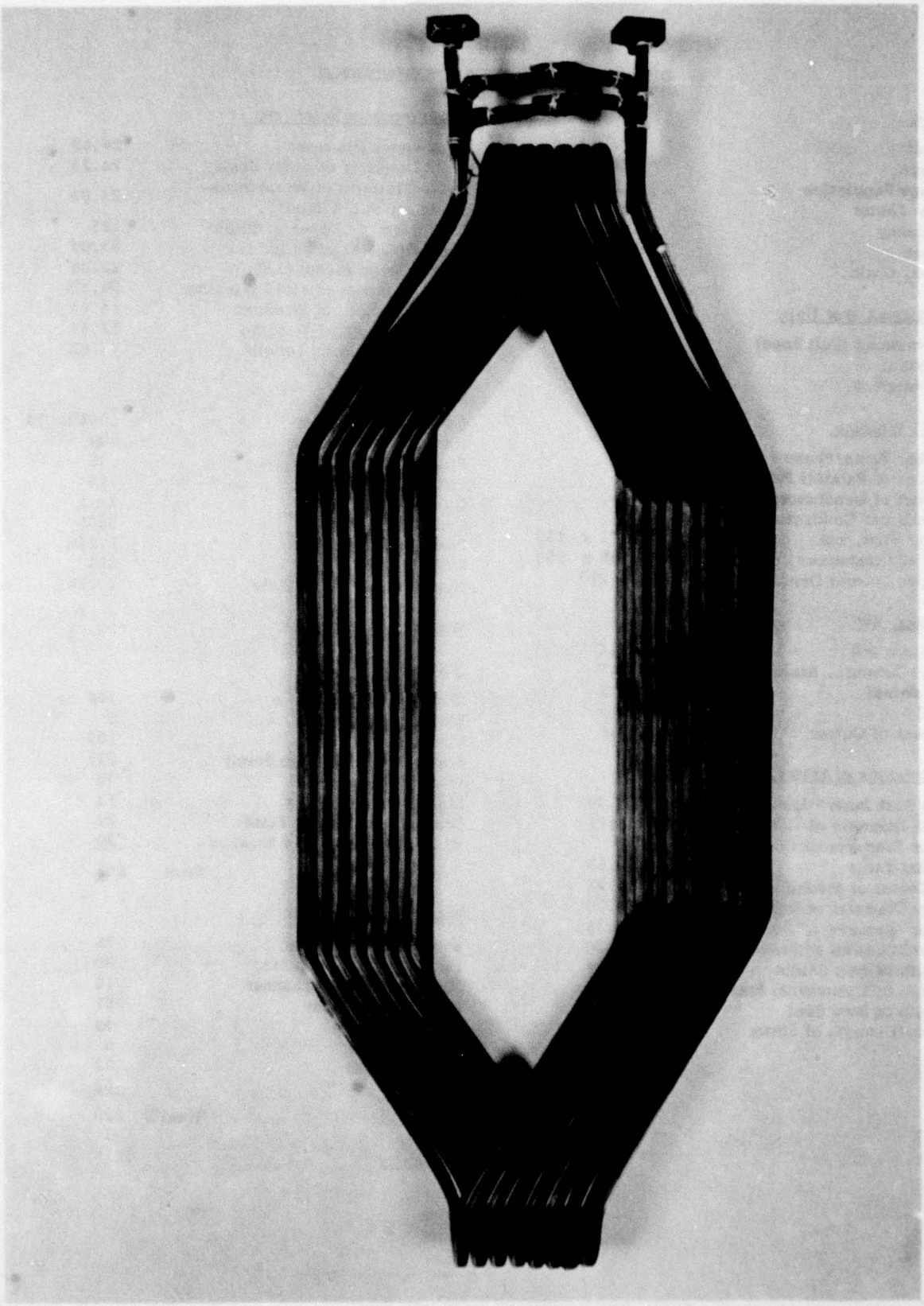


FIGURE 2 ARMATURE COIL

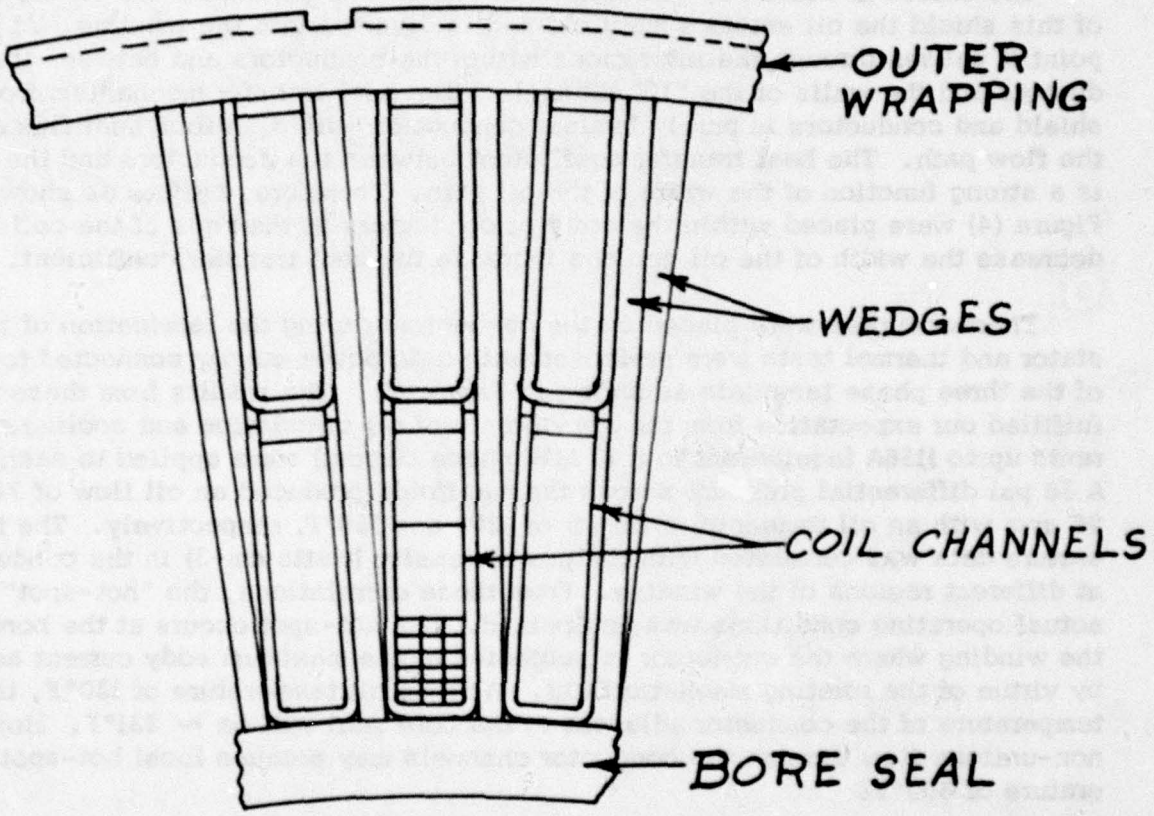


FIGURE 3 MECHANICAL SUPPORT FOR ARMATURE CONDUCTORS

Since the extra large bore would decrease the permeability of the magnetic circuits, the shield was constructed from laminated rings with separate halves. These rings were bonded to the winding assembly and were welded together on their outer surface to form a unibody structure which was subsequently machined to mate with the aluminum frames. The aluminum frames were pressed onto the shield, pinned and wrapped with an epoxy-glass roving to make an oil tight container.

The shield is cooled by circulation of transformer oil around it. At the center of this shield the oil enters a manifold and is diverted into the winding. At this point it passes through the interstices within the conductors and between the conductors and the walls of the "U" channels. The heat transfer mechanism from the shield and conductors is purely laminar conduction with a uniform heat flux along the flow path. The heat transfer coefficient between the conductors and the oil is a strong function of the width of the oil path. Therefore, baffles as shown in Figure (4) were placed within the array of conductors at the ends of the coils to decrease the width of the oil gap and increase the heat transfer coefficient.

Thermocouples were placed on the conductors during the fabrication of the stator and thermal tests were performed with a dc power supply connected to two of the three phase terminals as shown in Figure (5). The results from these tests fulfilled our expectation from the standpoints of oil circulation and cooling. Currents up to 1156A (equivalent to a 10 MW phase current) were applied to each phase. A 38 psi differential pressure across the manifolds produced an oil flow of 78 and 90 gpm with an oil temperature (inlet) of 120° and 150°F, respectively. The temperature data was correlated with the power density (watts cm-3) in the conductor at different regions of the winding. From these correlations, the "hot-spot" under actual operating conditions was determined. The hot-spot occurs at the bore of the winding where the conductor is subjected to the maximum eddy current heating by virtue of the rotating magnetic field. With an oil temperature of 130°F, the mean temperature of the conductor adjacent to the bore seal will be $\sim$ 231°F. However, non-uniform flow through the conductor channels may produce local hot-spot temperature of 300°F.

Rotor

The coils were wound in a fixture which controlled the height of each layer of turns. The number of turns in the layers was varied to obtain the step arrangement shown in Figure (6). A series of spacers (.76 x 19 mm) were placed between adjacent layers in each step to provide a (.76 x 6 mm) passage for helium. After completion of the winding operation, the coil and fixture were heated to the melting point of the polysulfone overcoating on the wire. This operation produced a bonded coil which could be handled easily.



FIGURE 4 BAFFLES BETWEEN CONDUCTORS IN THE CROSS-OVERS

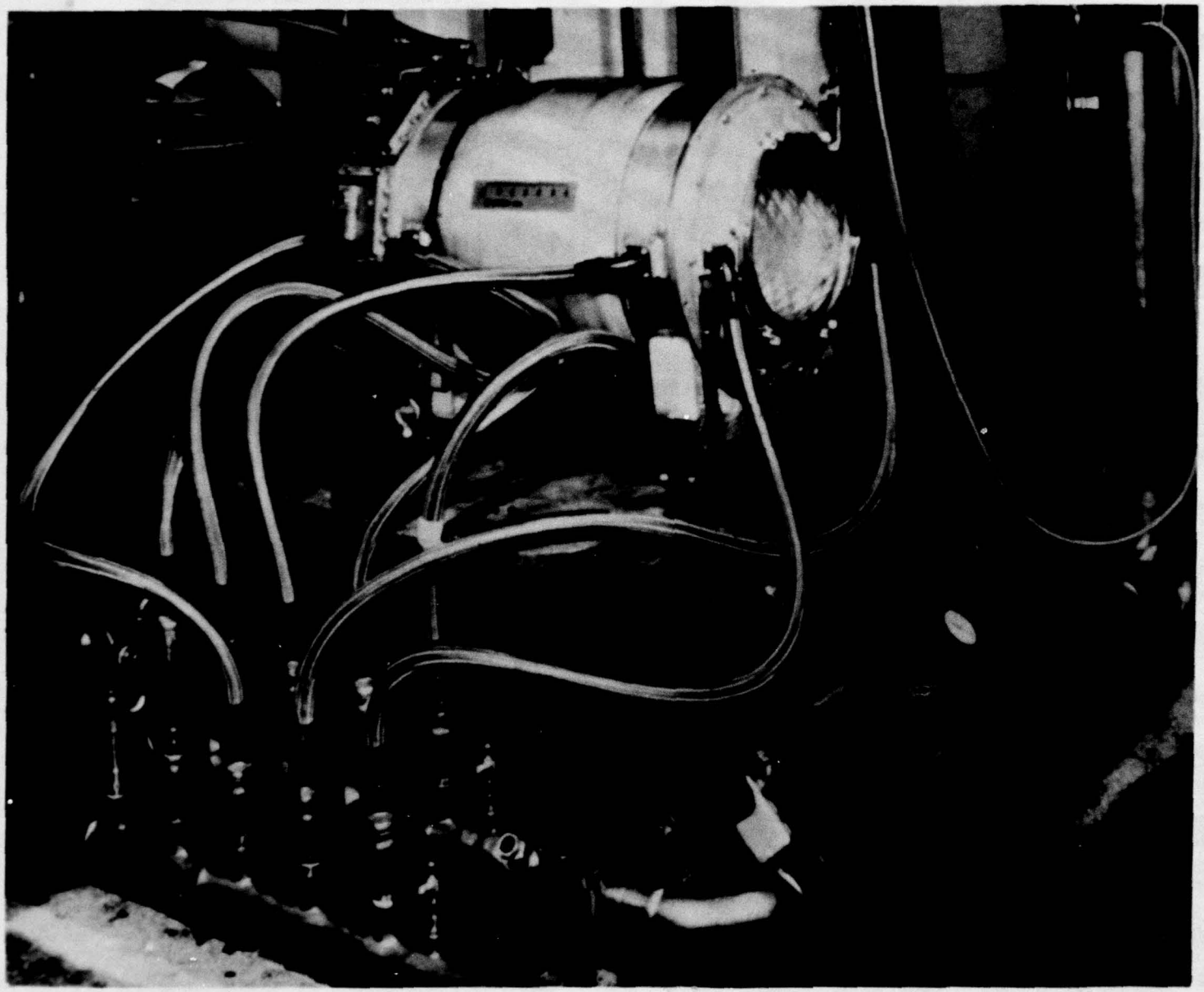


FIGURE 5 SUPERCONDUCTING GENERATOR ON TEST STAND FOR THERMAL TESTS

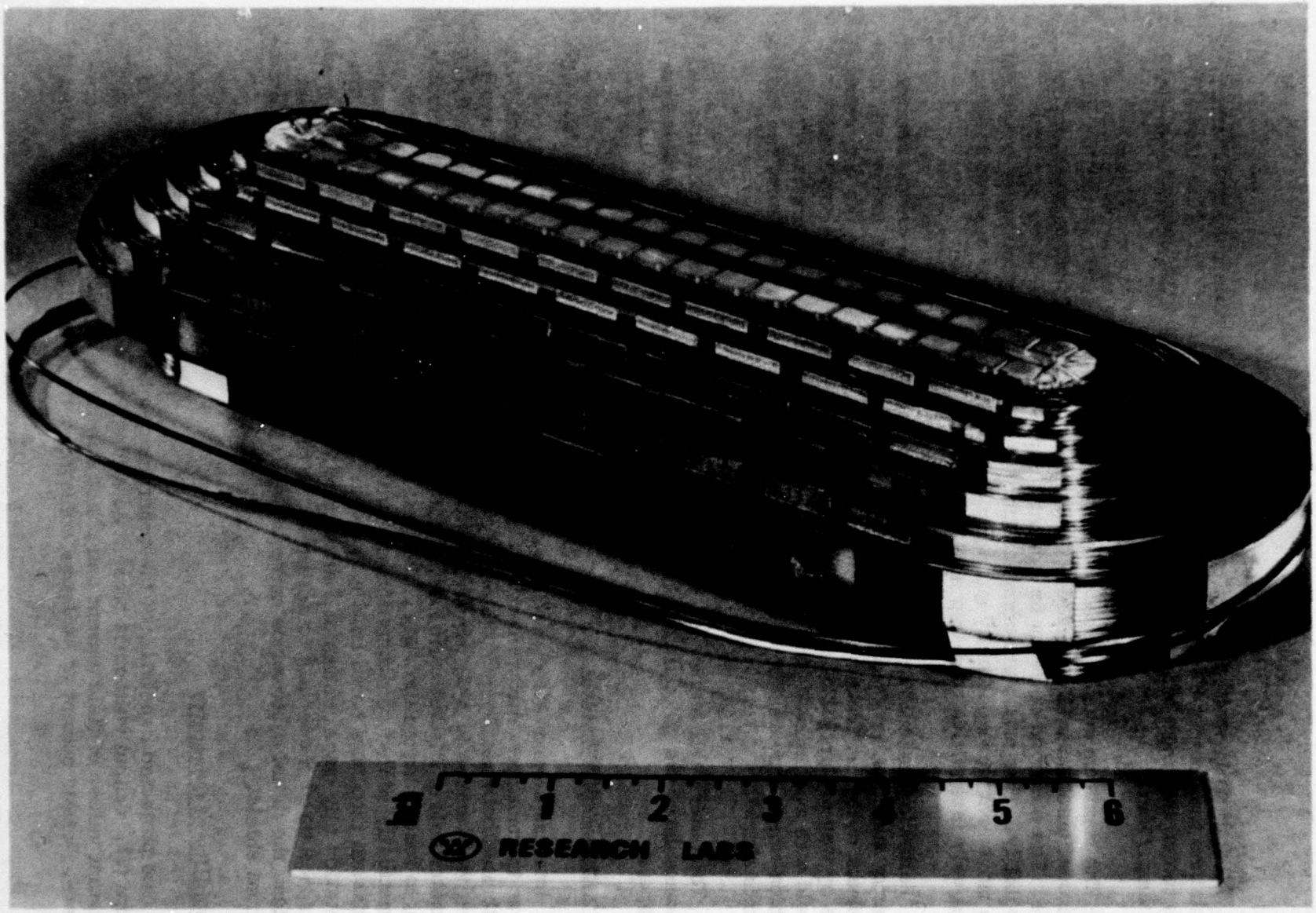


FIGURE 6 SUPERCONDUCTING COIL

All four coils were mounted on the rotor core and encased in structures that contained the counter form of the coils as shown in Figure (7). This assembly was tested in a bath of liquid helium at 4.2K and 3.4K at the sweep rates up to 144 Amp./Min.

The maximum current capability for this superconducting wire in this four-coil configuration is 410A based upon the performance of short samples of the wire. The observed currents for normalization were 60% of the projected capability. This premature normalization was attributed to conductor movement. The movement was apparently quite rapid since normalization appeared to be relatively insensitive to sweep rate.

Following the cold tests, closure welds were made on the casing and the exterior surfaces were machined for a .508 mm shrink fit with a heavywall, containment cylinder. Both ends of the cylinder were connected to the warm structure by way of duplicate, vapor-cooled transition tubes. An electro-thermal shield was mechanically and thermally connected to the transition tubes at a station which provides an intermediate temperature for interception of the losses in this shield.

The outer shell forms a vacuum jacket around the cold inner structures and accommodates the thermal contraction of these structures through flexible end-members.

Cryogenic Instrumentation

Internal thermometers were incorporated into the rotor during its assembly. These thermometers are ordinary 1/10W Allen-Bradly carbon resistors which were calibrated between 3 - 100°K using a calibrated Ge thermometer. Each thermometer was housed in a Cu support sleeve and was designed to fit within a 0.125 diameter hole. The Teflon insulated voltage and current leads were sufficiently long to reach outside the rotor. The leads were fed through special tubes to hermetically sealed connectors located in the drive coupling. These leads shall be passed through a bored hole in the gear box drive shaft to high speed instrumentation slip rings. Internal thermometer leads penetrated both the vacuum and He space through conduits to ascertain the temperature of the centerline inlet helium, the radial distribution across the superconducting coils, and the electro-thermal shield.

Capability of Generator

The projected capability of the generator can be described with the aid of Figure (8). Output voltage is present as a function of the output power (MVA). Constant values of field current and phase current are shown as arbitrary parameters. A field current of 245A was achieved during the static cold tests and the

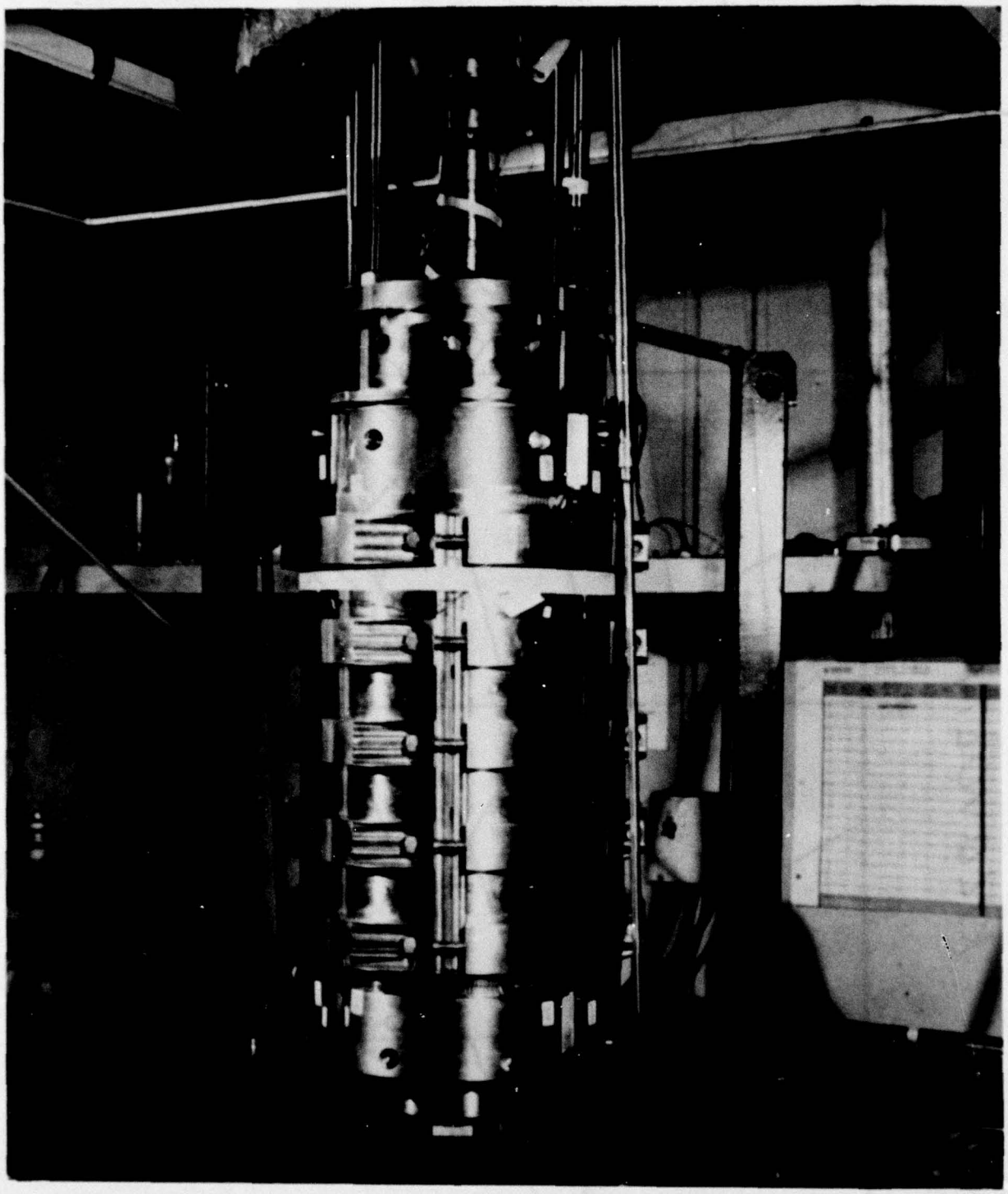


FIGURE 7 COLD TEST OF FOUR COIL ASSEMBLY

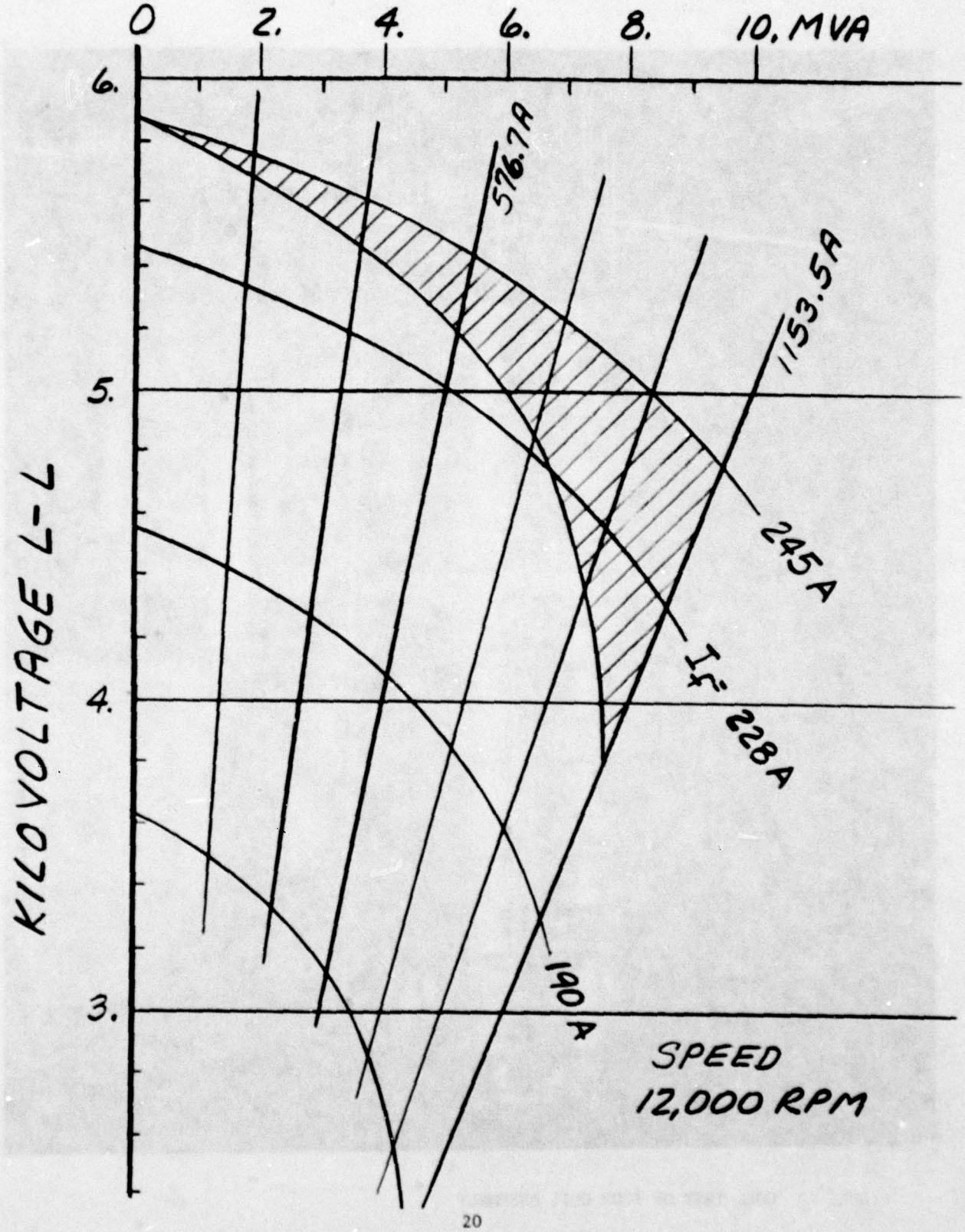


FIGURE 8 PROJECTED CAPABILITY OF THE SUPERCONDUCTING GENERATOR

armature winding was subjected to a dc phase current of 1154A. With these parameters as upper limits, the rating of the generator becomes 9.5 MVA at 4.76 kV. However, this is not a valid continuous rating for the generator since the static test on the stator did not reflect the eddy current heating of the armature conductors. The shaded area on Figure (8) shows the impact of the eddy current heating. A realistic maximum rating at 12,000 rpm is 7.7 MVA at 3.8 kV with a field current of $\sim$ 200A. In prejudgment, eddy current heating has a greater impact than premature normalization of the field winding since a 245A field current fulfills the needs of this generator with this amount of eddy current loss.

Reduction of the eddy current heating can be easily accomplished by decreasing the size of the strands in the conductor.

Generator Tests

Low power tests on the generator will follow directly after the construction is complete. These tests will include:

- Demonstration of design open circuit voltages.
- Demonstration of design armature current under steady-state three-phase short circuit.
- Sudden three-phase short circuit at reduced excitation to yield machine reactances and time constants.
- Determine electromagnetic shield performance under load unbalance at reduced excitation.
- Determine electromagnetic shield performance with short circuit rectified load at reduced excitation.
- Complete cryogenic characterization of the rotor during the above tests.

The main purpose of the rectified load test is to obtain information on shield heating in anticipation of future machine requirements.

While there is at present no scheduled commitment to a full-power test, it is the intent of the Air Forece to have such a test carried out sometime in the near future.

RARE EARTH PERMANENT MAGNET MOTORS AND GENERATORS

Sam Noodleman
Inland Motor Division,
Kollmorgen Corporation

In 1972, a visit was made to Wright Field to discuss with engineers in the Materials Lab their developments in rare-earth cobalt magnets. These developments sponsored by the Defense Department were directed to improving the properties of permanent magnets so as to provide higher fields and lighter weight components for traveling wave tube applications. The magnetic properties of Sm Co_5 materials at that time had relatively very high coercive force compared to permanent magnets used in motors, but low induction compared to the alnico materials which were the materials being used in Inland motors. Our evaluation of these materials and their cost indicated no possibility of using them for motors and generators for general purpose use. However, in looking further the new materials had some very attractive features and, because they could develop maximum energy levels that were very high in relation to magnet materials in use at that time, a program was started to study motors incorporating rare-earth cobalt magnets.

As a result of these studies it did appear that if these materials were to be used for permanent magnet motors new motor concepts would be required. In other words, the new motor con-

figurations would require a design which would allow the use of the minimum quantity of these materials since they were very expensive, and these designs would require new concepts different from the configurations used in the alnico motor designs. When we first started using Sm Co_5 materials the maximum energy product available at that time was 15×10^6 gauss oersteds. At the present time, all our designs use materials having maximum energy products of 18×10^6 gauss oersteds and some of the latest motors in production use rare-earth cobalt materials having a maximum energy product of 26×10^6 gauss oersteds.

The discussion today will cover two developments, one in motors and one in generators, to illustrate how rare-earth magnets are used in these types of products. A motor configuration which permits optimum use of the magnet material and provides improved motor performance is the inside-out type of construction. This configuration uses the magnets in the rotor or inside member for the rotating magnet structure and the windings are in the stator or stationary member. A major problem is how to best commutate the winding with this construction so as to develop the necessary rotating field. Considerable development and evaluation were necessary to produce a practical method that would provide suitable commutation for this concept.

Figure 1 shows the cut-away of an experimental rotor for one of the Industrial Drive motors using rare-earth cobalt magnets. The magnets are the rectangular blocks, and the light area shows the cast aluminum which holds the magnets and the steel pole piece laminations together. It took considerable development to learn how to cast the rare-earth magnet materials into a structure and to magnetize the multipolar structure to properly utilize the magnet materials.

Figure 2 shows the finished cast rotor as manufactured in volume production. The aluminum rings serve to hold the magnets as shown. The magnets are also entrapped by the laminated pole pieces which help to secure the magnets in place.

Figure 3 illustrates a production wound stator showing the commutator structure for this particular type of inside-out motor. Brushes contact the face-type commutator receiving their electrical energy from other brushes connected by pigtails which ride against slip rings providing a very compact structure. The basic electric power is applied to the stationary slip rings which transfer the energy to the rotating brush assembly feeding into the commutator to provide the commutation to the stationary windings. One of the major advantages of an inside-out type structure is that the windings are in the outside structure and can better dissipate the heat. The stator housing is also cast in aluminum with external fins so as to better dissipate the heat.

The inside-out construction provides about an 80% improvement in continuous torque rating for the same size over motors of conventional construction.

Figure 4 shows the assembled production motor. This motor develops about 82 lb.ft. peak torque and weighs 80 lbs. It has a continuous torque rating of 18 lb.ft. and a maximum acceleration of 7500 rad/sec^2. The motor which it replaced in alnico design weighed 75 pounds and developed 45 lb.ft. peak torque, slightly more than half of the present torque rating and had a 10 ft.lb. continuous torque rating and a maximum acceleration of 4500 rad/sec. The new line of motors out-performs the old alnico line in every respect. This line of motors in present production using rare-earth cobalt magnet materials started from a visit to Wright Field in 1972.

A different type product which could only be developed with rare-earth cobalt magnets is an alternator having very high efficiencies over 95%, with an output rating of 640 watts at 2000 R.P.M. Because of its very high efficiency the tests at its continuous rating showed a temperature rise on the windings of only 11^{o}C.

While customer requirements had specified alternator operation at 2000 R.P.M. tests were made at much higher speeds. Tests were also made at loads which would allow the windings to be worked up to their maximum continuous rating.

Figure 5 shows the plot of efficiency versus output at 3000 R.P.M. for this alternator at outputs up to 5 kilowatts. The efficiency exceeds 90% from about 300 watts to almost 4600 watts.

Figure 6 shows the stator and rotor construction of this alternator and Figure 7 its overall dimensions.

Figure 8 shows the rotor construction. By using a non-magnetic band over the rotor speeds considerably higher than 3000 R.P.M. could be achieved providing proportionally higher outputs.

The use of rare-earth cobalt magnets for d. c. motors became practical when methods were developed for assembling these materials into multipolar structures and the techniques were developed for magnetizing these structures in situ. New products are also being produced utilizing the improved magnetic properties of these cobalt rare-earth materials as they are made available for production. First prototype used materials having maximum energy products of 15×10^6 gauss oersteds. Most production motors now use 18×10^6 gauss oersted material with some production motors using samarium-praseodymium cobalt material having a maximum energy product of 26×10^6 gauss oersteds. New prototypes are presently being developed using materials having a maximum energy product of 30×10^6 gauss oersteds.

The materials can provide electromagnetic devices with the capability of improved performance in minimum size and weight which are not achievable by any other means, particularly for motors in ratings of 25 horsepower or less.

QUESTION PERIOD

Question: Please discuss the reliability of the properties of the higher energy rare-earth cobalt materials.

Answer: Are you talking now about 26 x 10^6 or 30 x 10^6 materials?

Question: Either materials.

Answer: Well, we are just starting production on motors using 26 x 10^6 material and we will be setting up incoming inspection to check the repeatability of these materials. The design of these motors allowed for more tolerance in the magnetic properties and we do expect that there will be some variation in the B-H characteristics of the material.

Question: What are the induction values?

Answer: Well, the B_r values of the present 26 x 10^6 material is about 10 to 10.5 kilogauss.

Question: Are you getting these kinds of flux density in the air gap?

Answer: No. That is the B_r value. We operate at a slope of about 6 or 7, so we are probably getting a B_d of about 8.5 to 9 kilogauss.

Question: Could you compare rare-earth designs with alnico designs?

Answer: Initially, we evaluated a number of designs and determined that for a comparable performance about one-fifth the volume of rare-earth cobalt materials as alnico material was required. At that time alnico material was selling for about $5.00 to $5.50 a pound. Consequently, to keep magnet costs comparable in production it was desired that we obtain this material for about $26 a pound. We presently obtain rare-earth magnets from between $26 to $40 per pound and we do have to buy relatively large volume to get our cost down.

Question: Are you able to magnetize magnets after assembly?

Answer: Yes, all of the multipolar structures are magnetized in place and this is a technique which was developed to allow the efficient use of these materials in production.

Question: In the last figure, Figure 8, were the magnets skewed?

Answer: That is correct. This particular machine is not only a generator, it also has to start as a motor. In order to get it to start properly and keep cogging torque to a minimum this particular rotor was skewed. The generator is started as a brushless motor to start up the Sterling engine which drives it as an alternator.

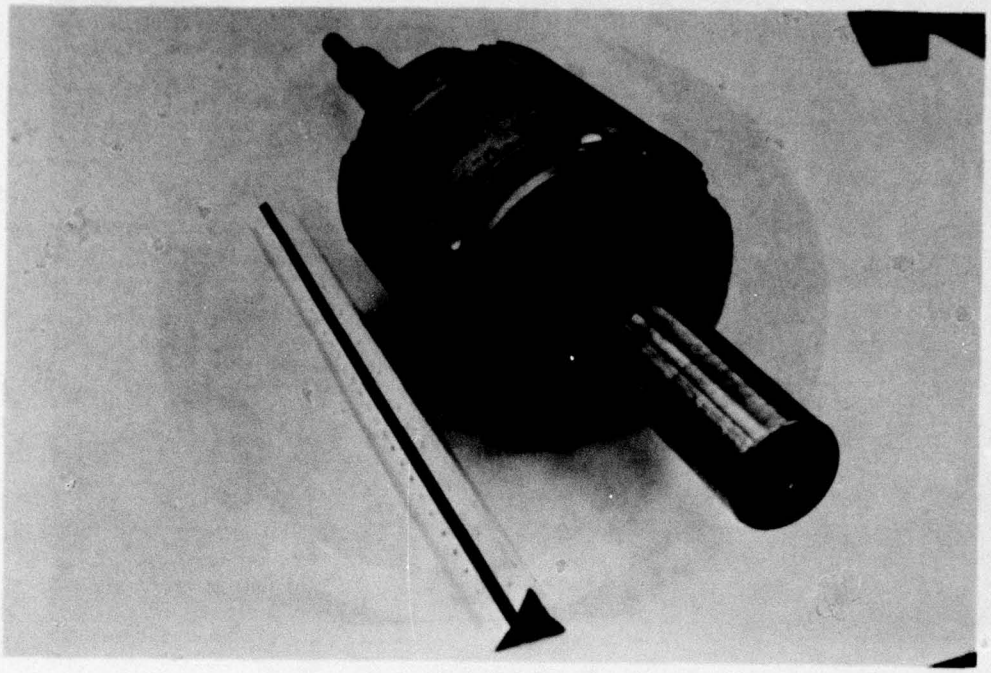


FIGURE 1

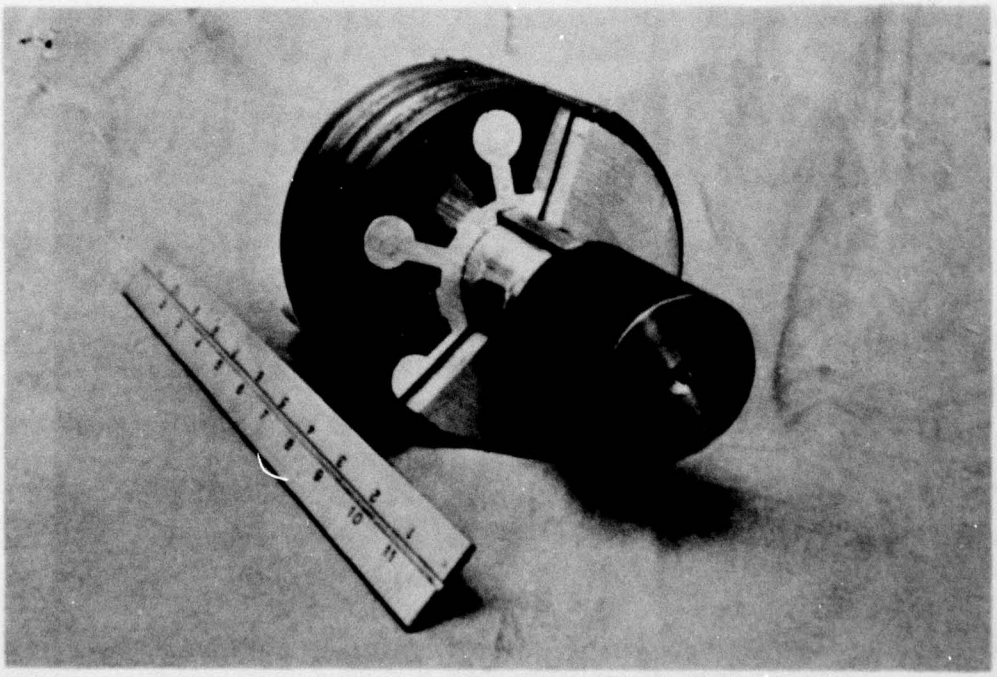


FIGURE 2

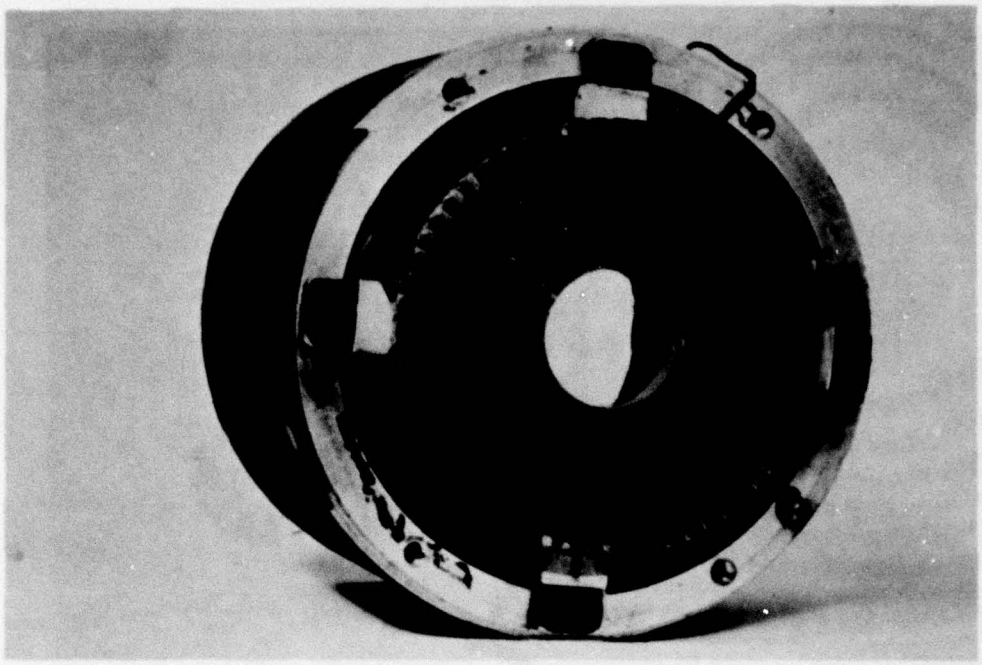


FIGURE 3

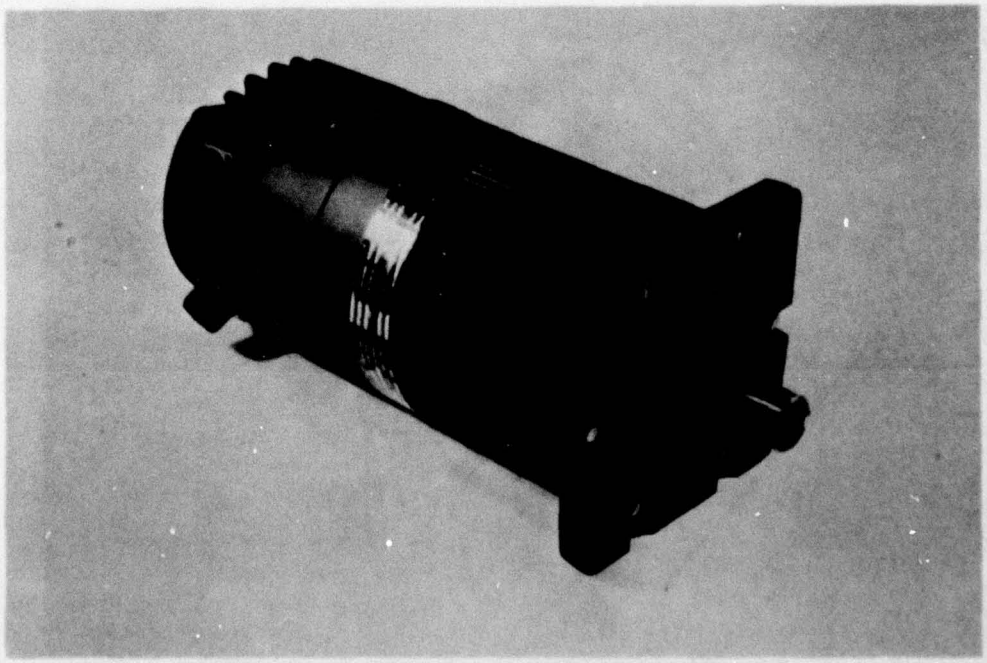


FIGURE 4

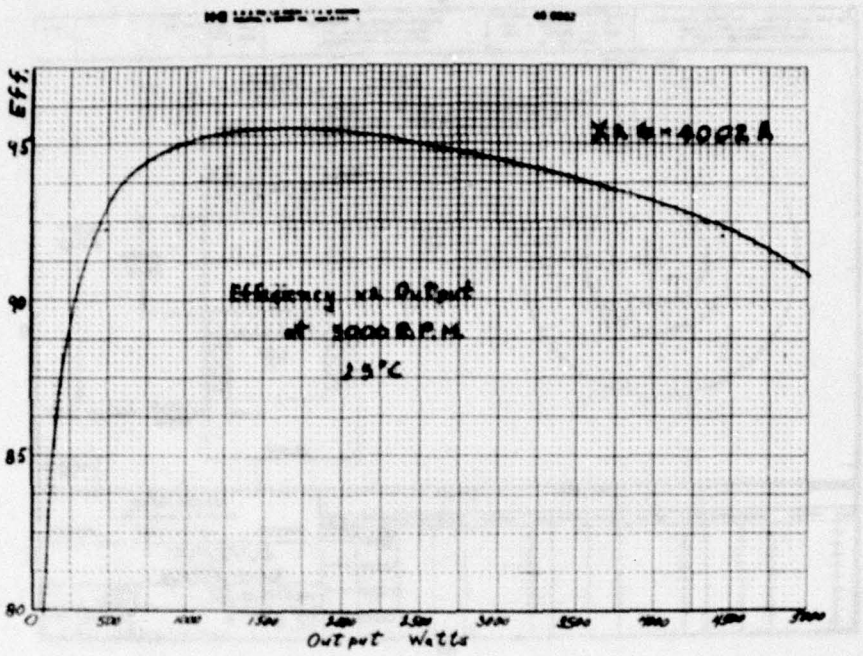


FIGURE 5

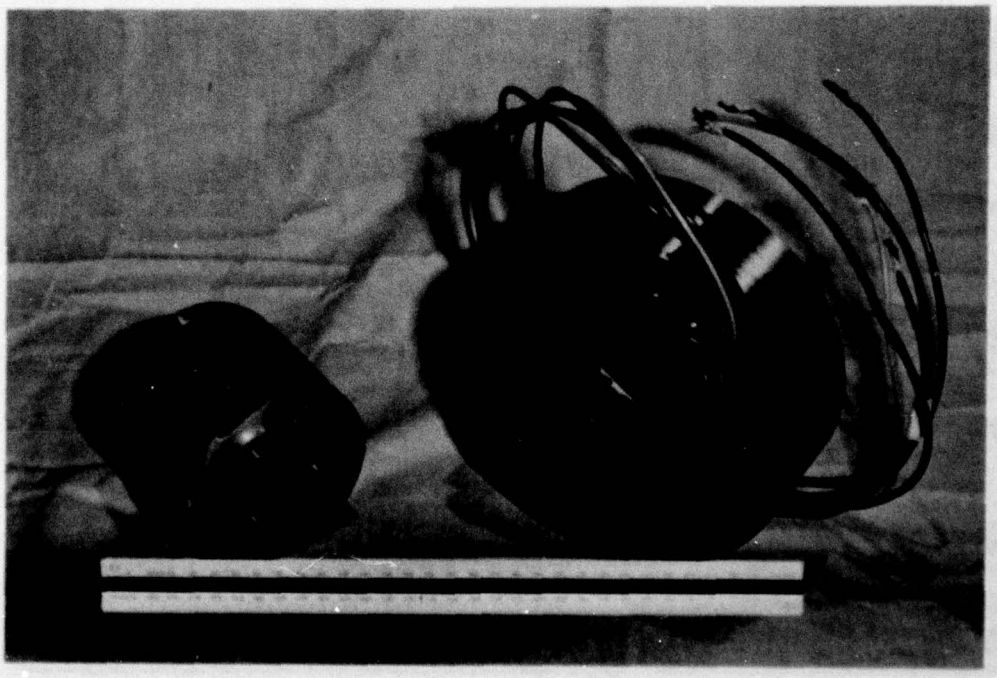


FIGURE 6

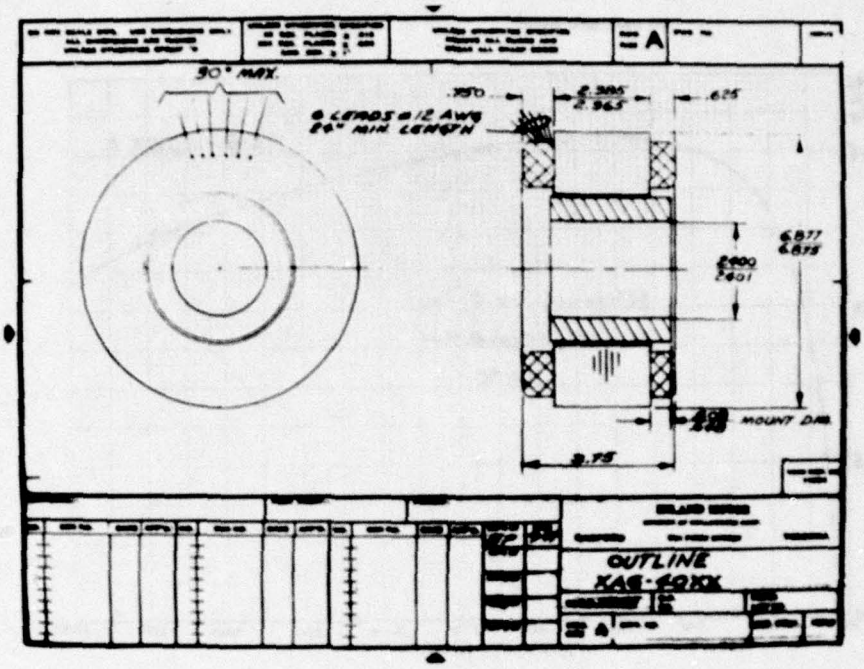


FIGURE 7

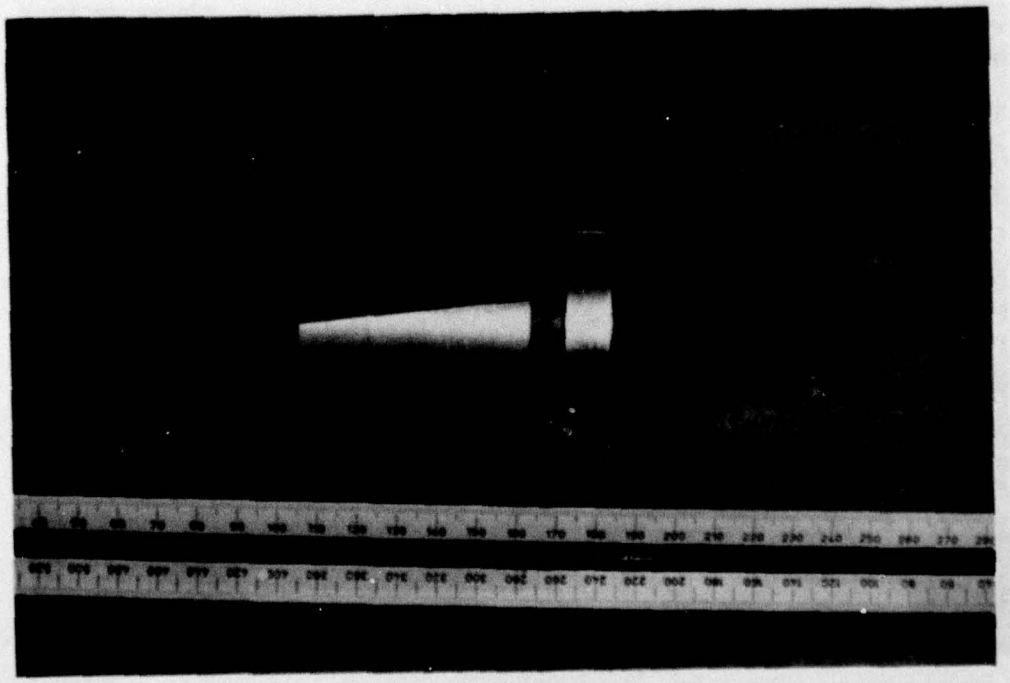


FIGURE 8

A NEW BRUSHLESS DC MOTOR CONCEPT

Milton S. Isaacson
President, Nu-Tech Industries, Inc.
Dayton, Ohio

Seven years ago our Company, Nu-Tech Industries, Inc. started work on a new approach in the design of a brushless DC motor. We were working with brushless DC because we believed that it was the best motor, the one that could produce the greatest output for size and weight, and the motor that would provide the best efficiency. Normally when speaking of a DC machine, one thinks of a brush commutator motor. That motor of course has its disadvantage because it has brushes and commutator. We were determined that our motor not only be brushless, but that it be better than the already existing brushless DC motors. If we could design a motor that had nothing attached to its shaft for purpose of indicating rotor position, and if at the same time we could provide speed control, this would certainly be a technical advantage over existing brushless DC machines. Lastly, if that speed control was synchronous, that would be better yet.

So, we started our work with the result that today we have a universal design that fully meets these objectives. The design is applicable to any size motor; it could be a motor as small as one to run a wrist watch, or as large as an alternator in a modern electric power plant.

Two major elements comprise the motor electronics, the digital electronics that senses back EMF voltage for commutation and speed control, which is the same for any size motor, and the

power electronics for power switching which varies in size according to the output of the motor.

To obtain an understanding of how the motor operates one may refer to the attached Nu-Tech Industries Technical Bulletin NT200. We would mention one item which is greatly stressed therein. The reason that a DC motor is better than other motors is that in a DC machine an average 90 degree torque angle is maintained between the two motor fluxes. This is the most important characteristic for creating maximum output for size as well as creating high efficiency in the DC machine.

Let us look at a few features of the motor. We have worked through the years toward the objective of having all the digital logic and analog circuitry on just one semiconductor chip. In recent studies we have determined that this can be done. The silicon chip would be approximately 150 thousandths on a side. That chip, if bought in sufficient quantity would cost less than one dollar. Once the chip is tooled and in production we will have achieved both our economic as well as our technical objective.

Also, during this period we have developed a microprocessor approach that does the same commutation and speed control that the custom chip does. When that approach is reduced to its minimum number of components it will consist of a microprocessor and a simple custom analog chip.

The motors we have built for test have been small motors, the largest being approximately two inches in diameter. Our work has been with small motors since they are easy to fabricate and

test. There is no reason however, that we could not build larger motors.

The power element for a motor that is relatively small, maybe an inch in diameter by an inch in length, could well be powered by two or three amps with an applied voltage between 28 VDC to 100 VDC. A single monolithic chip could be made to power this motor so that along with the custom digital logic chip only two chips would be required for the total system. As the motor increases in size, hybrid circuitry comes into play. In this case, on a one inch by one inch substrait we can safely operate with currents up to 20 amps at an applied voltage between 28 VDC and 100 VDC. With very large motors, SCR's and perhaps GTO type SCR's will be developed to handle very high currents efficiently. In the meantime, transistors are being produced today in ratings for hundreds of amps and hundreds of volts that offer immediate solution to power switching in the larger brushless DC motor.

In an inclusive sense we are striving in a simple way to control the motor shaft, whether that output be synchronous speed, normal commutation or a stepped function. If we put a string of speed control pulses into the motor, which are sinusoidal in frequency, the speed will be sinusoidal. In effect, we can cause the motor to follow any pattern of speed by the particular pulse applied. Also, by counting the pulses, we can tell where the rotor is at all times.

Typical applications being considered are sound and video systems, industrial drives and automobile accessory items. An

interesting application is the drive for the electric vehicle. Work is currently being done in developing drives for artificial heart devices.

THE K-I MOTOR

NU-TECH INDUSTRIES

AN ELECTRONICALLY OPERATED AND CONTROLLED BRUSHLESS DC MOTOR

FOREWORD

Major progress has been made in the field of brushless DC motors in the past decade: This progress came as a direct answer to the space program's need for small, efficient, reliable motors that could operate in a vacuum. High cost has slowed the transition of this technology to military, commercial and industrial fields. The development of a custom designed motor for the space program sometimes costs from $50,000 to $250,000. The engineers at Nu-Tech Industries felt there was a solution to this cost problem.

The development of micro electronics and power electronics provided technology for a new and truly universal brushless DC motor concept. This technology promised the universality so essential to commercial development at a cost and with a reliability previously unattainable. Two key problems had to be solved. First, the transducer used in previous concepts to sense rotor position had to be eliminated, and, second, a single electronics package had to be designed that was universal enough to provide constant speed or programmed speed changes regardless of changes in load or voltage.

After four years of development, a truly universal, brushless DC motor concept is a reality. In this concept, named the K-I (Knight-Isaacson) Motor, a single electronics package coupled with an appropriate power module can control two-phase or three-phase machines of any size. Digital electronics senses motor back EMF to provide commutation as well as control motor speed without using a transducer. The concept is the essence of simplicity.

The K-I Motor starts and accelerates along a straight line, DC, speed-torque curve like any DC commutator compound or permanent magnet motor. It can maintain a selected fixed speed under load and line voltage changes and can be reversed with a simple single-pole switch.

The machine can be of any size, can have any number of poles, and can have either a two-phase or three-phase winding. The armature and field need only produce a generated voltage when operated as a generator, to qualify as the mechanical apparatus for the K-I Motor. The digital electronics remains the same regardless of the size of the machine; the electronics will be two MOS chips. The power electronics on the other hand varies in size with the size of the motor. The power electronics will be different for different voltages and for two-phase or three-phase operation. Changing the number of poles does not have any effect on the design of the power electronics.

Replacing the brushes with electronic commutation does much more than just eliminate all the well-known brush problems. The digitally controlled commutation of the K-I Motor adjusts automatically with load to maintain an optimum flux configuration in a manner analagous to mechanically shifting the brushes in a comparable brush-type machine. In addition, it is possible to electronically accomplish the equivalent of shifting the brushes for optimizing performance in one direction of rotation.

The K-I Motor has much to offer. The range of application is limited only by the ingenuity and imagination of the design engineer. In the first section of this report we will discuss the motor theory essential to a clear understanding of this new motor concept, and in the second section we will discuss the specifics of the K-I Motor concept.

SECTION 1
INTRODUCTORY DISCUSSION

INTRODUCTION

Motor action may be defined as the conversion of electrical power to rotational mechanical power through the interaction of magnetic fields. There are several ways to approach a discussion of the theory of motor action, but the way that leads most directly to a clear understanding of the K-I Motor is to consider a set of vectors representing the magnetic fields involved. Rather than evolve a completely general theory, we will illustrate the pertinent principles by discussing the DC brush machine and the AC synchronous machine. Both of these machines generate a back EMF and an understanding of the phase relationship between this back EMF and the other magnetic fields involved is essential to understanding the K-I Motor. It will be shown that the DC and AC machines are similar in several other very important respects. The discussion of fields and back EMF's in Section I will lead to an explanation of the K-I Motor commutation concept and its electronic implementation in Section II.

STRUCTURE

Motor technology can be traced to the discovery of electromagnetic induction by Michael Faraday in 1831, but it is a commentary on the vagaries of the English language that we find it necessary to define a few terms before proceeding with our discussion. For our purposes, a DC motor is a brush-commutator machine that runs directly off a DC line. The armature rotates and contains windings as well as the commutator, and the magnetic member that remains stationary is referred to as the field. To simplify our discussions, we can, without loss of generality, consider the field as a permanent magnet even though in practice many fields are electromagnets. The AC machine we will discuss is a synchronous motor with a set of stationary windings called the stator or armature, and a rotating permanent magnet called the rotor or field.

ROTATING FIELD – AC MACHINE

For motor action to occur it is necessary to first establish a rotating magnetic field. This field then interacts with a second field to produce torque and rotation of a shaft. The AC machine is the easier to describe and we will address it first. Figure 1 illustrates a two-phase machine with coils A and B located 90 degrees apart in the stator. In a conventional machine, sine waves displaced by 90 degrees as shown in Figure 2 are applied to the two coils to produce the desired rotating field. Square waves may also be used to activate the coils and produce a rotating field. Figure 2 illustrates the required wave shape. The fundamental component of the square waves coincides with the sine waves of the conventional machine in Figure 2. The voltage is only on for 90 of each 180 degrees in a half cycle, a 90 degree on time condition, and the coil B wave is displaced from the coil A wave by 90 degrees. Note that the fundamental components of the square waves just described are sine waves displaced by 90 degrees.

Consider the square waves of Figure 2, applied to coils A and B in Figure 1. Using the sign convention established by vectors A and B in Figure 1, the flux is directed toward the top of the page for the first 90 degrees. At 90 degrees coil A is switched off and coil B is switched on to give a flux directed toward the right as shown in Figure 1b. The flux has effectively rotated 90 degrees clockwise. Ninety degrees later, coil B switches off and coil A switches on in the negative direction to give the flux shown in Figure 1c, which represents another 90 degrees of clockwise rotation. Similarly, during the last 90 degrees, coil A is not energized and coil B is negatively energized to give the flux vector shown in Figure 1d. At the end of this 90 degree segment the current and flux pattern revert to the initial condition. The flux has effectively rotated 360 degrees in 90-degree steps. This action is in sharp contrast to the sine wave case which results in a smoothly rotating constant-amplitude flux vector.

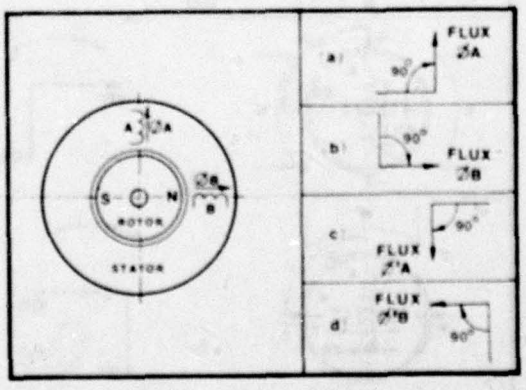


FIGURE 1

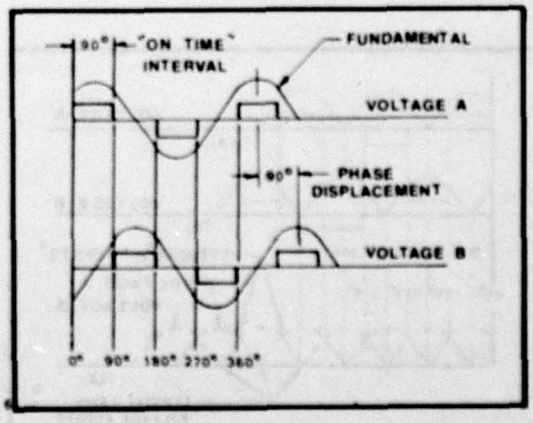


FIGURE 2

ROTATING FIELD – DC MACHINE

To visualize the equivalent rotating flux in a DC machine, imagine a motor with the shaft and armature fixed and the field magnets and brushes rotating. (The current would be brought to the brushes through slip rings). The geometry is illustrated in Figure 3. Coils A and B are displaced by 90 degrees as in the AC machine discussed above. The coils are connected to a four-segment commutator, each segment of which occupies 90 degrees. Leads from each coil are attached to segments 180 degrees apart. There are two brushes, "a" and "b", of negligable thickness located 180 degrees apart. For purposes of our discussion, current always flows in brush "a" and out brush "b". For the brush position shown in Figure 3, and during 90 degrees of counter clockwise brush rotation, current flows up through coil A and no current flows in coil B. During the next 90 degrees of rotation, current flows from right to left in coil B and coil A is not energized. During the last two 90-degree rotations, coil A is negatively energized, and then coil B is negatively energized in direct analogy with the AC case. The field set by the rotating brushes is, therefore, a stepwise rotational field just as in the AC case and the currents in the coils are two square waves with 90 degrees on time displaced by 90 degrees.

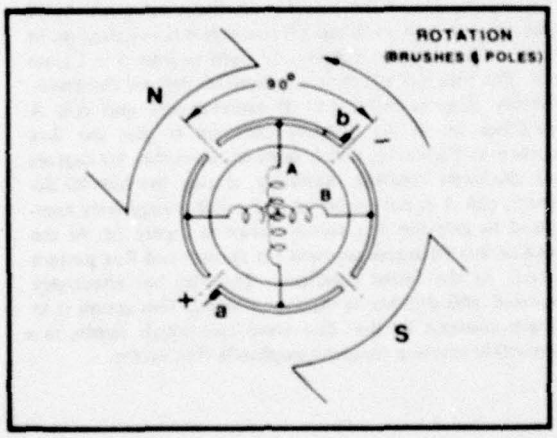


FIGURE 3

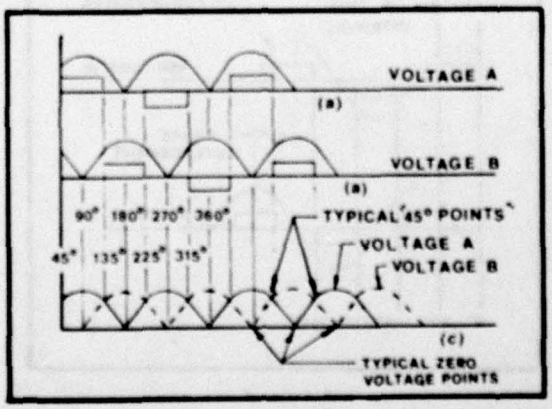


FIGURE 4

The fundamental component of the square wave is shown as a sine wave in Figure 2. The on-off points of the square wave occur at what we shall call the "45° points". To illustrate the location of these points more clearly, we have redrawn Figure 2 in Figure 4 (a and b) with the negative half-waves inverted. When the two inverted waveforms are superimposed in Figure 4c, the "45° points" lie midway between zero voltage points.

TORQUE ANGLE – DC MACHINE

The physical arrangement of the DC machine gives rise to a most important relationship between the flux of the permanent magnet and the armature flux, to illustrate this relationship we have drawn an idealized DC motor in four positions in Figure 5. To be consistent with our earlier discussions, we fixed the armature and commutator and let the field and brushes rotate. In Figure 5(a) the sign conventions are such as to result in a field flux directed from left to right and an armature flux directed upward. As the permanent magnet rotates 90 degrees counterclockwise, its field obviously rotates the same way; but since the brushes have also rotated 90 degrees, the armature current is now flowing through coil B in such a way as to have the armature flux directed from right to left.

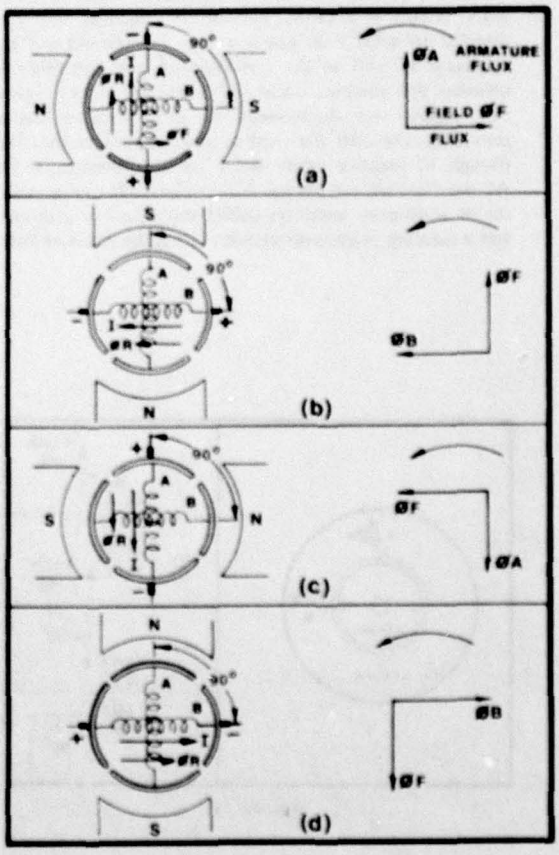


FIGURE 5

The relative positions of the two vectors is still the same, that is ❶B leads ❶F by 90 degrees. Similarly as the field continues to rotate, the armature flux moves with it. The angle between the fluxes is not a constant 90 degrees because the field is rotating through 90 degrees with no change in armature flux direction while the brushes are in contact with any pair of commutator segments. At the switching points, the armature flux suddenly jumps 90 degrees. The angle actually varies from 135 degrees to 45 degrees and then suddenly jumps to 135 degrees again. The result is that the average displacement between vectors is 90 degrees.

There are two very important consequences of having a 90 degree angle between the armature flux and the permanent magnet flux. First, since the torque produced is a function of the coil current, the field flux through the coil and the sine of the angle between the two fluxes, the torque is maximum for a 90-degree angle. Second, the efficiency is maximum for a 90-degree angle. We shall call the angle between the field flux and the rotating flux the torque angle.

TORQUE ANGLE – AC MACHINE

The torque angle is not fixed in the AC machine. The speed of a synchronous machine is fixed by the frequency of the supply voltage, but the torque angle is small for light loads and increases as the load increases. The efficiency, therefore, increases as the load increases. The DC motor is, therefore, generally more efficient and more powerful than the equivalent AC motor. If the AC machine is of the induction or hystersis type, the advantage of the DC motor is even more pronounced.

BACK EMF – AC AND DC MACHINE

We mentioned earlier that there is a back EMF voltage generated in both the AC and DC machines. For the DC machine, the peak of the back EMF wave coincides with the center of the applied square wave. In the AC machine the situation is not nearly so simple. The back EMF has a fixed relationship to the rotor; but since the torque angle is not fixed, the relationship between the impressed square wave and the back EMF will vary. When the torque angle is less than 90 degrees, the rotor is ahead of where it would be for DC operation and the generated voltage leads the applied voltage.

PERFORMANCE – DC MACHINE

In the DC machine the characteristic DC mode of operation is along a straight line speed torque curve as represented in Figure 6. At zero load the speed is maximum, chosen arbitrarily to be 3,000 RPM. When stalled the speed of course, is zero. The straight line curve, therefore, slopes negatively from 3,000 RPM to an arbitrarily selected stall torque of 30 oz-in.

The generated voltage is a function of turns times field flux times speed. Should we turn the rotor (of such a DC machine), in the direction that causes the device to act as a generator, we would find the open circuit voltage at 3,000 RPM to be slightly less than the value of the applied voltage as a motor. For precisely this reason, i.e., the back EMF essentially equals the applied voltage at 3,000 RPM, the no-load motor speed must turn out to be 3,000 RPM. The classical motor equation applied to this discussion is: $V_A = Eg + IR$

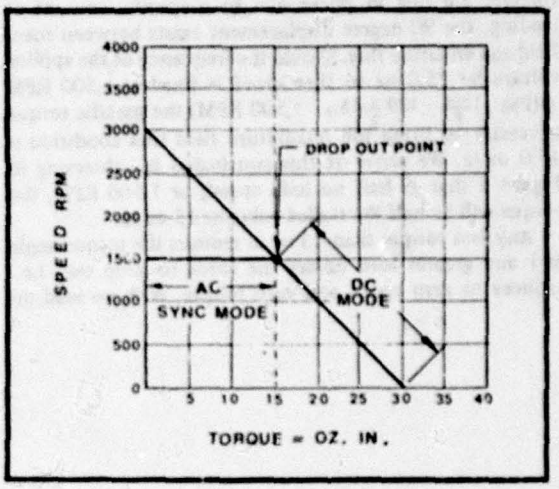


FIGURE 6

At no load, current I is nearly zero. At no load, the sinewave voltage in our illustrated DC machine lies practically on top of the fundamental sinewave of the applied squarewave voltage. It is slightly less in magnitude than the applied voltage at no load as a result of a slight IR voltage drop across the winding. Conversely, it is this slight difference in the two voltages V_A and Eg that causes the flow of no load current in the windings. This voltage difference increases greatly as the generated voltage diminishes -- a result of reduced motor speed as brought about by increased load. Speed and generated voltage are inversely proportional to load. At stall, there is no generated voltage and all applied voltage shows up as IR drop across the winding.

PERFORMANCE – AC MACHINE

In the standard AC machine, speed is not variable, hence the generated voltage magnitude remains constant. The two voltage wave forms, the generated back EMF and the fundamental of the applied voltage, if viewed on an oscilliscope, merely shift from an unaligned condition toward an in-phase condition as the load increases. For an AC motor with the same magnetic characteristics as the DC motor discussed in the previous section, when the voltages are just in phase due to a specific amount of loading, the 90 degree displacement exists between rotor field and armature flux. Should the frequency of the applied voltage be 25.0 hz so that speed is fixed at 1,500 RPM (RPM $= \frac{120f}{P} = \frac{120 \times 25}{2} =$ 1,500 RPM) the specific torque necessary to bring the quadrature field flux condition is 15.0 oz-in. We arrive at this conclusion by observing in Figure 6 that at half no load speed, or 1,500 RPM, the torque will be half the stalled value or 15 oz-in.

Any less torque than 15 oz-in reduces the torque angle and any greater load causes the rotor to drop out, i.e., reduces to zero speed and zero torque. With no load on the rotor other than the no load friction and windage and iron loss torques, the rotor moves to a position somewhere midway between 0 degree and 90 degrees. The changing torque angle is characteristic of the AC synchronous mode of operation. At 90 degree torque angle there is a condition in which operation is both AC synchronous mode as well as DC mode. This is the drop out point in the standard synchronous machine. If operating at this point, the K-I motor is in the DC synchronous mode of operation, and drop out will not occur.

FREQUENCY – AC MACHINE

In the AC machine, speed can be held constant or varied by control of applied frequency. The arrangement from a servo standpoint is simply an open loop servo. It should start to become apparent at this point that if the loop in the AC motor is closed in some manner as to maintain an average 90 degree torque angle, it becomes the same motor as the DC machine. Hence, we should see that the brushless DC motor emerges by closing the servo loop in the AC machine.

SECTION II
THE K-I MOTOR OPERATIONAL CONCEPT DISCUSSION

INTRODUCTION

The theory discussed in Section I of this report will now be used to explain the operation of the Knight-Isaacson (K-I) Motor. To summarize, we showed that an AC synchronous motor could be operated on square waves, that the magnetic field structure of the synchronous motor was similar to that of the DC brush-commutator motor and that a similar back EMF was generated in both machines. We now proceed to show how the K-I Motor uses the synchronous motor structure and electronic controls to produce a DC brushless motor.

The K-I Motor consists of three parts: the electromechanical assembly which is essentially an AC synchronous motor, an electronics package that performs all the low-level sensing and logic functions, and a power module that controls the flow of current to the motor. This section deals with the theory of operation of the K-I Motor and therefore addresses primarily the functions of the electronics package. The hardware implementation of these functions is left for a future report or for discussions with NU-TECH engineers. The functions of the electronics are:

1. **Commutation** - the electronics must sense the back EMF and provide the proper signal to the power module to switch power to the various motor windings as appropriate.
2. **Starting and Speed Control** - the electronics must be capable of starting the motor in the desired direction of rotation and must be able to maintain a constant, selected speed.
3. **DC Synchronous Mode Control** - the electronics must assure that the motor is operating in the DC synchronous mode regardless of changes in load or line voltage.

COMMUTATION

Rotor position sensing. Before commutation can occur, the electronics package must "know" the position of the rotor at certain key points in each revolution. There are numerous devices that could be connected to the shaft of an AC synchronous motor to provide the desired signal. A few of the devices are:

1. Permanent magnet generator
2. Potentimeter
3. Hall device
4. Eddy current device
5. Reluctance device
6. Optical sensor
7. Capacitance device
8. Resolver
9. Radiation device
10. Brush/Slip ring assembly

The first of these, the permanent magnet generator, will be discussed in some detail because this discussion leads most directly to an understanding of the K-I Motor.

Consider a two-phase permanent magnet generator (one that generates two sinewave voltages displaced by 90 degrees) mounted on the shaft of a two-phase synchronous motor. The stator of the permanent magnet generator is positioned circumferentially so that the back EMF voltages of the motor are in phase with the voltages generated by the permanent magnet generator. The stators of the two machines are fixed so as to prevent relative motion. The output from the permanent magnet generator is now directly analogous to the back EMF for both the AC and DC machines discussed in Section I.

The two sinewave voltages from the permanent magnet generator may be modified to obtain the composite wave shown in Figure 4 (repeated, as shown in Section I). You recall that we inverted the negative half cycles of both waves and that the "45° points" were mid way between the zero voltage points. These are the points at which we must switch the proper coil currents on or off to achieve brushless DC operation. If we determine these "45° points", we have the commutation signals required to switch the power transistors.

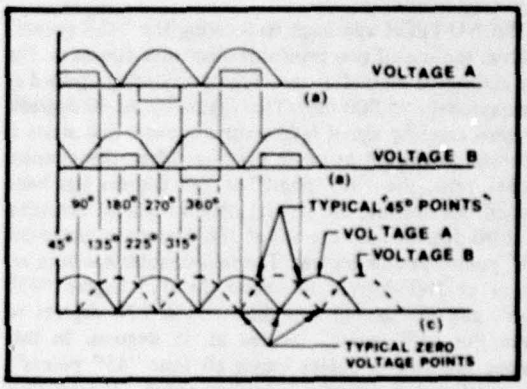


FIGURE 4

An implementation of the power switching function is shown in Figure 7. Each coil lead has two transistors connected to it; one for each direction of current flow. Only one coil conducts at a time so that the on time condition is 90 degrees and at any given time only two transistors are turned on. After these two transistors conduct for 90 degrees, a "45° point" is reached and the two conducting transistors are turned off and two transistors on the other coil are turned on. At the next "45° point" these last two transistors are switched off and the two transistors not used during the first 90 degree period are switched on to cause current to flow "backwards" through the first coil. Similarly, at the next "45° point" current is caused to flow "backwards" through the second coil for 90 degrees to complete the 360 degree cycle.

K-I Motor Commutation. The K-I Motor uses none of the ten transducer concepts listed above. One of the unique features NU-TECH engineers have developed for their motor is a transducerless approach to brushless DC motor operation.

The exact phase relationship between the voltages generated by the permanent magnet generator discussed in the preceeding paragraphs and the back EMF of the synchronous motor was recognized by NU-TECH engineers.

The engineers realized that if they could use the back EMF voltages in a manner similar to that described for the permanent magnet generator, the generator (or any transducer) could be eliminated. This was perhaps the most important single step in the K-I Motor development.

The back EMF is not available to the electronics during the entire cycle. When a coil is energized the applied voltage masks the back EMF voltage. Therefore, even though the back EMF voltage is available from the non-energized coil as shown in Figure 8, the "45° points" cannot be detected directly. A solution to this problem had to be found.

Digital Technique for Commutation. The commutation problem reduces to one of using the information available in the back EMF voltage to generate the switching signals. Note in Figure 8 that some information is available about the back EMF voltage even during the half-cycle the coil is conducting. The wave shapes near the zero voltage points (0°, 90°, 180°, 270°) are not masked. The "45° point" at which commutation must occur rest midway between these zero crossing points.

The NU-TECH approach to locating the "45° points" involves the use of two reversible electronic counters. The first counter is started at zero degrees counting upward at approximately 75,000 hertz (see Figure 8). At 90 degrees, the zero crossing signal reverses the counter and starts it counting downward at twice the rate. When this counter reaches zero, the "45° point" at 135 degrees has been reached. Meanwhile, the second counter started counting up at 90 degrees and reversed at 180 degrees to locate the "45° point" at 225 degrees. The first counter has been restarted at 180 degrees to locate the 315 degree "45° point" and the second counter starts at 270 degrees to locate the "45° point" located at 45 degrees. In this manner the two counters locate all four "45° points". This explanation assumes constant speed. Acceleration and deceleration cause the torque angle to vary slightly from the ideal 90 degree average.

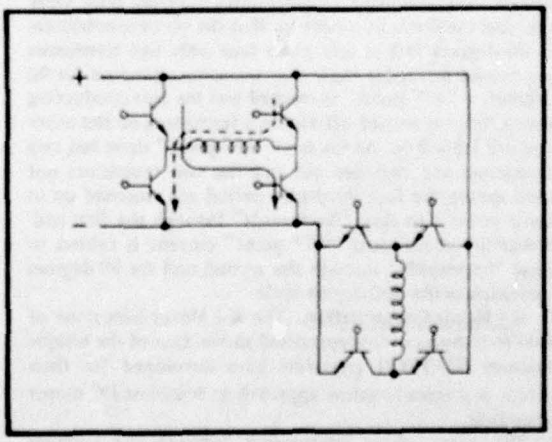


FIGURE 7

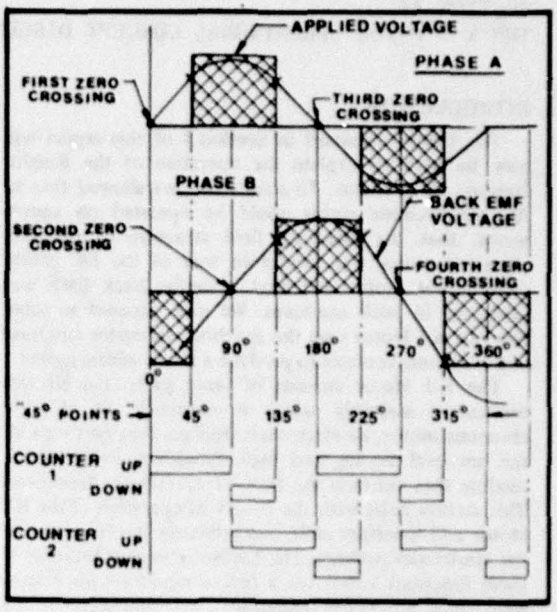


FIGURE 8

Multipole Machines. The entire discussion thus far has addressed two pole machines. The extension to multipole machines is straightforeward. Note that for a four pole machine, 90 electrical degrees correspond to 45 degrees of mechanical rotation of the rotor. However, the entire explanation given above is valid if all arguments are made in electrical degrees. The electronics does not change and any number of poles can be accomodated.

STARTING

There are two problems associated with starting a motor using the NU-TECH concept. First, there is no signal from the rotor position transducer before starting; and second, the motor must always start in the desired direction.

The NU-TECH solution to the first problem is to simply make the K-I Motor a stepping machine. A special clock generates a low frequency (equivalent to about 100 RPM) signal which is used to switch the power module until a sufficient back EMF voltage is generated. The back EMF is usually adequate within a quarter revolution to override the start-up clock, and the clock is effectively removed from the circuit until needed again for start-up.

The second problem, that of assuring proper direction of rotation, arises because of the symmetry of the back EMF voltage and the commutation circuitry used. Without special precautions, the motor would run equally well in either direction once started in that direction.

NU-TECH engineers developed electronic circuitry that allows only one direction of rotation. The signals from the start-up clock are applied to the coil switches in such a sequence as to ensure that the motor runs in the desired direction. Reversing the motor is a simple matter of changing that start-up sequence and is accomplished with

low-level signals. Another way of looking at start-up is to think of the clock as one that controls commutation at all speeds. This master control clock assures proper direction of rotation by sequencing the coil switches, runs at a speed proportional to the frequency of the commutating signal and has some minimum speed below which it cannot go.

SPEED CONTROL

The K-I Motor does incorporate a control clock as described above. It is a simple matter to fix an upper frequency for the clock which has the effect of causing the motor to not exceed the corresponding speed. As the frequency of the back EMF signal attempts to exceed the maximum clock rate, the rotor merely moves closer to the rotating flux. At this point the motor is operating at a lesser torque angle. It is functioning as a synchronous AC machine would if the load were suddenly reduced. This is a method in itself of maintaining constant speed, but because of its inherent inefficiency is not the K-I approach to speed control.

The operation of a typical machine is shown graphically in Figure 9. The motor starts with 30 oz. in. of torque and accelerates along the negatively sloped DC speed/torque curve until the top speed is reached. In this case the top speed is 1500 RPM and for any torque less than 15 oz. in. the motor will operate along the horizontal 1500 RPM line. For the AC synchronous machine, moving to the left along the constant speed line corresponds to a decreasing of the torque angle. The clock's top limit is easily adjustable so that programming motor speed is quite simple. If used this way, the motor would operate as a variable frequency synchronous motor until the maximum torque it could supply at any given speed would be exceeded, and then it would become a DC motor operating in the DC mode along the sloped curve.

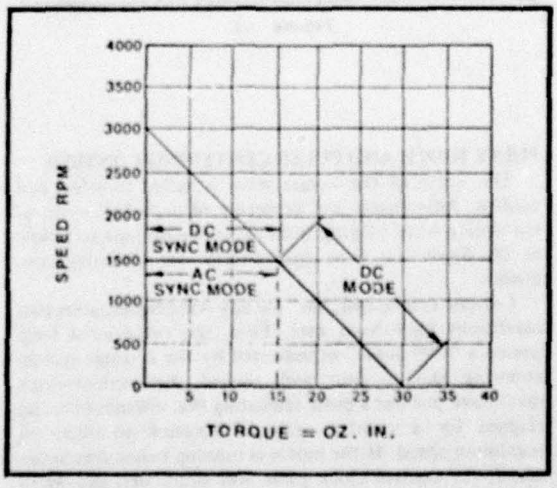


FIGURE 9

DC SYNCHRONOUS MODE OPERATION

The motor we have described so far is a completely functional hybrid machine. It operates as a DC motor during acceleration and as an AC synchronous motor at a constant preselected maximum speed. To show how the K-I Motor achieves its DC synchronous mode of operation (90 degree torque angle) throughout its operating regime, shown in Figure 9, consider the operation of our hybrid motor at varying applied voltage.

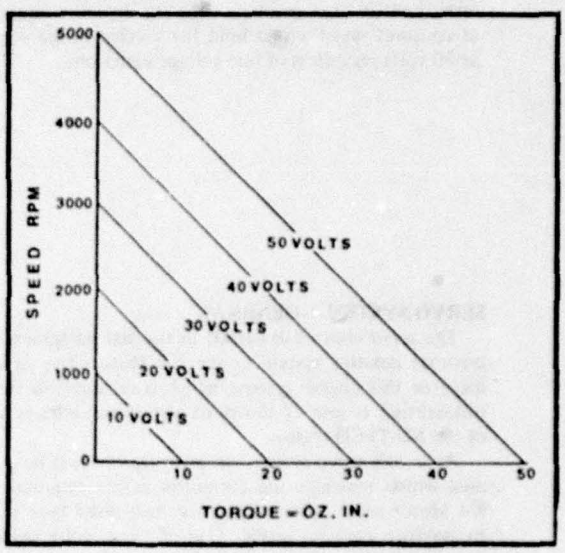


FIGURE 10

Changing the voltage applied to a DC motor with fixed field intensity simply causes it to operate along another constant slope speed/torque curve as shown in Figure 10. We have illustrated a motor that would produce 30 oz. in. of torque at stall and have a no-load speed of 3,000 RPM if operated at 30 volts. If we now reduce the voltage to 20 volts, the motor would have a stall torque of 20 oz. in. and a no-load speed of 2,000 RPM. Our hybrid motor would operate along this set of parallel curves until it reached the maximum speed set by the control clock.

Consider the case of the hybrid motor operating on 30 volts at a constant speed of 1500 RPM (see Figure 11). Suppose the torque required is reduced to 5 oz. in. The motor is now operating at a very low and inefficient torque angle. We can bring the average torque angle back to 90 degrees by reducing the voltage to 20 volts. If the torque required should now go back up to the original 15 oz. in., the speed of the motor would drop to 500 RPM and it would be necessary to increase the voltage to 30 volts to return the speed to 1500 RPM at which point we are again operating with the desired 90 degree torque angle.

We have just described what effectively happens in the K-I Motor. The voltage is varied through a servo control so that speed variations are kept to an absolute minimum while the motor operates very close to the drop out point

which is the intersection of the constant speed line and the appropriate DC speed/torque curve. The K-I Motor in its DC synchronous mode operates, therefore, at an average torque angle of 90 degrees at all times.

Consider the case of line voltage change while the motor is operating at constant torque. If the supply voltage drops, the speed of the uncontrolled motor would also drop. To illustrate, if the motor described by Figure 11 were operating at 1,500 RPM and 15 oz. in. of torque and the voltage dropped to 20 volts, the speed would drop to 500 RPM. In the K-I Motor, the same voltage servo control that maintains the 90 degree torque angle at constant speed would hold the voltage to the windings at 30 volts regardless of line voltage variations.

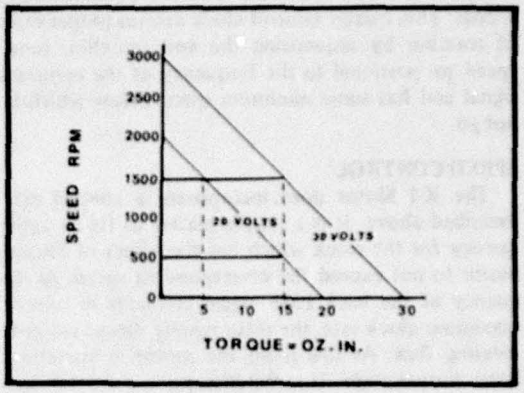


FIGURE 11

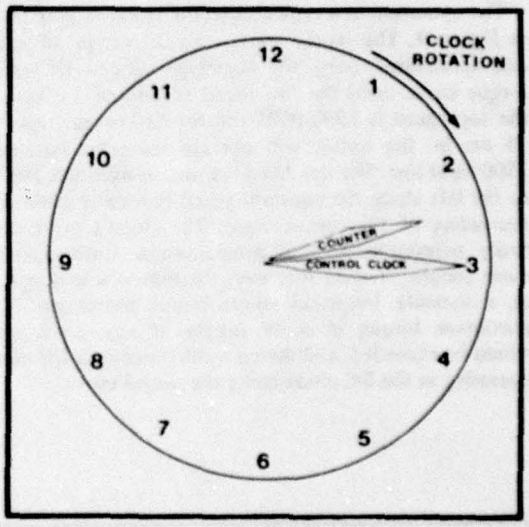


FIGURE 12

SERVO SYSTEM – GENERAL

The servo control described in the last paragraph is an intricate counter system in the K-I Motor. The development of this digital system, which is reliable and free of instabilities, is one of the most significant achievements of the NU-TECH team.

As in any servo system, an error signal must be generated which indicates the corrective action required. The K-I Motor servo system compares two pulse type signals to produce an error signal. One of these pulse signals is the constant frequency upper limit output from the control clock that consists of one pulse every quarter cycle. The other pulse type signal derived from the counter system also produces a pulse every quarter cycle.

The generation of the error signal may be visualized by considering a clock face as shown in Figure 12. Suppose the pulses from the control clock and the counter occur precisely at 3:00, 6:00, 9:00 and 12:00 o'clock. If at 3:00 o'clock the counter pulse, due to a sudden increase in load, is behind the control clock pulse as shown in Figure 12, the servo system raises the voltage to cause the rotor to catch up. If the counter pulse is ahead of the control clock pulse due to a sudden reduction in load, the voltage is decreased to cause the rotor to slow down. If the two pulse trains are exactly in step, there has been no change in loading and no error signal is generated and the voltage is maintained constant.

Line voltage changes are compensated for in exactly the same way. If the line voltage increases, the rotor speeds up and the counter pulse gets ahead of the clock pulse. The resulting error signal causes the servo to lower the voltage and return the rotor speed to its present value.

There are two means by which voltage is controlled. One, for rapid response is the width of the square wave and the other for greater range in either load, line voltage, speed or all three, is the square wave amplitude. The latter is not often required, since pulse width control provides ample variation for most applications.

PULSE WIDTH AND PULSE CENTERING CONTROL

The width of the square wave is varied to effect fast control. Adjustment and centering of each half cycle of the square wave ranging from 90 degree on time to as low as 20 degree on time compensates for changing conditions.

Current is switched "on" for any winding only after two conditions have been met. First, the rotor must have passed a "45° point" as indicated by the counter system counting back to zero; and, second, the control clock must have put out a pulse indicating that enough time has elapsed for a quarter cycle of rotation to occur at maximum speed. If the motor is running below maximum speed, the control clock pulse will occur first and when

the counter system reaches zero at a "45° point", current will be switched on to the appropriate coil. For this set of conditions, current is switched off for one coil when it is switched on for the other; the condition is that of 90 degree on time and the result is the DC mode of operation.

Now consider the condition, shown in Figure 13, wherein the motor is tending to run faster than the selected maximum speed either because the load was reduced or the line voltage suddenly increased. The counter system will indicate the passage of a "45° point" before the control clock puts out its quarter cycle pulse. The current will not be turned on until after the "45° point" has passed. The K-I Motor control logic measures the time T_1 from turn on until the next zero crossing is reached and then an equal time later T_2 turns power off. Thus the power pulse is centered about the mid point of the back EMF voltage. This arrangement results in an on-time condition of less than 90 degrees. Hence there is a period of time Δt about the "45° point" when neither coil is conducting current. The net effect of the control is a very rapid responses to load changes so that speed is maintained at the predetermined level.

AMPLITUDE CONTROL

The amplitude of the square wave voltage may be changed to improve speed control. If load and voltage changes are so great that varying the width of the square wave between 20 degrees and 90 degrees will not maintain constant speed, amplitude control may be employed. If the on-time of the square wave approaches 90 degrees, the control system increases the amplitude of the wave incrementally to maintain an on-time of slightly less than 90 degrees. Conversely, as the square wave width approaches some preselected lower limit, such as 20 degrees, the amplitude control causes an incramental decrease of amplitude. In this way, constant speed control can be provided over a wide range of load and voltage variations. At all times the pulse width control is providing rapid response to load and voltage changes. It should be noted here that for applications with limited speed and load variations, amplitude control may not be required.

SUMMARY

The K-I Motor starts, accelerates to a preselected maximum speed and operates at that speed regardless of voltage or load changes with the 90 degree torque angle characteristic of the DC motor. If the load exceeds the maximum the motor is capable of, the K-I Motor will decelerate along a linear speed-torque curve.

This operation is achieved by applying carefully controlled and regulated square waves to the phases of a synchronous machine. Typical waveforms are shown in Figure 13. The amplitude of the waves and the turn-on and turn-off points are automatically controlled by the K-I Motor to give optimum performance. Note that the square waves are centered on the 90 degree, 180 degree, 270 degree and 360 degree lines, mid points of the back EMF voltages, to assure a 90 degree torque angle.

The solid state logic that provides the desired square wave employs digital techniques to provide accuracy and assure reliability. A reversible counter started by the zero crossing of the back EMF of the motor locates the "45° points" and a master clock provides a reference so that the control logic can detect and correct for small changes in speed caused by changes in load or line voltage.

As an example of the versatility afforded by the K-I Motor, consider an application that requires many random changes in torque and yet requires constant speed operation. Instead of grossly over-sizing the motor or adding inertia in the form of a flywheel as would now be required, the K-I Motor would simply be designed with a Δt as defined by Figure 13, that could accomodate the load changes. The torque would effectively be adjusted to meet the demand every quarter cycle with the sacrifice of a little efficiency. This example is cited only to illustrate the extreme versatility of the K-I Motor.

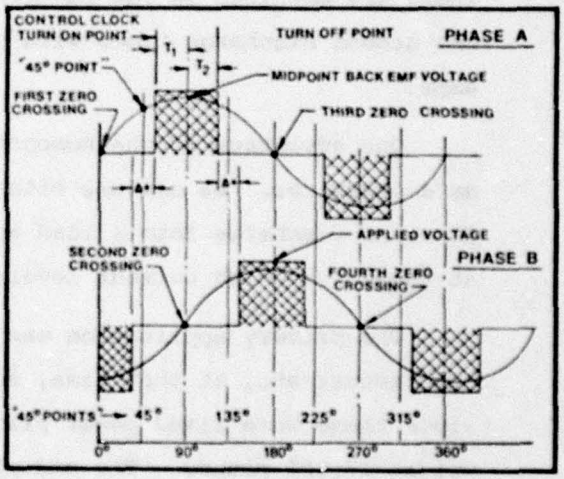


FIGURE 13

CONCLUSIONS

The K-I Motor employs advanced solid state sensing and logic technology to control the switching of DC power to an AC synchronous machine. The result is a motor with unprecendented flexibility. With only minor control system changes, a single unit can be operated as a DC motor, a stepper motor, or a speed programmed electromechanical control unit. Almost any speed-torque curve beneath the straight-line DC curve can be attained. The development of this unique motor is now complete and many laboratory demonstrations have proven the concept. The next step is production.

PULSED HOMOPOLAR GENERATOR RESEARCH

at The University of Texas at Austin

William F. Weldon

Center for Electromechanics

In 1972, the magnetic fusion community identified pulsed power supplies as a critical research issue. From a $100 million fusion budget, $62 million was proposed for power supplies. We could not afford to build experiments -- we couldn't even build power supplies for all the experiments. Among the ideas suggested was a national power supply for fusion experiments.

The Center for Electromechanics (CEM) at The University of Texas at Austin concentrated its efforts toward slow discharging homopolar machines. These are machines in the hundreds of megawatt to gigawatt power level, one second discharge times with output current ranging from 0.5-3 million amps.

One advantage of the homopolar system is that it models electrically as a capacitor. We can use either a critically, or slightly over-damped RC or LC discharge into a load and no interrupting switches are required. At these very high current levels, that is most desirable.

The primary application was charging large magnets for fusion experiments and, at that time, no real emphasis was placed on weight since these were fixed power plant type installations. The 5 MJ system weighs 17,000 pounds. The end plates of the stator are six-inch thick plates. We left the corners on them to act as legs for the generator. Strong emphasis was placed on cost, however. After reviewing several systems (systems in use as well as potential systems), it was apparent that flywheel energy storage was potentially the most economical for long-range pulsed power applications. However, the conventional motor-generator-flywheel sets in use at that time were unattractive. If an alternator was used, varying frequency during the discharge resulted in inefficiencies in the rectifier-transformer system. With the dc system the commutation problem at very high current levels is difficult. Consequently, homopolar conversion is very attractive. The flywheel is

actually the rotor of the homopolar generator and inertial energy stored in the flywheel is converted directly to electric power.

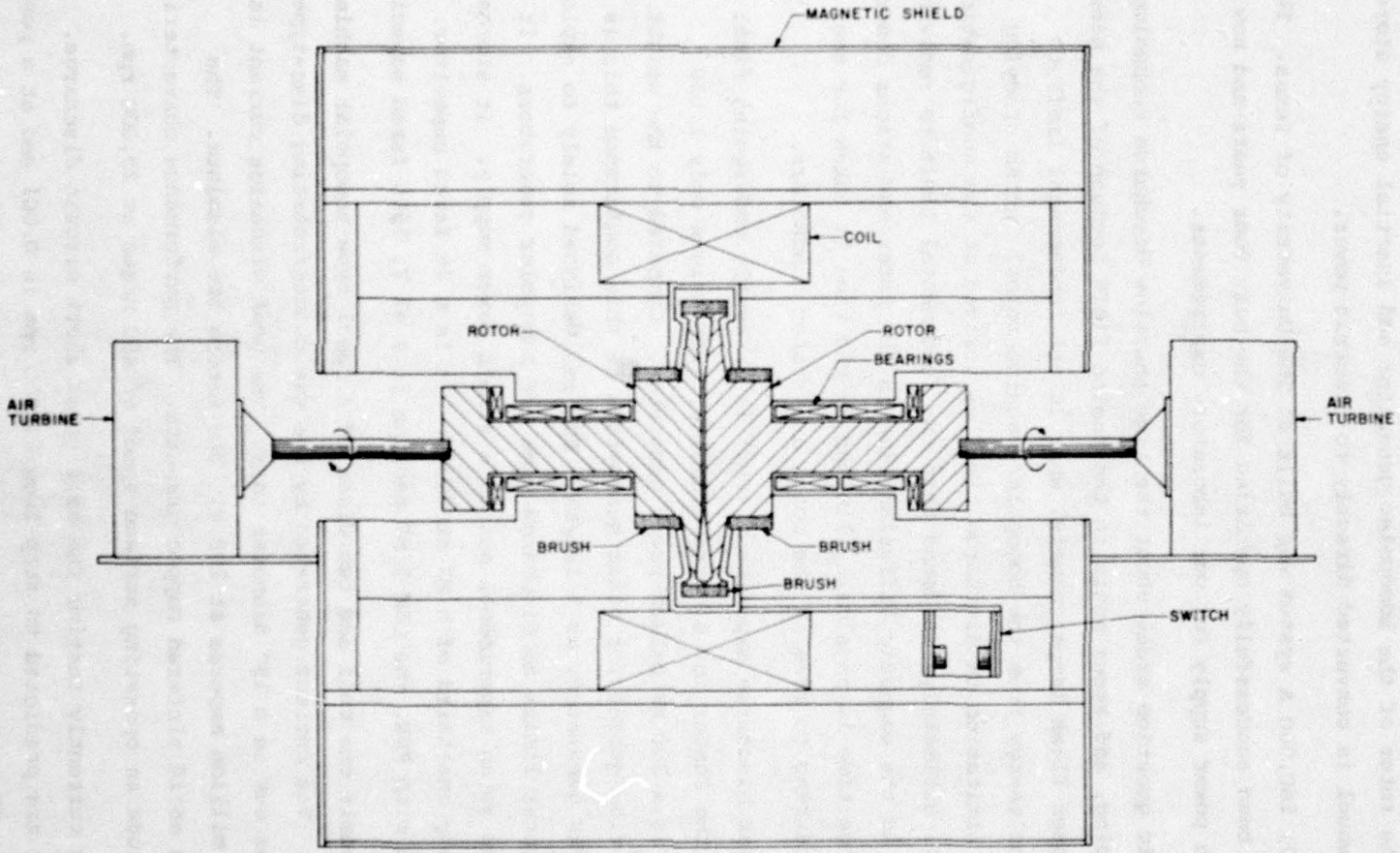
A 5 MJ, 560,000 A system was built at The University of Texas. The system has been successfully operating for the past four years and now acts as the power supply for our laboratory experiments.

A basic question arose about the time the slow discharge technology was developing, and arose again in the fusion field because of the need to power laser flash lamps; namely, what is the fundamental limit to removing the energy from the homopolar machine rotor? After studying the stress limitation on discharge time, we arrived at the configuration in Figure 1. Ultimately, we found that the fundamental limit to removing the energy is the magnetic diffusion time in the rotor and stator conductors. The discharge time is physically limited by the time it takes for the discharge current to rise in the rotor and stator conductors.

The Fast Discharge Experiment (FDX) is currently undergoing final testing at the Centor for Electromechanics. FDX weighs only 1,000 pounds and is a 200 MW pulsed power generator. Compared to the weight to power ratios quoted for other generators at this conference this is a 0.005 lb/kW generator, or 5 lbs/MW. FDX was designed solely to explore the fundamental limits to discharge time for homopolar generators. It was designed as an experiment, not as a viable power supply. It stores approximately one-third of a MJ at 208 V. It is a 16 farad capacitor. As compared with FDX, the CEM 5 MJ machine is a 42 V, 5500 farad capacitor.

FDX models one coil and two discs of a spool type homopolar machine (Figure 2). The current generated by the two counterrotating disc-type rotors comes out in a 15" diameter coax. The peak discharge current is almost two million amperes at 208 V. The rotors are aluminum. The brushes are solid sintered copper graphite. The performance characteristics of FDX include an operating surface speed of 450 m/sec at 28,000 rpm.

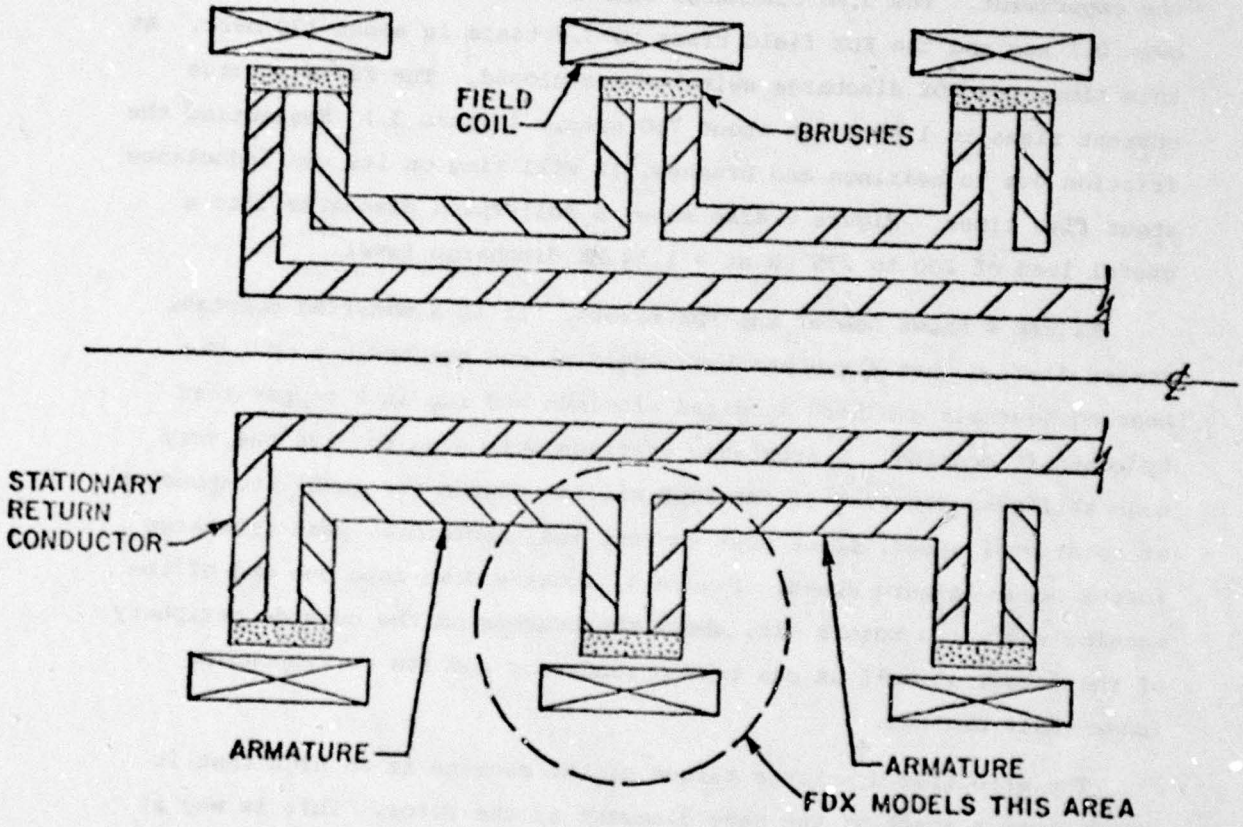
CEM is currently testing the half-speed short circuit discharge. Both rotors are predicted to stop from 14,000 rpm in 0.001 sec at a peak current of 1.88 MA. In the second millisecond, the rotors reverse to 80% of their speed, i.e. the machine is of low enough capacity so that



FDX HOMOPOLAR MACHINE

CROSS SECTION

Figure 1



SPOOL TYPE HOMOPOLAR GENERATOR

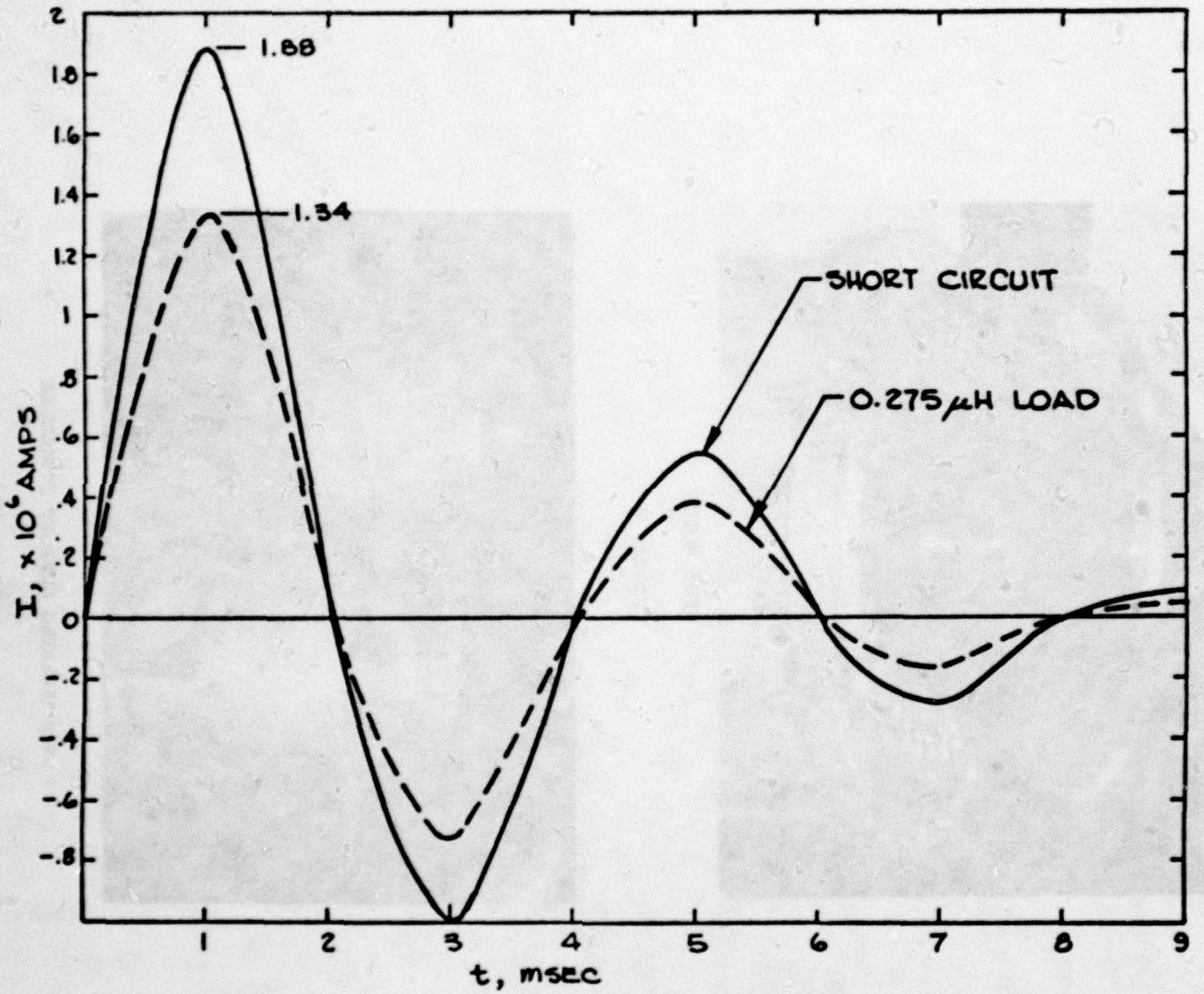
Figure 2

it rings on its own internal inductance. To operate at this power level, the machine requires a high pulsed magnetic field. This pulsed field is provided by the CEM 5 MJ homopolar generator. For portable applications, a superconducting coil would be required, but the room temperature coil was chosen for FDX to keep the costs low and to expedite the experiment. The 5 MJ discharge current rises to 360 kA in a little over 0.1 sec and the FDX field rises to 3.7 tesla in about 170 msec. At this time, the FDX discharge switches are closed. The FDX discharge current rises to 1.88 MA in about 750 μsec. (Figure 3.) Neglecting the friction due to bearings and brushes, it will ring on its own inductance about five times. Figure 3 also shows a full-speed discharge into a useful load of 200 to 275 μH at a 1.34 MA discharge level.

Figure 4 shows one of the FDX rotors. It is a modified constant stress disc in that a rim has been added to run the brushes on. The bearing journals are hard anodized aluminum and run in a copper lead hydrostatic bearing. Hydrostatic bearings were used to give the very high stiffness required (about four million pounds per inch) independent of rotational speed, since peak current and, therefore, peak discharge forces occur at zero speed. Figure 5, looking down into one end of the machine where the rotors fit, shows the brushes on the outside periphery of the rotor, as well as one return conductor and its corresponding inner shaft brushes.

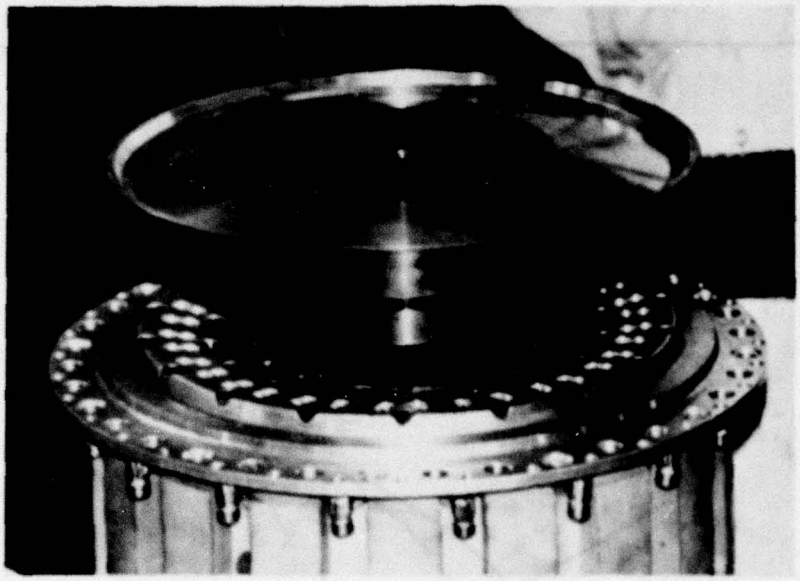
The effective discharge torque of the machine is so high that it would shear a shaft of the same diameter as the rotor. This is why it is impossible to use motor-generator-flywheels at these power levels. Since we actually stop the rotors with body forces ($\bar{J} \times \bar{B}$ forces in the rotor material) the peak stress during discharge is only about 2,000 psi.

The bearing support structure (Figure 5) is non-magnetic G-10 epoxy-glasscloth laminate, but it maintains an overall stiffness of about three million pounds per inch at the bearing. Since the two million amp current rises in about 700 μsec, doubts concerning the ability to close a switch uniformly around the discharge coax lead to



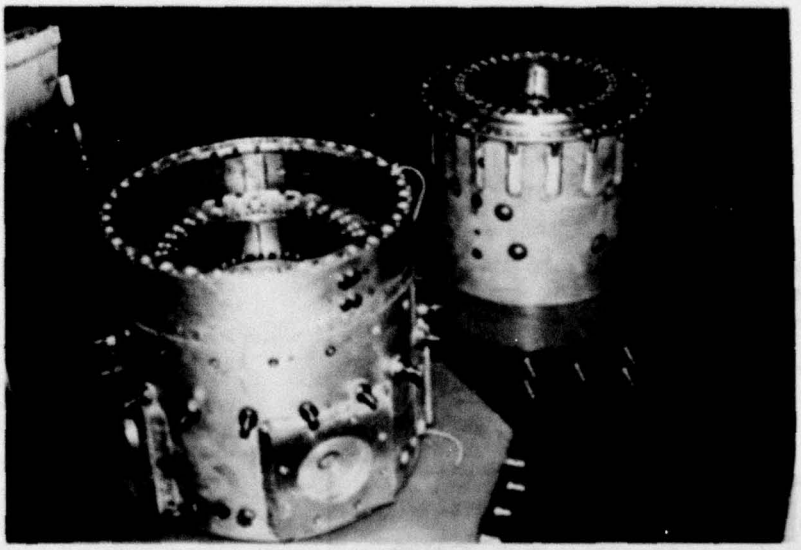
FDX OUTPUT CURRENT.

Figure 3



FDX ROTOR

Figure 4

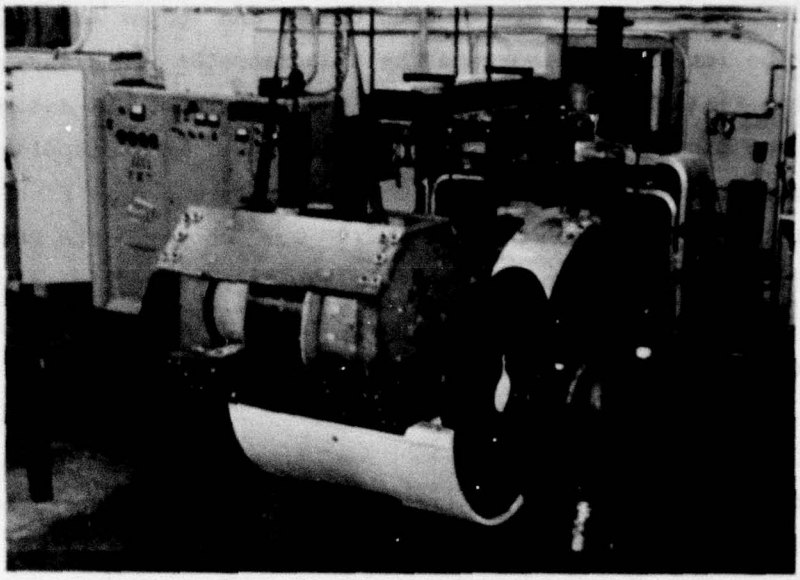


FDX BEARING SUPPORT STRUCTURE

Figure 5

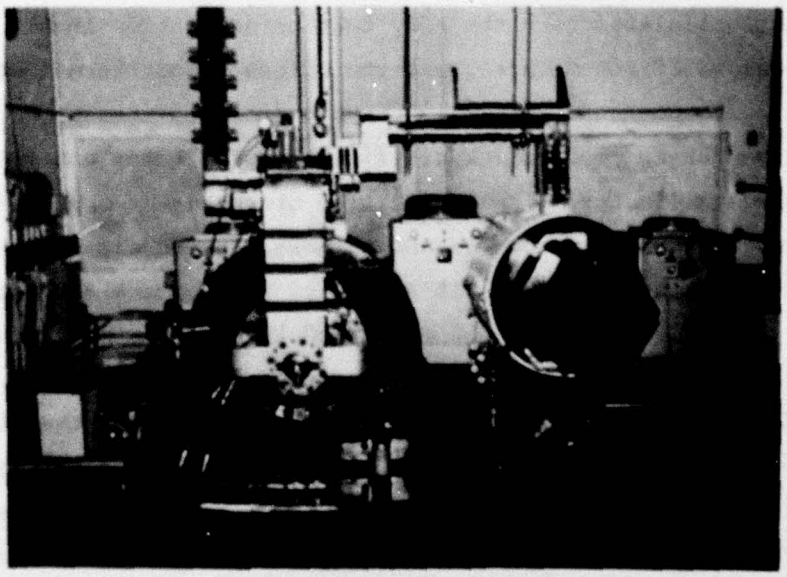
the development of four very fast-acting switches equally spaced around the coax. These switches are on stub coaxes and longer transmission lines can be inserted to increase the inductance of the discharge circuit to simulate realistic loads. Figure 6 is a picture of FDX assembled in place in the magnetic shield. The 5 MJ generator, which supplies 360,000 A of pulsed power to the FDX field coil, is also shown in Figure 7. It is a four-turn coil, edge-wound of 1-1/2" x 3" copper. The magnetic pressure in the coil is approximately 1,500 psi. There is an epoxy-graphite filament wrap on the coil to sustain the magnetic pressure. The prime movers for the rotors are air turbines. With a superconducting magnetic field, the rotors could self motor. They could also be driven with any other kind of prime mover. The air turbines are attractive in an aircraft application because they could possibly be run on bleed air from the turbines.

In support of the homopolar projects, the Center for Electromechanics has expanded its research efforts into several other areas. Since CEM was running a pulsed magnetic field of very high field level with a fast rise time, we developed a nonlinear, transient magnetic field-mapping program that calculates both the eddy current generation in all the metal components of the machine, and the stresses and thermal effects on these machine components. CEM also has a controlled atmosphere brush tester for measuring coefficient of friction, wear rates and voltage drop for sliding electrical contacts. The brush tester operates at pressures up to three atmospheres and has been run in air, carbon dioxide and hydrogen. It has controllable pressure, temperature and relative humidity. It will operate at 450 m/sec and 10,000 A/in.^{2}. With the 5 MJ machine, we have operated the brushes at 15,000 A/in.^{2} for 0.7 sec pulses. The FDX machine will operate at 45,000 A/in.^{2} on the sliding contacts for one msec pulses. CEM frictional heating models that correlate with the 5 MJ and brush tester data predict the temperature rise at the brush interface to be about 146°F. Another use for the 5 MJ generator, which is becoming quite an attractive research program, is in welding applications. Conventional resistance welding power supplies are limited to 100,000 A. It takes about 50,000 A/in.^{2} to resistance weld steel.



FDX ASSEMBLED IN SHIELD

Figure 6



FDX AND 5 MJ

Figure 7

We are now welding large pipe sections and have designed machines large enough to weld pipe like that used in the construction of the Alaskan pipeline. Welding time would be a few seconds as opposed to about four hours presently.

THE SEGMENTED MAGNET (SEGMAG) MACHINE DEVELOPMENT PROGRAM

Dr. D. L. Greene
Westinghouse R&D Center

For sometime now, Westinghouse has had a program sponsored by the Office of Naval Research to develop light-weight, low volume, and low cost electric machinery. Specific applications under investigation have included ship propulsion. This program has as its objective a demonstration of the technology required to achieve high power density to the forty thousand horsepower level by 1979. The program is designated the SEGMENTED MAGNET (SEGMAG) Machine Program. The basic concept of these machines incorporates three technologies which are novel to propulsion machines. First, the machines are water cooled to increase power density. Second, the current collection portion of the machine operates at a very high current density by conventional standards, using liquid metals or solid brushes. Finally, by proper selection of the electromagnetic geometry, the size and weight of the machines is reduced.

The program was initiated with a configuration similar to a simple drum-type homopolar machine. Later, the designs were segmented to provide machines with modular construction. These machines are characterized by rotor conductors rotating in a radial field. The flux path is shown in Figure 1 by the dotted line. Current collection is accomplished at the ends of the rotor conductor. There is a compensating stator winding for control of armature reaction and to provide a return path for series connection of the modules. The two module machine of Figure 1, for example, has six current collection sites.

One of the first objectives in the program was to build a machine of this modular type at the three thousand horsepower level. The machine in Figure 2 was constructed with liquid metal current collectors, and the machine was tested successfully in 1975. It was felt that, in order to

have satisfactory machines of this type, the voltage rating must be high enough to make them more attractive for a system application. To increase voltage, investigation of the compounding of turns on the rotor was initiated. This was accomplished with series and parallel connection of circuits. Current is taken off the rotor by brushes and passed to the next electromagnetic turn many times around the machine. This yields several steps of increasing voltage. In order to make this type machine sufficiently power dense, it is still necessary to operate at a very high current, because even with this voltage compounding, the voltages are lower than achieved in conventional dc machines. In order to achieve a practical machine, the brushes used must be very high current density solid brushes, instead of liquid metal, since switching current from one bar to the next requires a solid, rather than liquid, contact.

The program has, as its technological centerpiece, the development of these high current density solid brushes. In the first application, we are designing and constructing a three thousand horsepower motor and generator for tests. Additionally, preliminary design studies for a forty thousand horsepower ship system have been undertaken. The detailed design of a three-thousand-horse-power, twin-drive system is also in progress. This drive system will use four machines and demonstrate the interaction of two, interconnectable propulsion trains in a laboratory setting, similar to the diagram of Figure 3.

This particular program offers an extremely attractive option for the Navy of the future. Westinghouse has worked extensively with superconducting machinery, and it is apparent that such equipment certainly is an attractive alternative for ultra-lightweight applications, where the high cost can be justified. Segmented magnet machines with water cooling will offer substantial promise where cost prohibitions exist, but where lightweight machinery is sought. Superconducting machinery, for example, appears favorable for surface effect ships, while SEGMAG machines will be appropriate for displacement ships, submarines, and heavy vehicle drives.

The baseline application under analysis is a displacement hull which has a twin screw system. It is nominally a two thousand volt,

fifteen thousand ampere system. The generator has been rated at thirty-two thousand horsepower, and since it is gas turbine driven, it is unidirectional. The forty thousand horsepower motor must be capable of regeneration and reverse operation. It operates at 168 rpm. For this requirement, the typical motor characteristics are shown in Figure 4. A forty thousand horsepower machine is in the 120- to 150-thousand pound class. The efficiency at full load is about 97 percent. Part-load efficiency is about 96 to 97% at the ship's established cruise condition. Of interest in this kind of a machine is the amount of brush surface area that is required. On the motor, it is approximately 810 square inches. The number of circuits represent the number of turn amplifications. There are four segments with three circuits per segment in the generator, providing twelve voltage amplifications. The weight of the generator is about 17 to 24 thousand pounds or about one-and-a-half to two horsepower per pound. The generator has a full load efficiency of about 98 to 99%, and the size of the brush area in this machine is about 192 square inches.

The three thousand horsepower machines, presently in detailed design, are five hundred volt machines, and the generator operates at 3600 rpm. This is a five thousand ampere machine operating at thirty-six hundred rpm at a rated efficiency of about 97%. The motor will be a twelve hundred rpm machine with a rated efficiency of about 96%. When construction of these two, and an additional two machines, is completed, they will be incorporated in a laboratory test system, incorporating a control system, load devices, prime movers, and the four machines. Demonstrations of parallel operation, reversing, and various maneuvers and configurations of the machines will be accomplished.

There are four major development areas in this program. First, there is the development of high current density, solid brushes. Second, because current is switched from one bar to the next, a phenomenon not unlike that in a commutator, and the ability to predict and control the amount of reactive voltage which is present during switching is important. The final two areas are, perhaps, more engineering than development, but it is necessary to use an air gap winding, which must be held on the rotor at very high tip speeds. It must also be a stranded and transposed conductor

with a very high packing density to reduce eddy current losses. At the same time, the rotor conductors are water cooled. Because the current density of the brushes is so high, the heat from the brushes must be removed, and they must be applied in a carefully controlled load pattern.

In a program jointly sponsored by DARPA and ONR, a good deal of long duration brush tests have been run at about one-and-a-half meg/amps per square meter. This is the equivalent of about a thousand amps per square inch. Previous screening tests with brushes at fairly low speeds have been in the range of 2500 amps per square inch. In a long-term project with DARPA, the goal is about five thousand amps per square inch. It is expected that this goal can be met with a multi-element brush. The brushes that will go into machines at this time are monolithic, however. The 3000 hp machines are designed with brushes having a thousand ampere per square inch current collection capability.

In the brush testing program, two high speed, high current density brush test rigs have been built. The rig shown in Figure 5 operates at a brush sliding speed of fourteen thousand feet per minute. Figure 6 shows a brush holder which is fully instrumented to measure the voltage drop and the dynamics of the brush. Figure 7 is the second brush test machine. Both of these rigs have water cooling directly under the slip ring surface to control the temperature at the interface. The brush test rig of Figure 7 is capable of testing four rows of brushes. It is virtually a drum-type homopolar machine with a very high current capacity, capable of testing brushes at two thousand amps per square inch. It is chiefly employed for testing the load sharing of a multiplicity of brushes around the ring. Twenty-four brushes can be applied per ring in this machine.

Operations have started with a machine constructed to demonstrate the current switching phenomenon and verify analytic models in this area. A conventional dc machine was modified and fully instrumented as a test vehicle for current switching.

Major program milestones include complete machine construction of the first two-three thousand horsepower machines in 1979 and complete system tests in 1980.

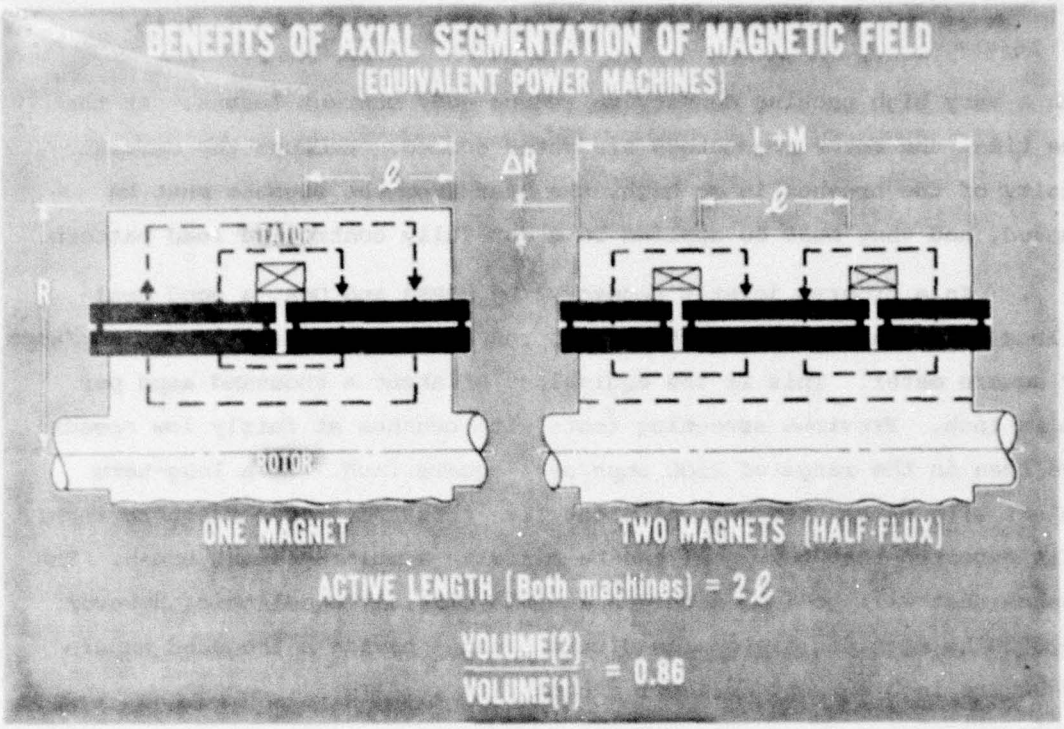


FIGURE 1

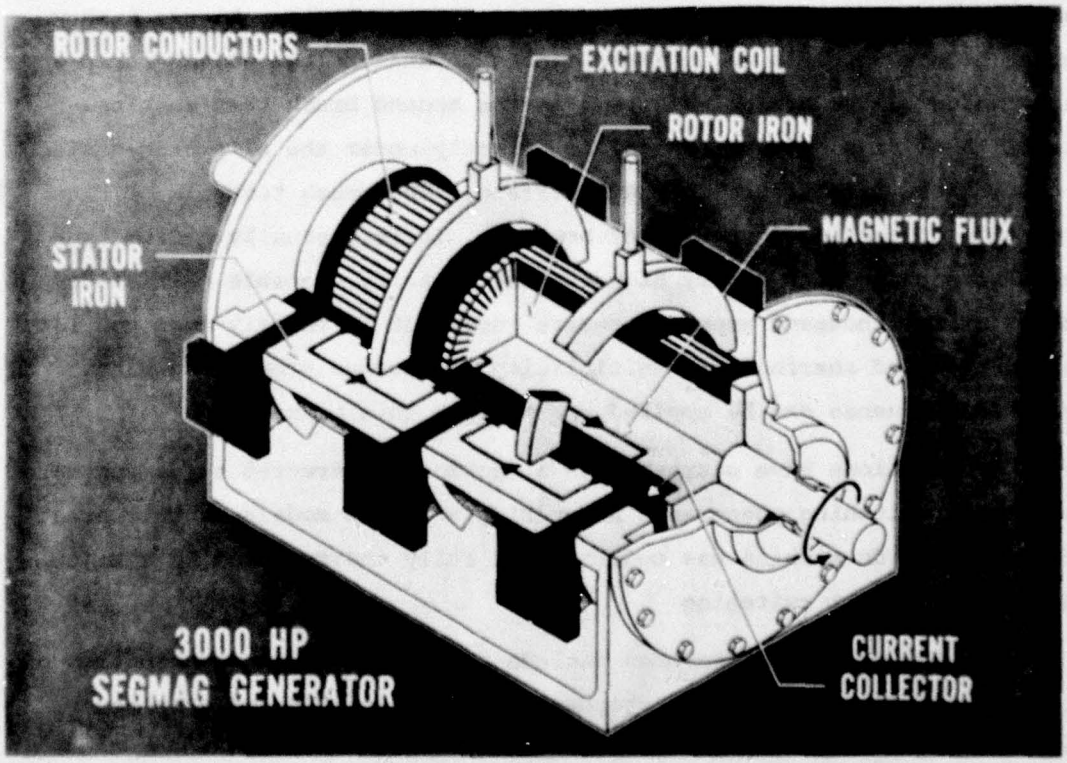


FIGURE 2

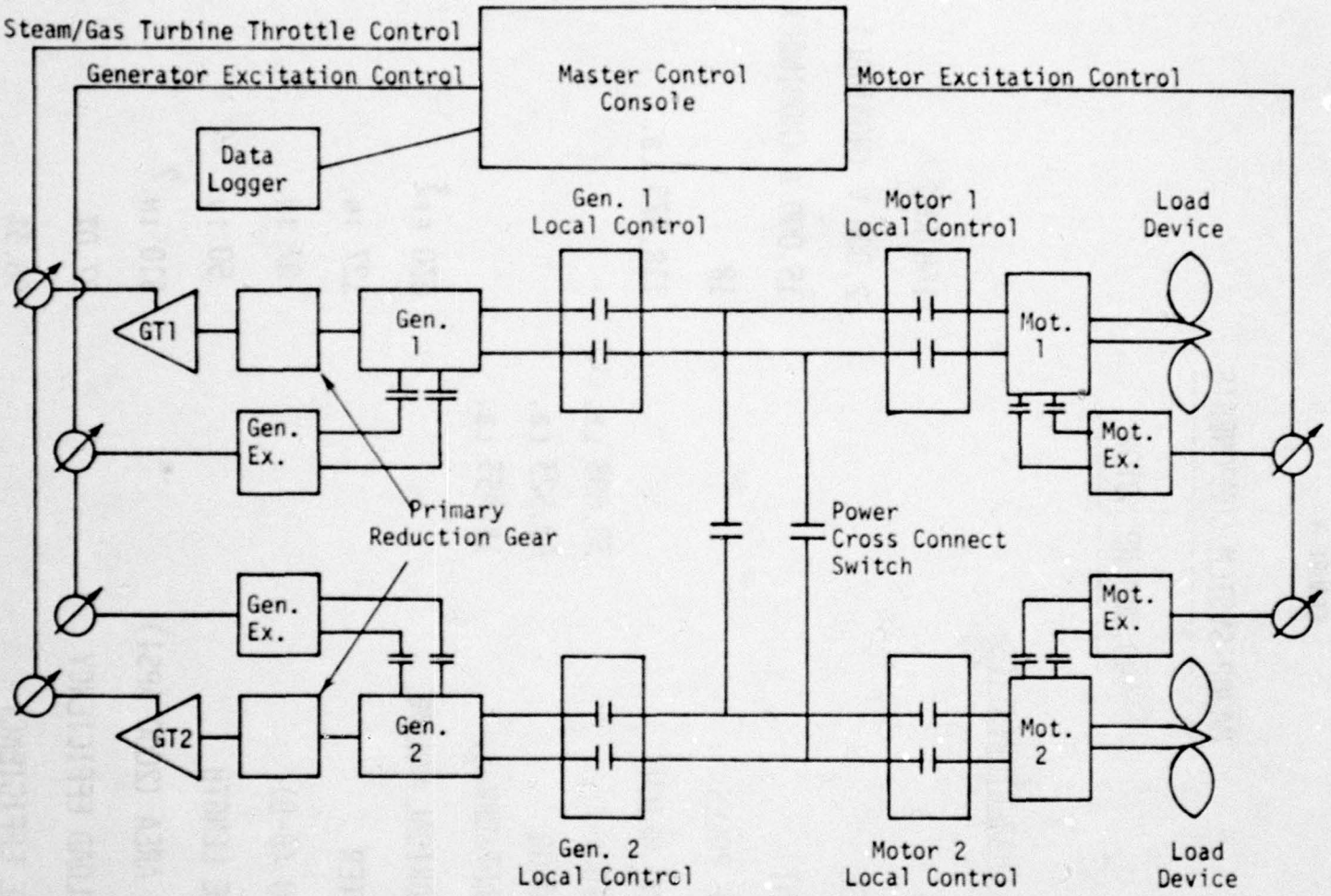


FIGURE 3. 3000 hp/shaft test system.

FIGURE 4

MAJOR SYSTEM COMPONENTS

40,000 HP MOTOR

PRINCIPAL CHARACTERISTICS:

SPEED		168 RPM
VOLTAGE		2,000 V (NOMINAL)
CURRENT		15,000 A (NOMINAL)
NO. OF POLES		18
MACHINE WEIGHT		118,675 LB.
ROTOR	39,698 LB.	
STATOR	60,523 LB.	
SHAFT/BRNGS.	18,453 LB.	
CYLINDRICAL VOLUME		630 FT^3
DIAMETER		127 IN.
LENGTH (B-B)		87 IN.
ACTIVE LENGTH		50 IN.
BRUSH AREA (2000 APSI)		810 $IN.^2$
FULL LOAD EFFICIENCY		97.0%
CRUISE EFFICIENCY		96.3%

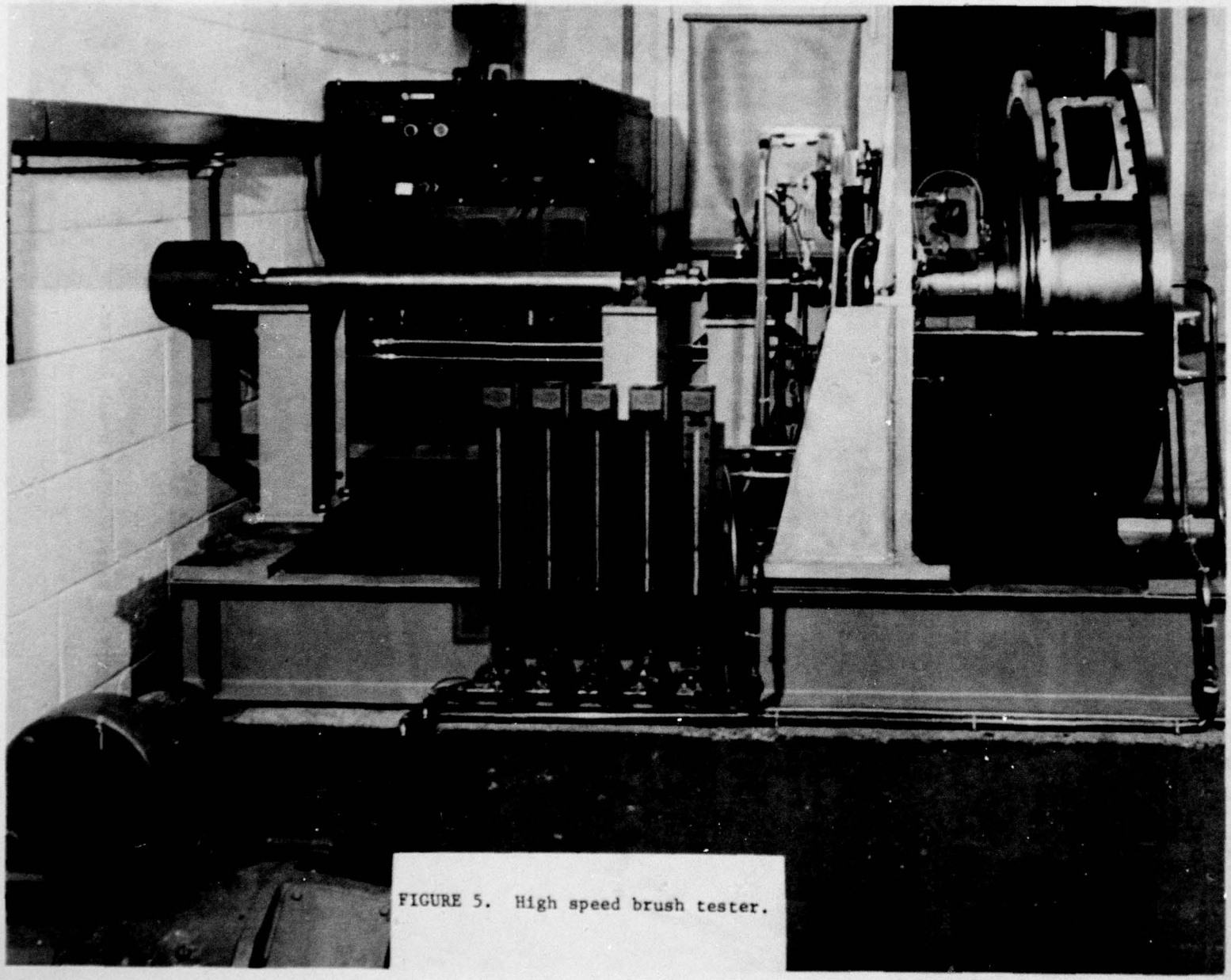


FIGURE 5. High speed brush tester.

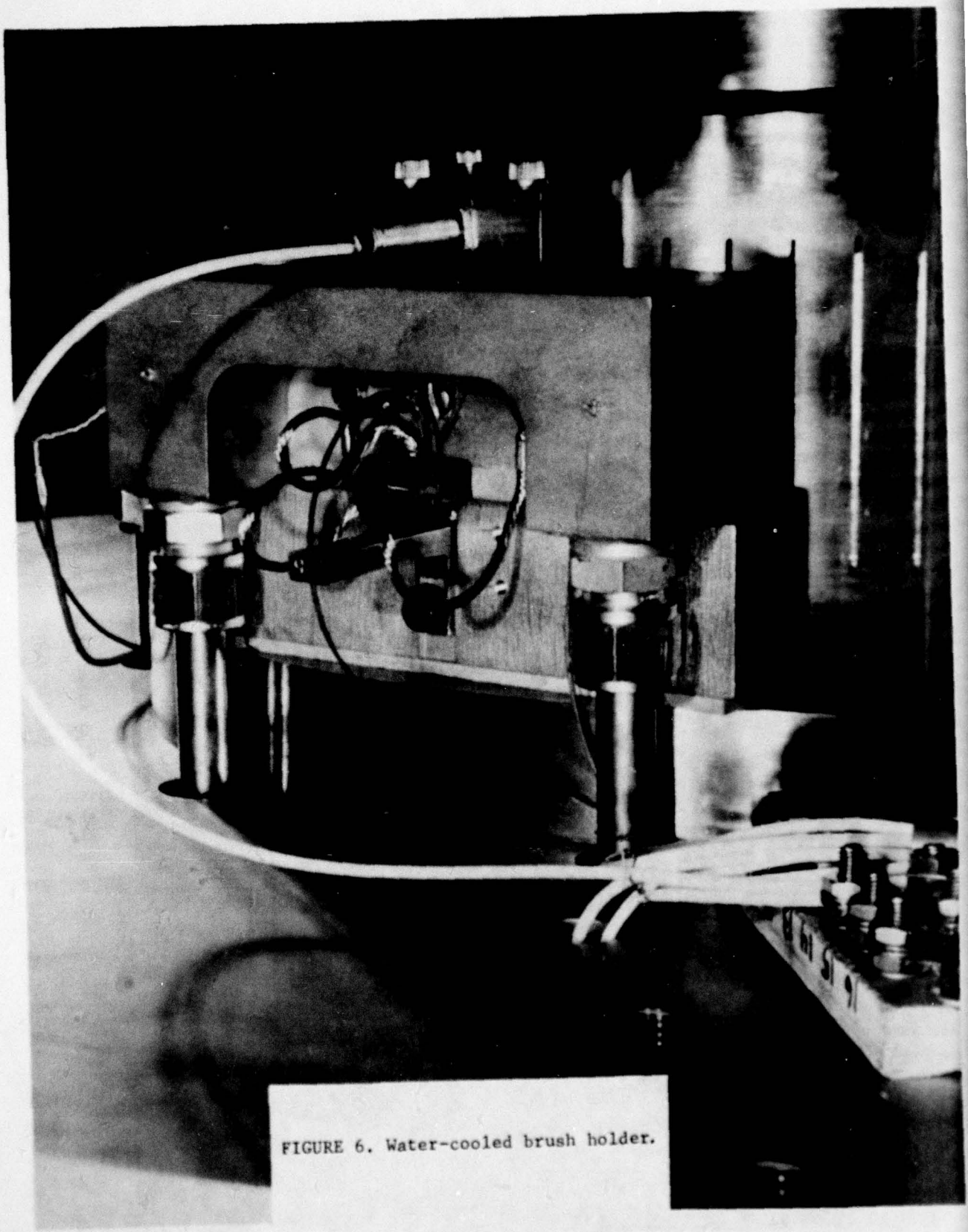


FIGURE 6. Water-cooled brush holder.

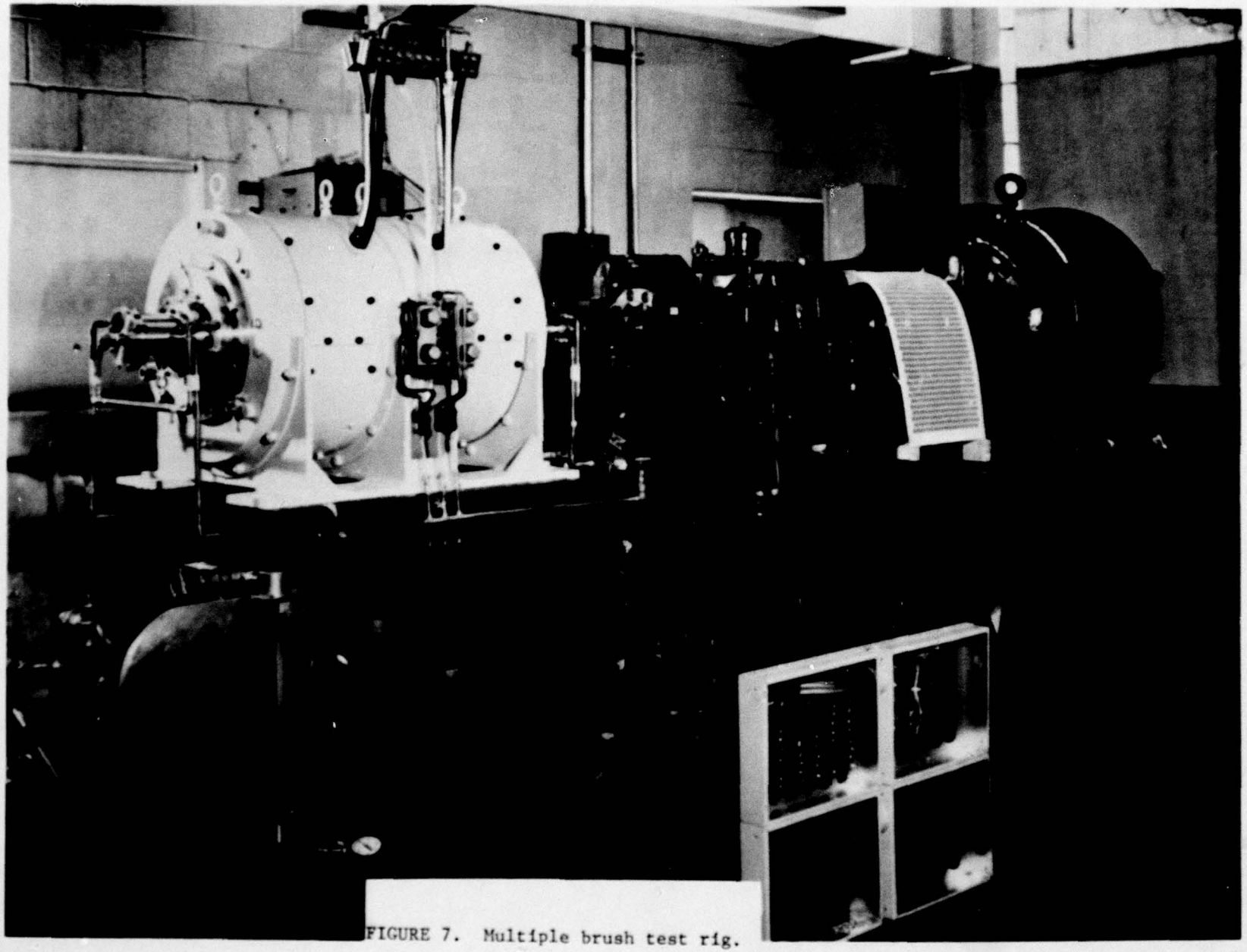


FIGURE 7. Multiple brush test rig.

SECTION IV

MATHEMATICAL MODELING PRESENTATIONS

HIGH POWER, AIRBORNE GENERATOR MODELING IN THE U. S. AIR FORCE

H. L. Southall, Capt, USAF

U. S. Air Force Aero Propulsion Laboratory, Wright-Patterson AFB OH 45433

INTRODUCTION

This paper describes a methodology for mathematically modeling high power, airborne electrical generators for the purposes of reducing specific weights (kg/kw or lb/kw) and improving performance. Modeling of generators and power systems began with relatively simple analyses and has developed into the present use of computer-aided design/simulation (CAD/S) programs[1-6]. Types of U. S. Air Force (USAF) high power generators and their operating conditions are described. The different kinds of models and the relationships among them are discussed and finally, future requirements in specific areas of modeling are considered.

USAF HIGH POWER, AIRBORNE GENERATORS

Generators of primary interest include salient pole wound-rotor, cylindrical wound-rotor, rare earth permanent magnet and superconducting-coil field structures. The power range for permanent magnet machines is 1 to 10 Megawatts, and 10 to 30 Megawatts for superconducting machines, with specific weight goals of 0.1 lb/kw (.045 kg/kw).

Mission requirements are high power, pulsed operation as shown in Fig. 1 for an assumed electrical load profile of 5 MVA. The term pulsed is used since the power is on for a much shorter period than the total mission time. A comparison with a load profile for an Advanced Airborne Command Post (E4B) is shown[7]. Each high power "spike" or pulse can last for seconds or tens of seconds, and may require direct current or pulse-train (hundreds or hertz) current operation. The electrical load consists of a primary load with a voltage range of 15 to 40 KV and a secondary load which is about 10 percent of the primary power with a voltage requirement of about 150 KV. The power split occurs in the power conditioning subsystem between the generator and the loads. In the DC case, the generator operates into a rectifier or transformer/rectifier and filter depending upon the design voltage of the generator. In the pulse-train

case, the generator operates into a pulse former. The load seen by the generator is not a steady state sinusoid in either case, due to power conditioning switching operations. Operation near saturation in the magnetic circuits (for maximum power per pound of material) and transient loading conditions (including load, feeder and power conditioning faults), require the inclusion of saturation effects in modeling USAF high power generators.

KINDS OF MODELS

Three kinds of generator models are described. The primary emphasis is on the electrical performance of the machine since the mission success depends upon the delivery of high quality electrical power to the load.

The first (and simplest) kind of model is a weight and volume algorithm (a mathematical expression) which expresses the weight, volume and geometry of a generator in terms of input variables such as RPM, power rating, voltage, rotor tip speed, current densities, material properties, magnet strengths, etc. This model is useful for comparing generator (or system) concepts and for parametric studies, since the model requires relatively small amounts of computer time.

The second kind of model is a simulation model which predicts the dynamic (time-varying) performance of a machine for given system operating conditions. This model is useful for predicting performance under varying load conditions and comparing the results of mathematical models with test data for model validation. The electrical simulation model is generally a lumped parameter equivalent circuit consisting of resistances, self and mutual inductances. The circuit equations can be formulated and solved for instantaneous voltages and currents given appropriate initial conditions, input parameters and load conditions. One equivalent circuit approach (Fig 2a) considers self and mutual inductances which vary with rotor position relative to the stator because of differences in winding alignment and permeability path changes with the relative motion. This is the so called "direct phase variable" equivalent circuit approach[2-3]. Another approach is illustrated in Fig. 2b where a coordinate transformation applied to the phase variables results in two equivalent "stator" windings which are stationary with respect to the field windings[1&3]. One

magnetic axis is aligned with the direct magnetic axis of the field winding and the other one in quadrature. Since there is no longer relative motion, the self and mutual inductances in the equivalent circuit are independent of rotor position. The resulting circuit equations with constant coefficients are referred to as Park's equations[1&3]. In either representation, the electrical effects of damper bars or other closed electrical paths for currents on the rotor structure are represented as two equivalent windings on the rotor, one winding is in alignment with and the other in quadrature with the main field excitation winding.

One of the problems in using circuit models for simulation is the accurate determination of the circuit parameters. There have been several USAF efforts to solve this problem and to determine the sensitivity of predicted transient performance to changes in the parameter values[3&8].

The simulation of a generator operating with various loads such as resistive, open circuit, short circuit, unbalanced and a rectifier bridge has been accomplished by implementing the equivalent circuit of Fig. 2a using the SCEPTRE (System for Circuit Evaluation and Prediction of Transient Radiation Effects) circuit analysis program to predict transient terminal characteristics[5]. The SCEPTRE simulation program in Ref. 5 was also modified to simulate a superconducting generator.

The third kind of model is the design model used to generate dimensions, types of material required and a large number of physical parameters necessary for machine fabrication. The starting point is a specification list which must be met (within tolerances, of course) by the machine to satisfy mission requirements. The specification might include values for weights, time constants, or inductances. The design process utilizes math models for electrical, magnetic field, thermal and mechanical analyses. This kind of model is the most complex and exacting since it is interdisciplinary and involves different "sub-models" which must be coordinated to assure that the machine will meet specifications. The individual sub-models may be empirical relations, rule of thumb or more sophisticated approaches such as finite element modeling and other CAD/S tools which relieve the designer of numerical dog work and free him to concentrate on physical and logical ideas and concepts.

MODELING RELATIONSHIPS

A three level modeling heirarchy is illustrated in Fig. 3 for the progression from system concept to the detailed design of a generator which will satisfy mission requirements. System modeling is required since the generator is a component (subsystem) and must be designed to interface with other subsystems for successful operation of the entire power supply (the system). This must be accomplished with stringent weight and volume constraints for aircraft applications.

The block labeled SYSTEM MODEL includes weight and volume algorithms and a system simulation model. The process is iterative in that an initial generator "parameter set", α_i, which is a list of physical dimensions; RPM; frequency; inductances; time constants; etc, is assumed for the system models. The output, 0_1, of the system model is a set of generator "performance measures", β_i, which is a list of alternator variables such as weight; volume; stability; voltage regulation; heat dissipation; torque limits; overload capability; fast start capability; etc. The output, 0_1, is compared with specifications such as maximum allowable weight, RPM, volume, etc. If the specifications are met, represented by YES for the logical decision $L(0_1)$, then a more detailed model of the alternator is formulated to simulate the dynamics of the machine using a new parameter set, α_2, to obtain a more accurate performance measure set, β_2. Again, a logical decision determines if the specifications are satisfied by the generator represented by the parameter set α_2. If the measures of performance are satisfactory, the DESIGN MODEL is initiated by implementing detailed, sophisticated and experimentally proven design models. A logical decision based on performance measures predicted by the design model results in fabrication go-ahead if the measures meet specifications. A change in the parameter set and a return to system modeling is required if specifications cannot be met.

FUTURE REQUIREMENTS FOR CAD/S MACHINE MODELING

A list of areas for development or improvement in existing state-of-the-art modeling approaches is given in this paragraph. Math models for discrete damper bars have been developed; however, a need exists for more

accurate modeling of cylindrical, sleeve type damper or shield members. The improvement of present models by including magnetic saturation effects on machine parameter values is also required. Finite element analysis programs offer promise in these areas. For superconducting generators, the active length of the machine can be small compared to the rotor diameter, therefore, three dimensional computer programs must be used to properly account for effects due to the three-dimensional nature of the problem. In more general terms, requirements exist for "optimized" designs through modeling; modeling of machines which are not necessarily three phase, sine wave generators; and, simplified models (terminal modeling, transfer functions, etc) for including the generator as a component in system simulation.

REFERENCES

1. Park, R. H., "Two Reaction Theory of Synchronous Machines," AIEE Transactions, V. 48, Jul 1929, p. 839.

2. Subramaniam, P., and Malik, O. P., "Digital Simulation of a Synchronous Generator in Direct-Phase Quantities," Proceedings IEE, V. 118, No. 1, January 1971, p. 153.

3. Webb, R. P., et. al.,"Alternator Modeling, Part 1. Simulation, Parameter Estimation, and Output Sensitivity," AFAPL-TR-75-87, Oct. 1975.

4. Tan, O. T. and Shokooh, F., "Synchronous Machine Analysis Using State Equations with Simple and Relevant Coefficients," Proceedings of the 1975 IEEE Southeast Conf., V. 2, p. 4B-4-1.

5. Kuhler, R. J., "Application of Generator Analysis Methods," AFAPL-TR-77-31, Apr. 1977.

6. Stuart, T. A. and Tripp, M. W., "Computer-Aided Design of Rectified Superconducting Alternator Power Supplies," CAD: Applications and Techniques, Midcon 77, Session 24.

7. Lloyd, W. M. and Stewart, A. A., "Development of a 1200 KVA Aircraft Electrical Power System," National Aerospace and Electronics Conference (NAECON) '76 Record, Dayton OH, p. 962.

8. Webb, R. P., Brice, C. W. and Tan, O. T., "Parameter Estimation for Generator Simulation Studies," AFAPL-TR-77-69, Nov. 1977.

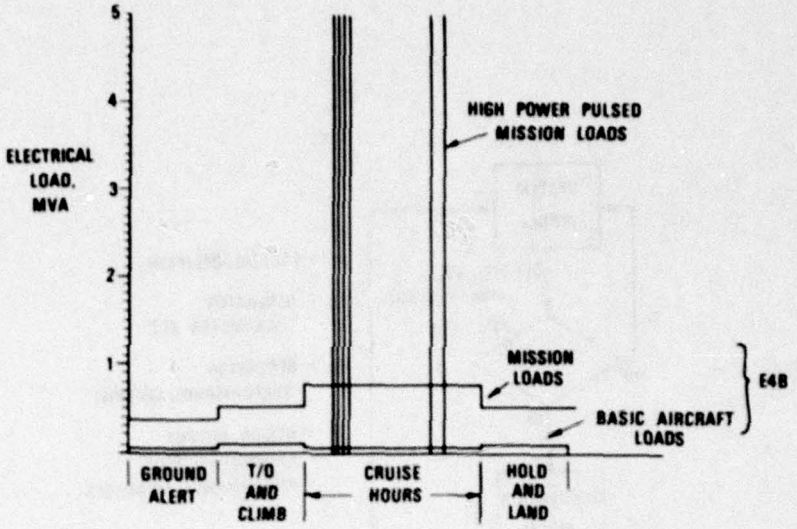


FIGURE 1 Comparison of High Power Pulsed Loads with Existing High Power Loads (E4B Advanced Airborne Command Post)

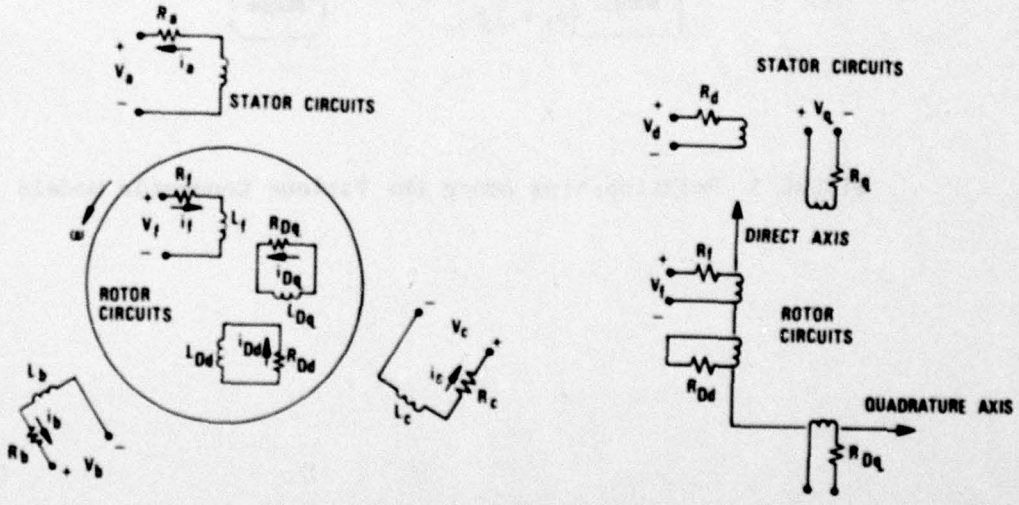


FIGURE 2 Generator Equivalent Circuits, (a) Direct Phase Variables (b) Direct and Quadrature Circuit Variables

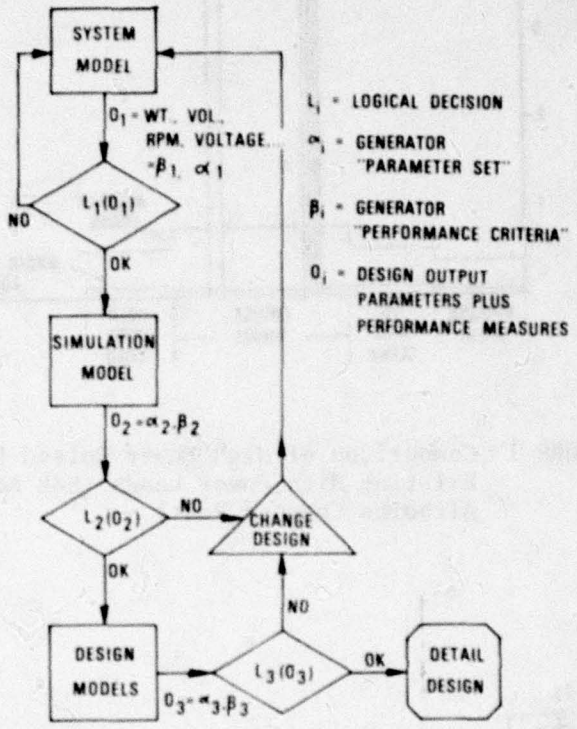


FIGURE 3 Relationships Among the Various Generator Models

EVOLUTION OF MACHINE DESIGN MODELS *

W. J. Shilling
Westinghouse Electric Corporation
Aerospace Electrical Division
Lima, Ohio

THEN AND NOW -

This discussion might be more aptly titled: "Electrical Machine Design - Then and Now". The "Then" being B.C. - Before the Computer and the "Now" being A.C. - After the Computer. The author has had the fortune of being on the scene as the industry passed through this "international dateline" - the epic milestone - the arrival of the IBM digital computer. This arrival was in the latter half of the decade of the 50's. The event was not heralded in with a 21 gun salute. It was like today's pocket calculators - suddenly you noticed they were here.

Even then though (as sometimes now) the computer was greeted with much trepidation. The author still remembers his complete skepticism and consternation when he was assigned the task of designing a computer program that would calculate a generator no-load voltage saturation curve. How could a computer do a decent job? It had no french curve available to it. It certainly couldn't do as good a job as a man because it had to deal with specific points. Recently the boss that made the assignment admitted he too had a lot of reservations. Other engineers assigned similar tasks, also viewed the whole matter with a jaundiced eye. However the computer soon proved itself by showing it could not only spit out no-load saturation curves with alacrity, but, when told how, it could actually design generators - and not just one or two designs for a given application but tens or hundreds of designs.

---

* Presentation to be made October 20, 1977, at Generators and Motors Seminar, Air Force Aero Propulsion Laboratory, Wright Patterson Air Force Base, Dayton, Ohio, 45433

There were "fringe benefits" also. The author was told by the computer experts that the computer doesn't make mistakes - at least he wouldn't likely live long enough to see it. And sure enough two decades later, the author, having waded through multitudes of his own programming errors, is still watching and waiting for the computer to make its first. There was still another fringe benefit that had nothing to do with rapid, accurate calculations. The computer was programmed for neatness. It always gave its answers very neatly typed with each specific item located precisely at the same position on the page. This meant that much detailed information was readily retrievable at the glance of an eye.

But enough lauding the computer. Let us telescope back to the B.C. times.

THE GOOD-OLD-DAYS

Back in the early 1950's generator design was approached similarly to how an artist might start his day. A calculation figuring book was opened. The engineer, with compass in hand, struck an arc representing a new stator punching outside diameter (O.D.) which would meet the customer's envelope requirements. Next an arc was struck representing the rotor punching O.D. This was a first try and was a critical diameter. Then a specific number of stator slots was picked. Calculations followed yielding such things as stack length, pole width, field turns, and wire size. With this work done, the designer then made crucial estimates. Would the stator winding cool? Were the field winding losses low enough that the field would operate below critical temperatures? If, for example, the field would not cool, there was one thing to do, get the compass out, increase the rotor diameter so there would be room for a larger field, and begin calculations again. Such a process netted one design in one or two days - not including performance calculations such as voltage unbalance.

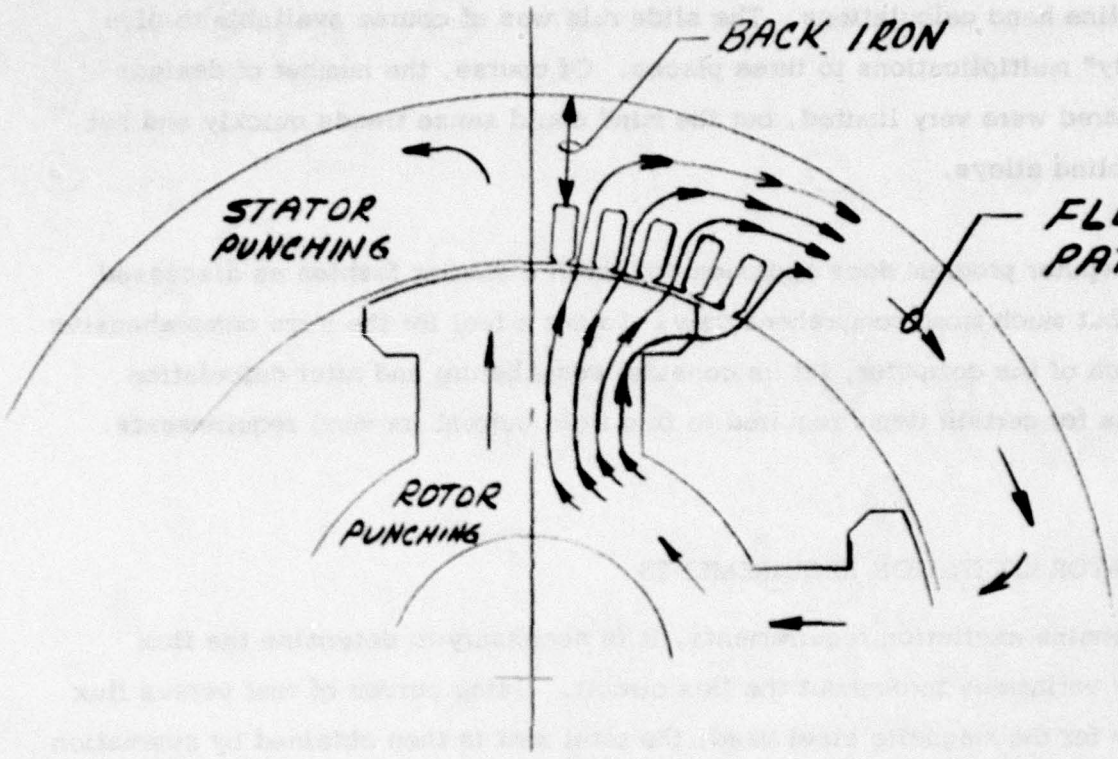
All of this really was not as rough and crude as it sounds. The human mind is a pretty good computer too. Operations such as eye-balling in the correct rotor diameter was an art learned quickly. Charts, tables, and curves were used to streamline hand calculations. The slide rule was of course available to give "speedy" multiplications to three places. Of course, the number of designs considered were very limited, but the mind could sense trends quickly and not go up blind alleys.

Our computer program does approach design in a similar fashion as discussed above but much more comprehensively. To get a feel for the more comprehensive approach of the computer, let us consider some before and after calculation methods for certain items required to find field current (or mmf) requirements.

GENERATOR EXCITATION REQUIREMENTS

To determine excitation requirements, it is necessary to determine the flux density variations throughout the flux circuit. Using curves of mmf versus flux density for the magnetic steel used, the total mmf is then obtained by summation of the mmf drops. As the flux flows through its circuit, (Figure 1), it gets squeezed at various points. One such point is in the stator teeth. At the stator I.D. the flux density is high but diminishes as the flux moves radially outward. When calculating by hand, the flux density is usually assumed constant throughout the tooth and equal to the density one-third the way up from the tooth root (at the stator I.D.). This assumption is not bad; however, it is usual to operate the tooth highly saturated. This means at the narrowest portion of the tooth (at the slot wedge), the saturation is extreme. The computer has an advantage here through a more thorough approach. Our program* cuts the tooth length including the wedge zone into 55 segments and calculates the mmf requirements of each segment. The computer also makes another refinement in this area. The

* Calculation methods and computer programs discussed are based on methods and programs at Westinghouse Electric Corporation, Aerospace Electrical Division, Lima, Ohio



FLUX PATHS IN GENERATOR PUNCHINGS

FIG. 1

mmf drop across the radial dimension of the tooth is also across the slot. Using this mmf, the program calculates the flux flowing radially through the slot and adds this flux to the tooth flux.

Still another item is the mmf drop in the back iron (between the stator slots and the punching O.D.). In hand calculations it is normal to assume this flux is sinusoidally distributed. The computer on the other hand breaks the back iron into twelve segments for each pole. The teeth and air gap are next considered as twelve parallel flux paths feeding flux into the back iron. In this manner mmf drops in the back iron are calculated using the actual flux distribution.

Another refinement which has a minor effect on excitation calculations but can be significant to temperature calculations, is the eddy current factor of the ac winding. This is the factor by which the dc winding resistance must be multiplied to obtain the high frequency skin effect. Determination of this factor is not simple and was rarely done in the days of hand calculations especially since it usually was not critical in our applications at that time. Now the computer calculates the factor for every design.

These various refinements have resulted in good calculations of generator excitation requirements. There are many variables in the manufacture of machines such as punching stacking factors, steel permeability, building tolerances but in general we expect the computer to agree within 3 to 5% of actual field current requirements.

DESIGN ASSURANCE

Another plus for the computer is the use of design checks. For example, in our program every design considered is automatically checked to see:

if the number of slots chosen is windable,

if the rotor damper bar pitch relative to the stator slots will cause excessive damper bar losses,

if pole face losses will be excessive,

if the stator slots are too full of wire,

if waveform meets specification,

if critical mechanical stresses are excessive,

if end extensions of ac winding are likely to collapse together on a three phase short,

if tooth width is too narrow to punch,

if voltage unbalance is excessive,

etc.

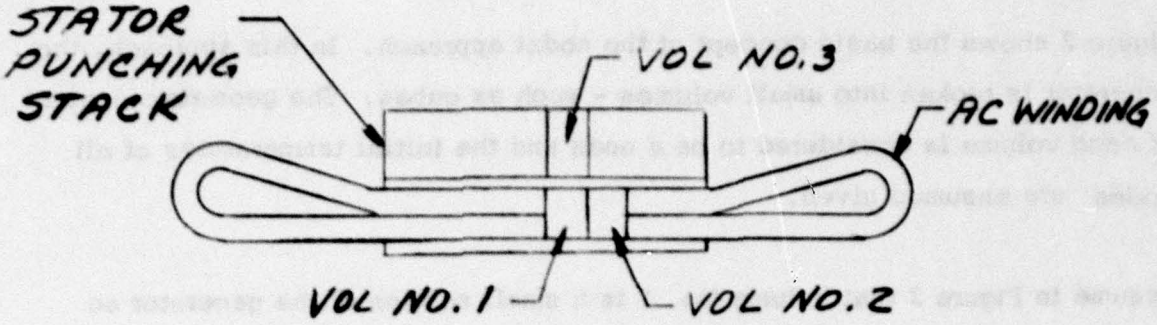
These design checks represent a real design assurance policeman. Who knows how many goofs the computer has prevented?

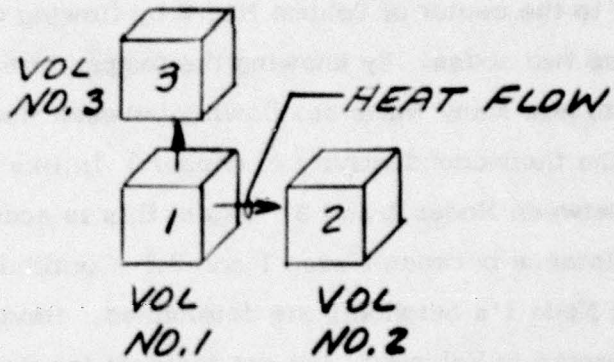
THERMAL ANALYSIS

One important aspect of electrical design is thermal. Insulation is usually the weak thermal link in a machine. In the good-old-days, simple thermal calculations were made based on temperature drops through the slot cells and back iron. Sometimes even a simpler approach was used whereby current densities in the wire of proposed designs were compared to densities in previously built machines. Today at Lima we have programs available based on a nodal approach to thermal calculations which is a three dimensional approach.

Figure 2 shows the basic concept of the nodal approach. In this approach, the generator is broken into small volumes - such as cubes. The geometric center of each volume is considered to be a node and the initial temperatures of all nodes are assumed given.

Assume in Figure 2 that Volume No. 1 is a small section of the generator ac winding condutor. Let Volume No. 2 be the next segment of the copper wire, and let Volume No. 3 be the back iron over the slot. Vol. 1 is a segment of copper wire carrying current so heat is being generated in this volume. Volume No. 2 is Volume No. 1's neighbor. Heat can flow from the center of Volume No. 1 (Node No. 1) to the center of Volume No. 2 by flowing through the copper wire connecting these two nodes. By knowing the temperatures at Nodes 1 and 2, we can calculate how many watts are flowing between Nodes 1 and 2. (This is done by using the thermoconductivity of copper.) In like manner we can find the watts flowing between Nodes 1 and 3. (Again this is accomplished by knowing the thermal resistance between Nodes 1 and 3.) Continuing this process, watt losses to all of Node 1's neighbors are determined. Having already calculated the losses generated in Volume 1, the net residual losses can be obtained (generated losses minus outgoing losses). These residual losses will heat up Volume No. 1 just as a coffee pot heats on the stove. This rate of temperature change is determined using the specific heat of the material in Volume No. 1 (copper). A small incremental time such as .001 seconds is next chosen and temperatures of Volume No. 1's neighbors are assumed constant during this time. The temperature of Volume No. 1 can now be calculated at the end of .001 seconds. In this manner the temperatures of all nodes can be calculated at the end of this .001 second time increment. Using this concept then, a transient temperature calculation can be made for all nodes starting with initial given temperatures. If a stabilized solution is desired, the same concept is used except in this case the residual heat in each volume is zero and simultaneous equations are used.





t = TIME, SECONDS
T = TEMP. °C

AT TIME = t_0 LET $T_1 = 25°C$

$W_{1-2} = (T_1 - T_2) \times K \times \frac{A}{L}$

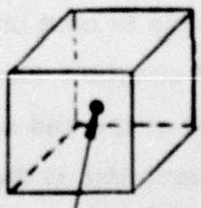
NET WATTS = $W_{gen} - W_{1-2} - W_{1-3}$ ETC

C_p = SPECIFIC HEAT

$C_p = \frac{\text{WATTS - SECONDS}}{\text{LB °C}}$

$\Delta T_c^\circ = \frac{\text{NET WATTS}}{C_p \times \text{LB}} \times \text{SECONDS}$

AT .001 SEC: $T_1 = 25 + \Delta T_c^\circ$



NODE 1 IS AT GEOMETRIC CENTER OF VOLUME NO.1

VOLUME AND NODAL CONCEPTS FOR TEMPERATURE TRANSIENT CALCULATIONS

FIG 2

Obviously, the above approach would be very tedious for hand calculations. The computer on the other hand loves such a calculation method which is readily adaptable to "Do Loop" and "If" statement programming.

Lima has such a program that is used routinely for spray oil cooled generators. It uses 54 temperature nodes and calculates both a transient and stabilized solution. (If more nodes and sophistication is desired, such programs are also available using as many as 400 nodes.) Figure 3 shows a comparison of calculation (using the 54 nodal program) versus test for the ac winding average temperature transient of a 75 kVA generator with a 6 second line to neutral short circuit fault applied. The curves are not meant to imply absolute accuracy of the temperature calculation method as there are too many variables involved in both the calculation and test. However, it does give a feel for the program capabilities.

VOLTAGE TRANSIENTS

Another area that must be considered by the electrical designer is the voltage transient response of the generator. Before computers, the approach usually was to compare the machine constants of a new design with constants of previously built machines. Using these machine constants in the form of ratios and charts, estimates were made of the new machine transient response. This method is normally a good approach but is not comprehensive. The method failed in one particular application years ago and required a major generator redesign involving significant time and money. The computer was on the scene at that time so a program was initiated to calculate voltage transients in a more comprehensive form.

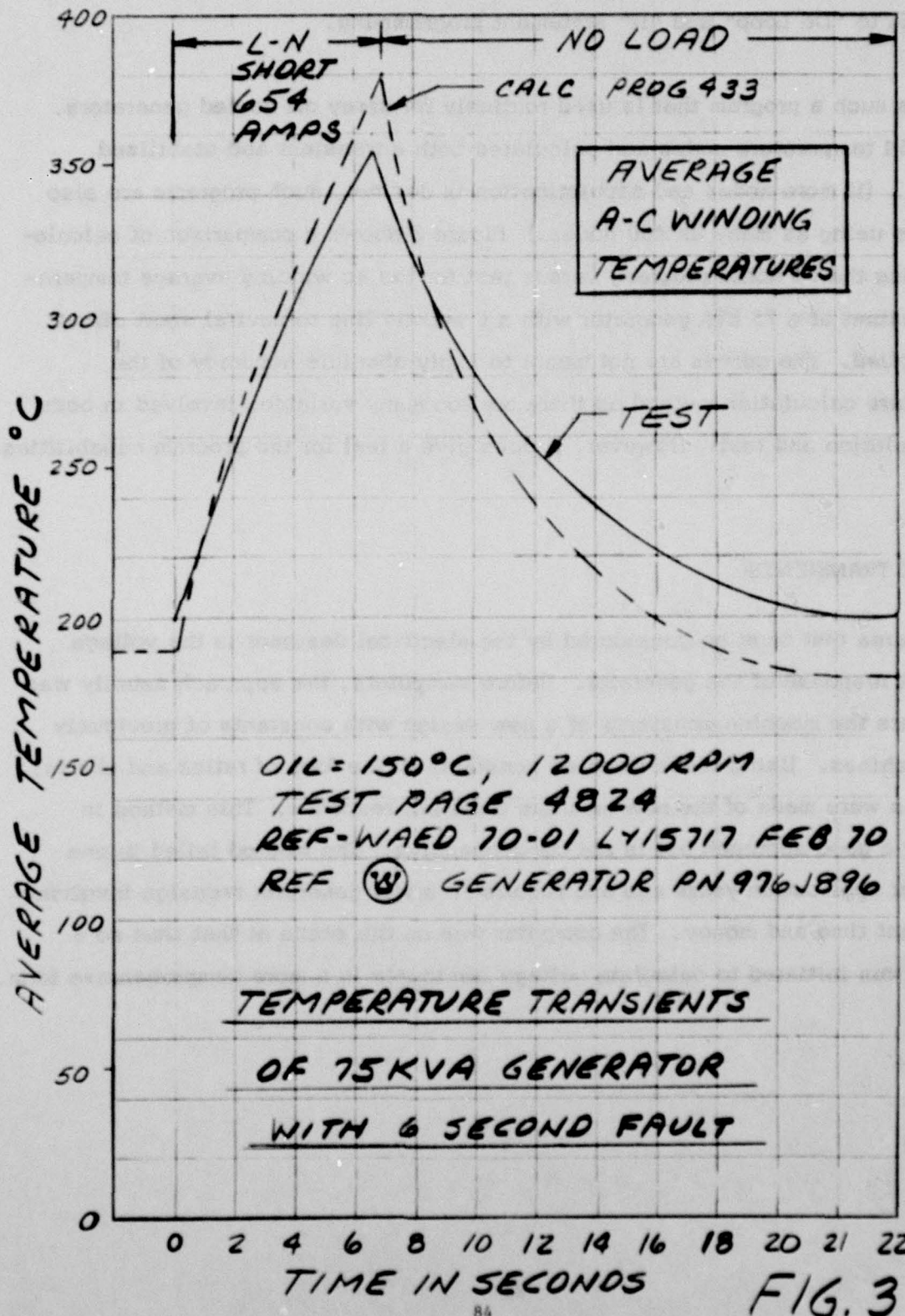

400
350
300
250
200
150
100
50
0
AVERAGE TEMPERATURE °C
L-N SHORT 654 AMPS
NO LOAD
CALC PROG 433
AVERAGE A-C WINDING TEMPERATURES
TEST
OIL = 150°C, 12000 RPM
TEST PAGE 4824
REF-WAED 70-01 LY15717 FEB 70
REF (W) GENERATOR PN 976J896
TEMPERATURE TRANSIENTS
OF 75KVA GENERATOR
WITH 6 SECOND FAULT
0 2 4 6 8 10 12 14 16 18 20 21 22
TIME IN SECONDS

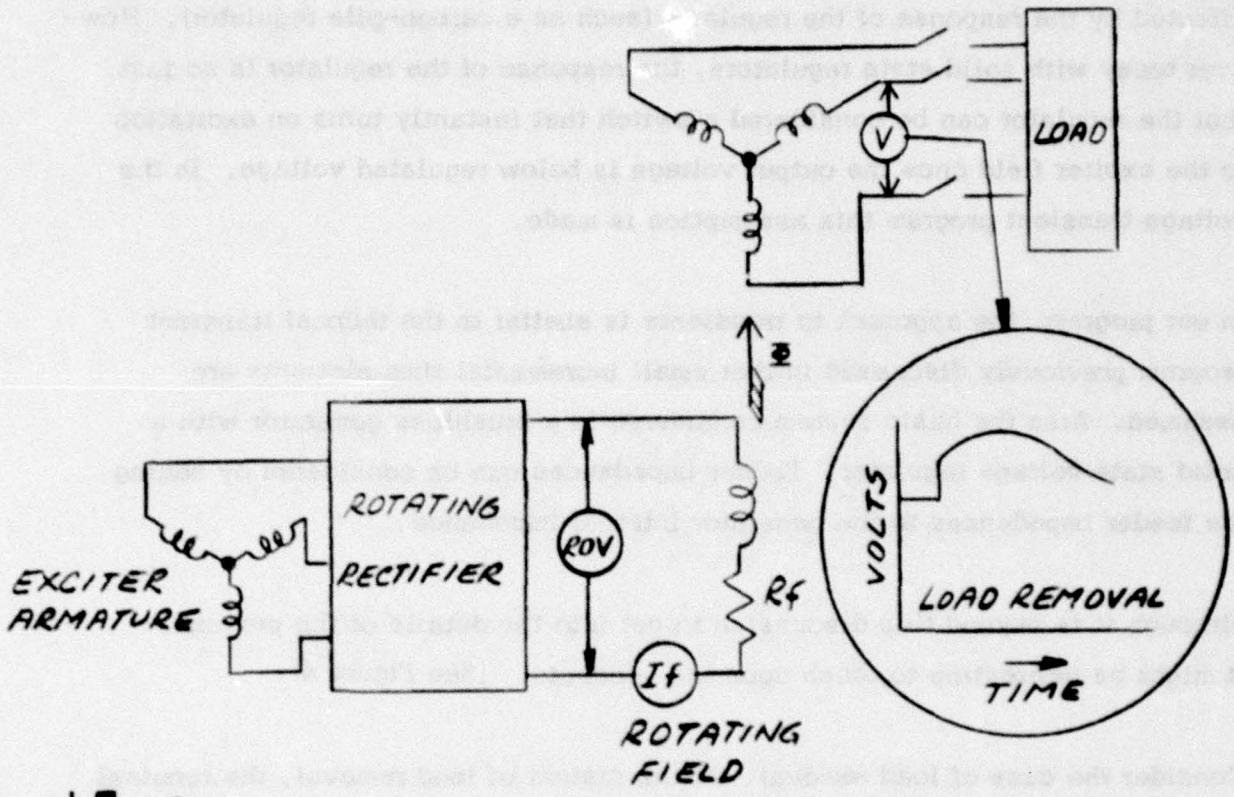
FIG. 3

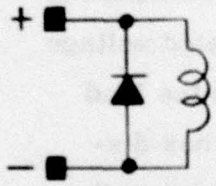
In the past, voltage transients of a generator-regulator system were significantly effected by the response of the regulator (such as a carbon-pile regulator). However today with solid state regulators, the response of the regulator is so fast that the regulator can be considered a switch that instantly turns on excitation to the exciter field once the output voltage is below regulated voltage. In the voltage transient program this assumption is made.

In our program, the approach to transients is similar to the thermal transient program previously discussed in that small incremental time elements are assumed. Also the basic system considered is a brushless generator with a solid state voltage regulator. Feeder impedances can be considered by adding the feeder impedances to the generator internal impedance.

Although it is beyond this discussion to get into the details of the program, it might be interesting to touch upon the concepts. (See Figure 4).

Consider the case of load removal. At the instant of load removal, the terminal voltage suddenly jumps because we suddenly see the internal generated voltage (required during the load condition) at the machine terminals. Since the load current has been suddenly removed, however, the armature reaction has disappeared. This means the rotating field current suddenly drops. However the voltage supplied to the field from the exciter does not significantly change. There is now an inequality, the voltage supplied to the field is greater than the IR drops in the field. This inequality must be corrected and this is done by a rate of change of the main generator flux. In this case the change is in a direction so as to increase the main flux. This rate of change of flux flowing through the rotating field generates a voltage across the field that corrects the inequality. This can be expressed in equation form as:





EXCITER
FIELD

$$ROV = I_f R_f + N_f \frac{d\Phi}{dt}$$

$$V = K \times \Phi$$

ROV = RECTIFIER OUTPUT VOLTS

I_f = ROTATING FIELD AMPS

R_f = ROTATING FIELD RESISTANCE

N_f = ROTATING FIELD TURNS

Φ = MAIN FLUX

V = VOLTS OUTPUT

K = CONSTANT

CONCEPTS USED IN VOLTAGE TRANSIENT PROGRAM

FIG. 4

$$ROV = IR + N \, d\Phi/dt$$

Where:

- ROV = rotating rectifier output volts with the exciter supplying the source voltage
- I = rotating field current
- R = rotating field resistance
- N = field turns
- $d\Phi/dt$ = rate of change of the flux through the rotating field

A similar equation is applied to the ac exciter. Using a small time increment and the above equation, the main generator flux and therefore the terminal voltage can be determined as a function of time. By the use of "Do Loops" and "If" statements the computer program is quite versatile. The program has been used to calculate:

Load removal and application

Short circuit removal

No load buildup and decay

Constant impedance buildup and decay.

Figure 5 shows calculation versus test for load application of a 250 kVA generator. Again the comparison involves many variables and is not meant to show inherent accuracy (or inaccuracy) of the calculation method. (In the calculation the regulator is assumed to turn off at 5% below rated voltage to account for anticipatory action of the actual regulator.) In another example in which there are less variables involved, a 591 kVA generator was suddenly excited with a constant dc voltage of 24 volts supplied to the exciter field. Figure 6 shows a comparison of test and calculation.

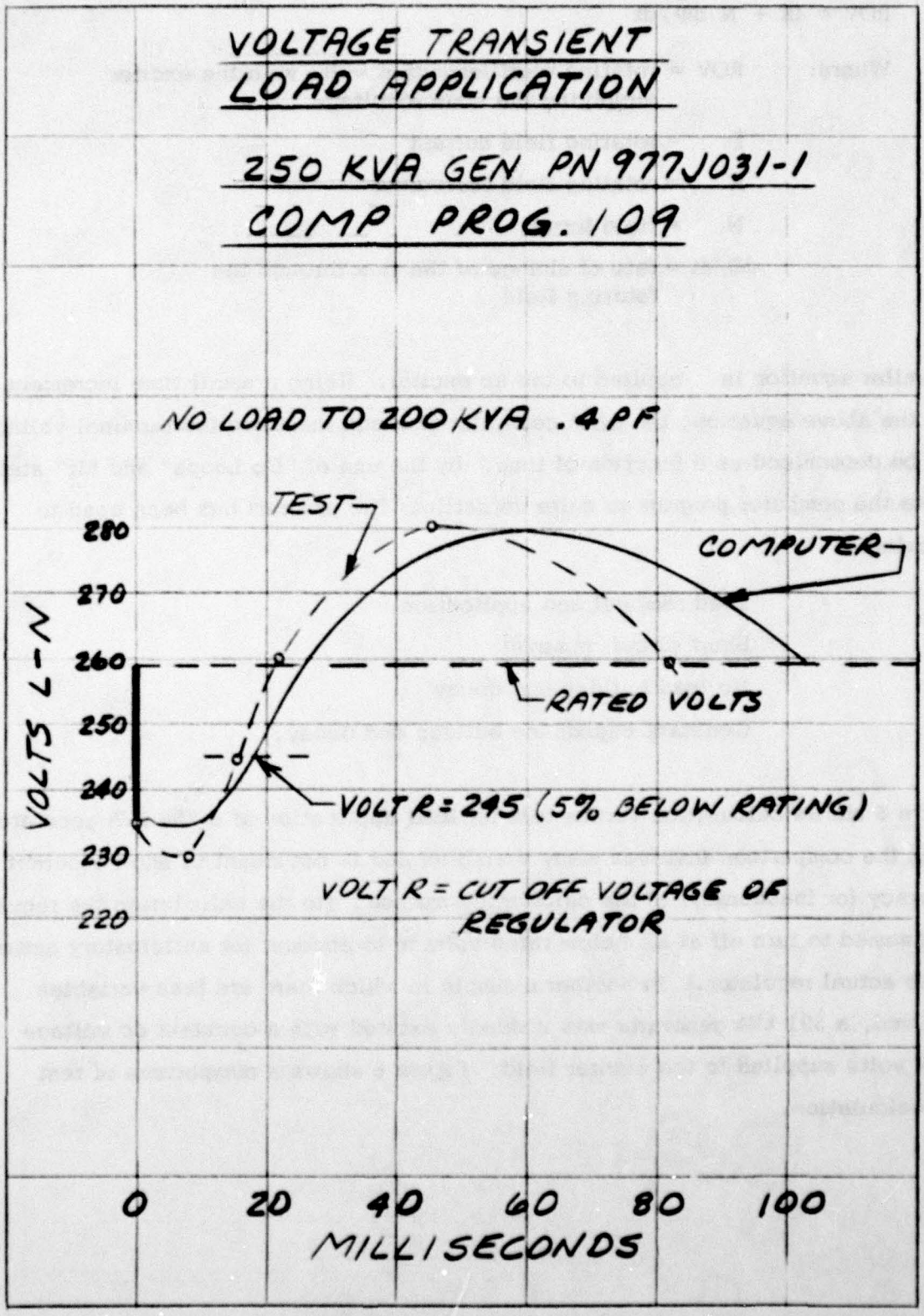

VOLTAGE TRANSIENT
LOAD APPLICATION
250 KVA GEN PN 977J031-1
COMP PROG. 109
NO LOAD TO 200 KVA .4 PF
TEST
COMPUTER
RATED VOLTS
VOLT R = 245 (5% BELOW RATING)
VOLT R = CUT OFF VOLTAGE OF REGULATOR
VOLTS L-N
280
270
260
250
240
230
220
0
20
40
60
80
100
MILLISECONDS

FIG 5

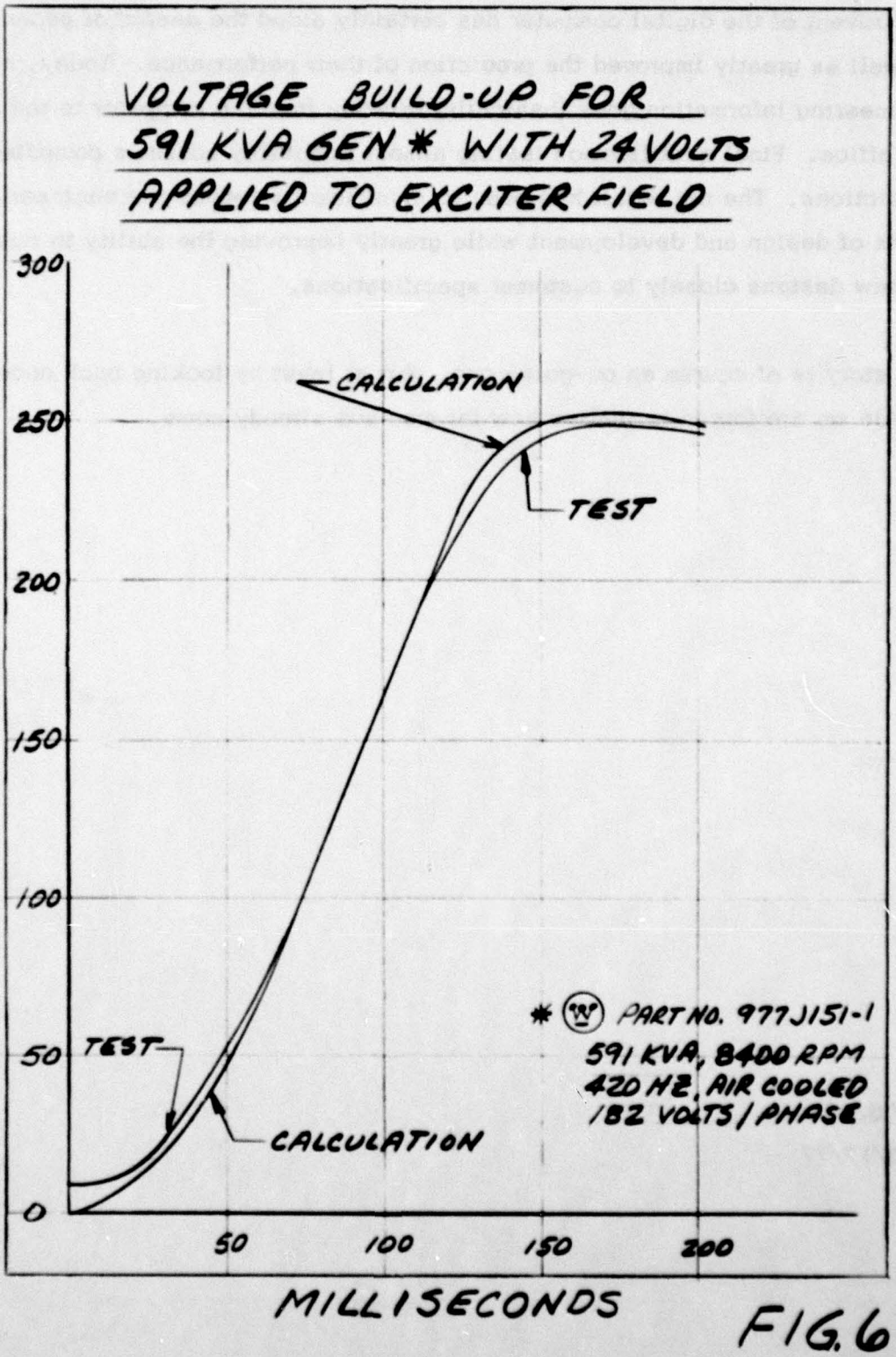

VOLTAGE BUILD-UP FOR
591 KVA GEN * WITH 24 VOLTS
APPLIED TO EXCITER FIELD
VOLTS PER PHASE
300
250
200
150
100
50
0
CALCULATION
TEST
TEST
CALCULATION
* PART NO. 977J151-1
591 KVA, 8400 RPM
420 HZ, AIR COOLED
182 VOLTS / PHASE
50
100
150
200
MILLISECONDS

FIG. 6

CONCLUSIONS

The advent of the digital computer has certainly aided the design of generators as well as greatly improved the prediction of their performance. Today, most engineering information goes (basically) directly from the computer to the drawing office. Final qualification testing almost invariably confirms computer predictions. The net result has been to significantly reduce the engineering costs of design and development while greatly improving the ability to custom fit new designs closely to customer specifications.

The story is of course an on-going one. But at least by looking back once in awhile we are forced to realize how far we have already come.

WJS/pdw
10/17/77

MECHANICAL FORCES IN DAMPER SHIELDS FOR SUPERCONDUCTING GENERATORS

J.L. McCABRIA
WESTINGHOUSE ELECTRIC CORP., AEROSPACE ELECTRICAL DIVISION

Superconducting generator uses a rotating electrical shield between the field winding and the armature to initially exclude and slow down a sudden demagnetizing flux from the armature. Under steady-state condition this shield also attenuates asynchronous magnetic fields and prevents a strong ac field from entering the superconducting winding. The electric shield is a necessary component which keeps the superconducting field winding from being driven normal.

In a radial gap machine the shield takes the form of hollow cylindrical shell.

1. Electric requirements demand a material with a high conductivity;
2. Mechanical stresses in the shield demand a material with high strength; and
3. Minimization of the deformation demands a material with a high modulus of elastics.

Both aluminum alloys and copper alloys have been considered for the electrical shield. Recent conceptional design shows that the shield should operate at room temperature or above. The losses in the shield will place excessive demands upon a cooling system at cryogenic temperatures.

AD-A078 341 AIR FORCE AERO PROPULSION LAB WRIGHT-PATTERSON AFB OH F/G 10/2
PROCEEDINGS OF THE AFAPL GENERATOR AND MOTORS SEMINAR (1ST), HE--ETC(U)
AUG 79 H L SOUTHALL , J L MCCABRIA

UNCLASSIFIED AFAPL-TR-79-2090 NL

2 OF 3
AD-
A078341



The critical problem which must be resolved by the designer of the shield is to obtain a structure which does not yield when subjected to electromagnetic forces associated with faults on the machine. Initially the fault forces on the rotor are experienced by the shield.

The fault force field has unidirectional tangential component and a unidirectional normal component of force which varies sinusoidally around the shield.

Since a thin wall cylinder is easily deformed by a sinusoidally normal component of force, this shield can experience large bending stresses when a fault occurs.

I shall now describe a model I have used to calculate the stresses in a shield when it is subjected to a harmonic pressure.

The stress distribution for a cylinder in two-dimensional, polar coordinates is:

$$\sigma_R = \frac{1}{R}\frac{\partial \phi}{\partial R} + \frac{1}{R^2}\frac{\partial^2 \phi}{\partial \theta^2}$$

$$\sigma_\theta = \frac{\partial^2 \phi}{\partial R^2}$$

$$\tau_{R\theta} = -\frac{\partial}{\partial R}\left(\frac{1}{R}\frac{\partial \phi}{\partial \theta}\right)$$

$$\phi = f(R, \theta)$$

Where ϕ is a stress function expressed in terms of R, θ . These equations are derived from static equilibrium of an element rd θ by dr . In order to obtain a valid solution the stress functions must satisfy the condition of compatibility - continuity of deformation or deformation without cracks or overlapping. The compatibility equation in polar coordinates is:

$$0 = \left(\frac{\partial^2}{\partial R^2} + \frac{1}{R}\frac{\partial}{\partial R} + \frac{1}{R^2}\frac{\partial^2}{\partial \theta^2}\right)\left(\frac{\partial^2}{\partial R^2} + \frac{1}{R}\frac{\partial}{\partial R} + \frac{1}{R^2}\frac{\partial^2}{\partial \theta^2}\right)\phi$$

We can find the stress distribution for a cylinder subjected to uniform exterior pressure (P_u) by using stress functions:

$$\phi = C_1 + C_2 \ln R$$

This function provides the familiar equations for hollow cylinders under external pressure:

$$\sigma_R = -P_u \frac{(1 - R_I^2/R^2)}{(1 - R_I^2/R_o^2)}$$

$$\sigma_\theta = -P_u \frac{(1 + R_I^2/R^2)}{(1 - R_I^2/R_o^2}$$

To find an analytical solution for a cylinder subjected to a harmonic external pressure, we use the stress function:

$$\phi = (aR^N + bR^{N+2} + cR^{-N} + dR^{-N+2}) \cos N\theta$$

Where a, b, c, and d are coefficients which can be calculated by satisfying boundary conditions.

Substituting this stress function into Equation (1) gives:

$$\sigma_R = [N(1-N)aR^{N-2} + (2-N)(1+N)bR^N - N(1+N)cR^{-N-2} + (2+N)(1-N)dR^{-N}]\cos N\theta$$

$$\sigma_\theta = [-N(1-N)aR^{N-2} + (2+N)(1+N)bR^N - N(1+N)cR^{-N-2} + (2-N)(1-N)dR^{-N}]\cos N\theta$$

$$\tau_{R\theta} = [-N(1-N)aR^{N-2} + N(1+N)bR^N - N(1+N)cR^{-N-2} + N(1-N)dR^{-N}]\sin N\theta$$

Four boundary conditions are applied to determine coefficients a, b, c, and d.

They are:

$\sigma_R = -p_a \cos N\theta$	AT	$R = R_o$
$\sigma_R = 0$	AT	$R = R_I$
$\tau_{R\theta} = 0$	AT	$R = R_o$
$\tau_{R\theta} = 0$	AT	$R = R_I$

If we let

Let

$$A = N(N-1)a$$
$$B = (N+1)b$$
$$C = N(N+1)c$$
$$D = (N-1)d$$
$$E = R_I / R_o$$

---

and solve for coefficients A, B, C, and D they become

$$D = \frac{\Omega_R R_o^N}{2} \left\{ \frac{1 - E^{2(N+1)} + (N-1)(1-E^2)}{(N^2-1)(1-E^2)^2 + (1-E^{2(N+1)})(1-E^{-2(N-1)})} \right\}$$

$$B = \frac{\frac{D(N+1)(1-E^2)}{R_o^N} - \frac{\Omega_R}{2}}{R_o^N (1 - E^{2(N+1)})}$$

$$C = R_o^{2(N+1)} B - (N+1)(R_o^2 D) + \frac{R_o^{N+2} \Omega_R}{2}$$

$$A = -(N-1) B R_o^2 - R_o^{-2(N-1)} D + \frac{R_o^{(2-N)} \Omega_R}{2}$$

Now simple equations for the stress intensities due a harmonic external pressure become:

$$\sigma_R = \{A_R + B_R + C_R + D_R\} \cos N\theta$$

$$\sigma_\theta = \{A_\theta + B_\theta + C_\theta + D_\theta\} \cos N\theta$$

$$\tau_{R\theta} = \{A_S + B_S + C_S + D_S\} \sin N\theta$$

Where

$$A_R = -A R^{N-2}$$

$$A_\theta = A R^{N-2}$$

$$A_S = A R^{N-2}$$

$$B_R = -(N-2) B R^N$$

$$B_\theta = (N+2) B R^N$$

$$B_S = N B R^N$$

$$C_R = -C / R^{N+2}$$

$$C_\theta = C / R^{N+2}$$

$$C_S = -C / R^{N+2}$$

$$D_R = -(N+2) D / R^N$$

$$D_\theta = (N-2) D / R^N$$

$$D_S = -N D / R^N$$

A review of these solutions shows that:

- the stress intensities are proportional to the applied pressure.

P_u or P_e

- the stress distribution is independent of the absolute dimensions of the cylinder - a cylinder with a diameter of 10 feet and a 1 foot wall has the same stress intensities as a cylinder with a 10 inch diameter and 1 inch wall when subjected to same pressure (uniform or harmonic).

- the stresses depend upon R_I/R_o, the number of full size waves around the periphery, and the crest value of the pressure. Strength of material considerations did not affect the solution.

- the stresses in a hollow cylinder subjected to N full sine wave of pressure is a strong and complicated function of N.

- Figure (1) shows the solution graphically.

  Here we have

$$\left(\sigma_\theta/P_e\right)_{max} \sqrt{S.\ N}$$

  for several values R_I/R_o

- It can be noted that 2 sine waves cause a large bending stress as one would expect since this distribution of external pressure causes the cylinder to flatten.

- The stress intensity due to bending decreases rapidly as the number of sine waves increase from 2 to 4 to 6 etc. Also, increasing the thickness of the hollow cylinder decreases the ratio of the maximum bending stress to the crest value of the applied external stress.

- I have compared the stress intensities obtained via this analytical solution with stress intensities calculated using curved-beam theory. I found the stress intensity calculated by the solution present here are 8 to 10 percent higher than one would calculate using a curved-beam model.

- Figures 2, 3, and 4 gives the stress intensities when external loads of the form $p = p_0(1 + \cos N\theta)$ are applied. In a SC generator N is equal to the number of poles or a product of this number.

- It can be noted from Figures (2) and (3) that it is possible to select a thickness for the shield so the tensil bending stress is equal or less than the uniform compressive stress. For eight sine waves this occurs when the thickness is greater than 10% of the outer radius. A similar condition exists for six sine waves when the thickness is greater than 17% of the out radius.

TRANSIENT RADIAL FORCE DISTRIBUTION

FOLLOWING A 3 - PHASE FAULT:

A sudden change of the phase currents in the armature will produce a change of the field which is initially excluded from the field winding via currents in the electromagnetic shield. As the shield currents decay, the armature field will penetrate the shield and a new dc field and force distribution will be established in the field winding. During the transient, forces are exerted on the shield. Unidirectional tangential force appear which equalize the torques on the stator and rotor. A unidirectional crushing force acts upon the shield when the armature current increase and unidirectional dilative force appear when the armature current is suddenly decreased.

The fault currents for superconducting generator are high and produce large crushing force on the electromagnetic shield following the fault.

The components of normal stress resulting from a three-phase fault from open circuit are shown in Figure (5).

The normal stress given by this equation is made of

(1) A component

$$-(B_{AS}B_F + B_{AS}^2 + B_{AT})$$

which independent of of angular position and time;

(2) A component

$$+(B_{AT}B_F + 2B_{AS}B_{AT})\cos\omega t$$

which is dependent upon time only;

(3) A component

$$(B_{AS}B_F + B_{AS}^2)\cos 2M\theta$$

which is a second spatial harmonic and independent of time.

(4) A component

$$-(B_{AT}B_F + 2B_{AS}B_{AT})\cos(\omega t + 2M\theta)$$

which is a traveling wave relative to the rotor and stationary relative to the armature, and

(5) A component

$$B_{AT}^2\cos 2(\omega t + M\theta)$$

which is a wave traveling at twice the speed of rotor.

The net results of all these components to produce uniform crushing pressure around the shield superimposed upon the second spatial harmonic which has an amplitude equal to uniform pressure.

At $\omega t = 0$ the external applied stress is zero. At $\omega t = \pi$, the radial applied stress is a maximum and has the form of $P = P_0 (1 + \cos 2M\Theta)$ where M = number of pole pairs.

Figures (6) and (7) illustrate the amount of electromagnetic stress that can be endured by a copper shield and by an aluminum shield, respectively. The allowable electromagnetic stress is based upon a reasonable allowance for centrifugal stress and the yield strength of these materials. It can be noted from Figure (6) the electromagnetic stress in a copper shield must be limited to approximately 10,000 psi if the surface speed of the shield is 570 fps. On the other hand, an aluminum shield with a surface speed of 570 fps. could with an electromagnetic stress around 60,000 psi without yielding. Figure (8) shows the required thickness of a shield as a function of the applied external magnetic pressure.

SUMMARY

- An analytical solution for the stresses produced by a harmonic radial load around a cylinder has been obtained.
- This solution represents an exact solution for the boundary conditions imposed upon the problem.
- A comparison of the stress intensities obtained from the exact solution and from a curved-beam model showed good agreement - within 90%. However, the curved-beam model must be used with prudence or an incorrect bending stress is obtained. I have noted stress intensity in the literature based upon a curved-beam model which appears to be in error.
- The compressive stress due to the uniform pressures around a shield should not be neglected for 4, 6, and 8 pole machines. This compressive stress offsets a significant portion of the harmonic stress.
- An AL of Cu alloy can be used for a shield if the rotor has four or more poles. The thickness required to withstand a three phase fault appears to be reasonable.
- Up to this point, I have only considered the thickness of the shell from the standpoint of withstanding the normal fault forces. The diffusion time and the attenuation of the synchronous field impact upon the shield dimensions as previously discussed by Dr. Parker.

  Under steady-state operation forced vibration of the shield will be produced by the electromagnetic forces. The cylinder must be designed so the frequency of the natural modes of vibration under rotation do not coincide with the frequencies of the electromagnetic forces. The frequency of the natural modes of motion are a function of the density, radius, and the thickness of the shell. Thus, the selection of the dimensions of the shield must be made on the basis of vibration and electromagnetic considerations as well as its ability to withstand the fault forces.

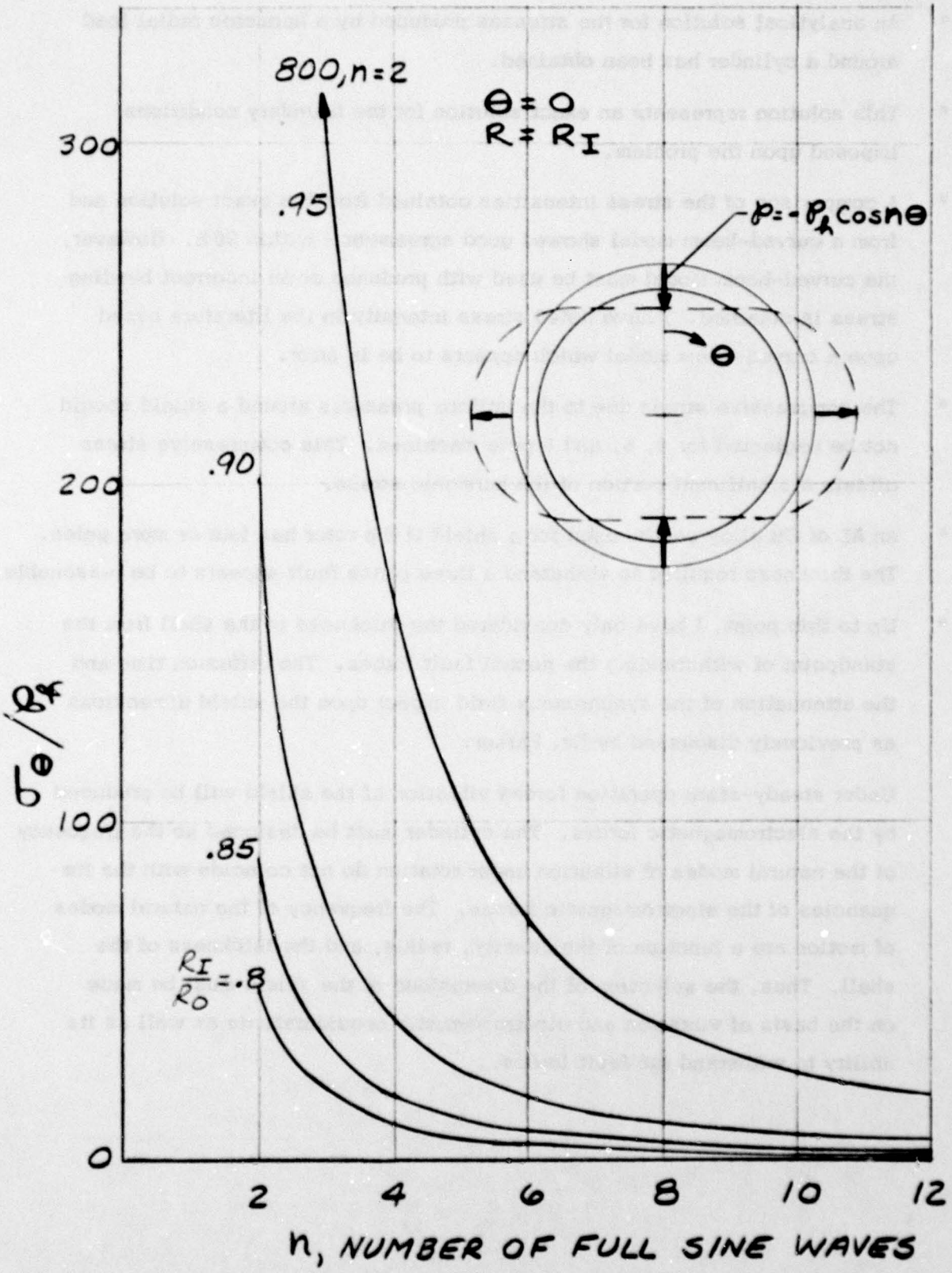

800, n=2
θ=0
R=R_I
p=-p_1 Cosnθ
θ
.95
.90
.85
R_I/R_O=.8
300
200
100
0
σ_θ/p_1
2
4
6
8
10
12
n, NUMBER OF FULL SINE WAVES

Figure (1)

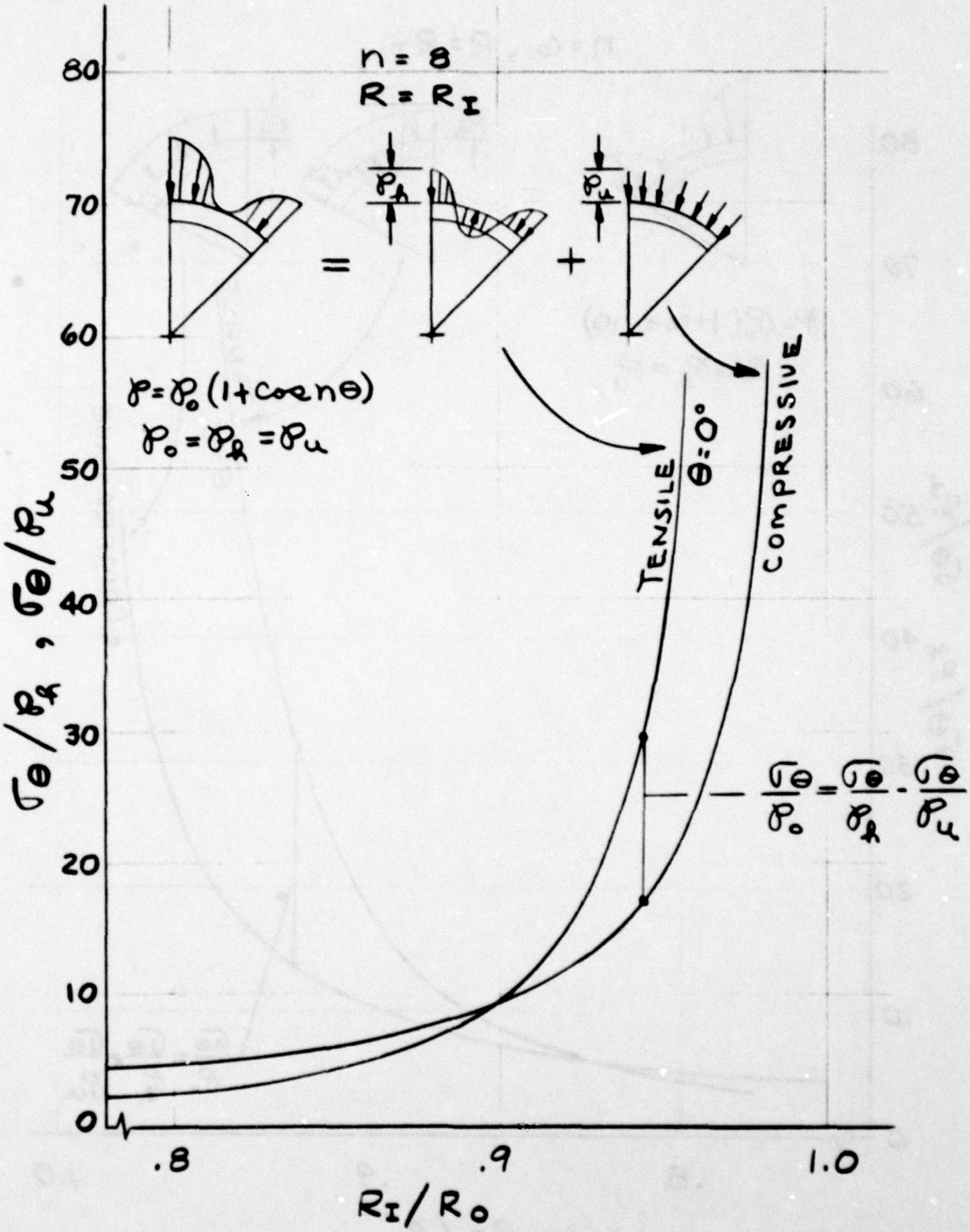

n = 8
R = R_I
p = p_0 (1 + cos nθ)
p_0 = p_i = p_u
=
+
p_i
p_u
σθ / p_i , σθ / p_u
80
70
60
50
40
30
20
10
0
.8
.9
1.0
R_I / R_o
TENSILE
θ = 0°
COMPRESSIVE
σθ / p_0 = σθ / p_i - σθ / p_u

Figure (2)

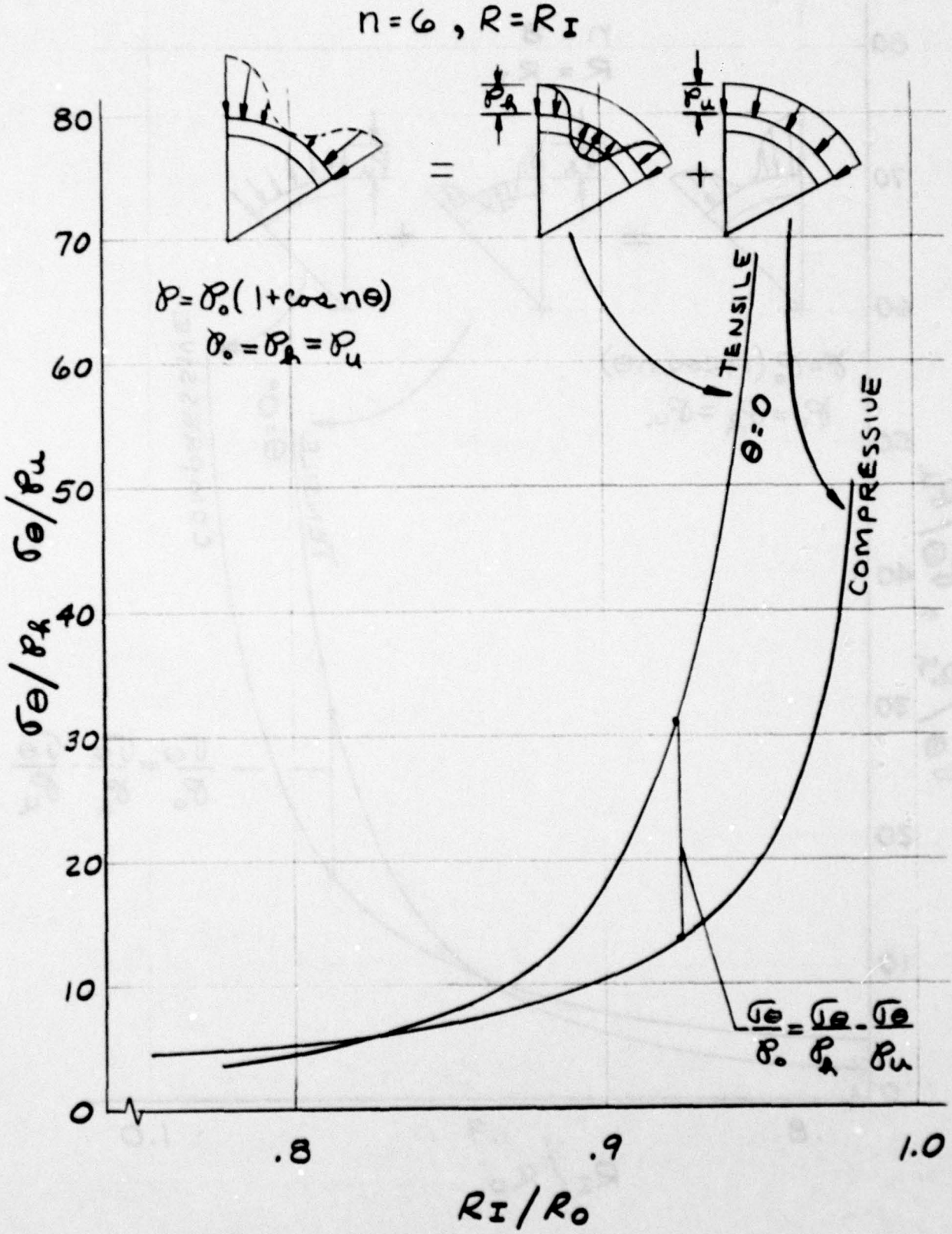

n=6 , R=RI
=
+
p=p0(1+cos nθ)
p0=pA=pU
80
70
60
50
40
30
20
10
0
σθ/pU
σθ/pA
TENSILE
θ=0
COMPRESSIVE
σθ/p0 = σθ/pA - σθ/pU
.8
.9
1.0
RI/R0

Figure (3)

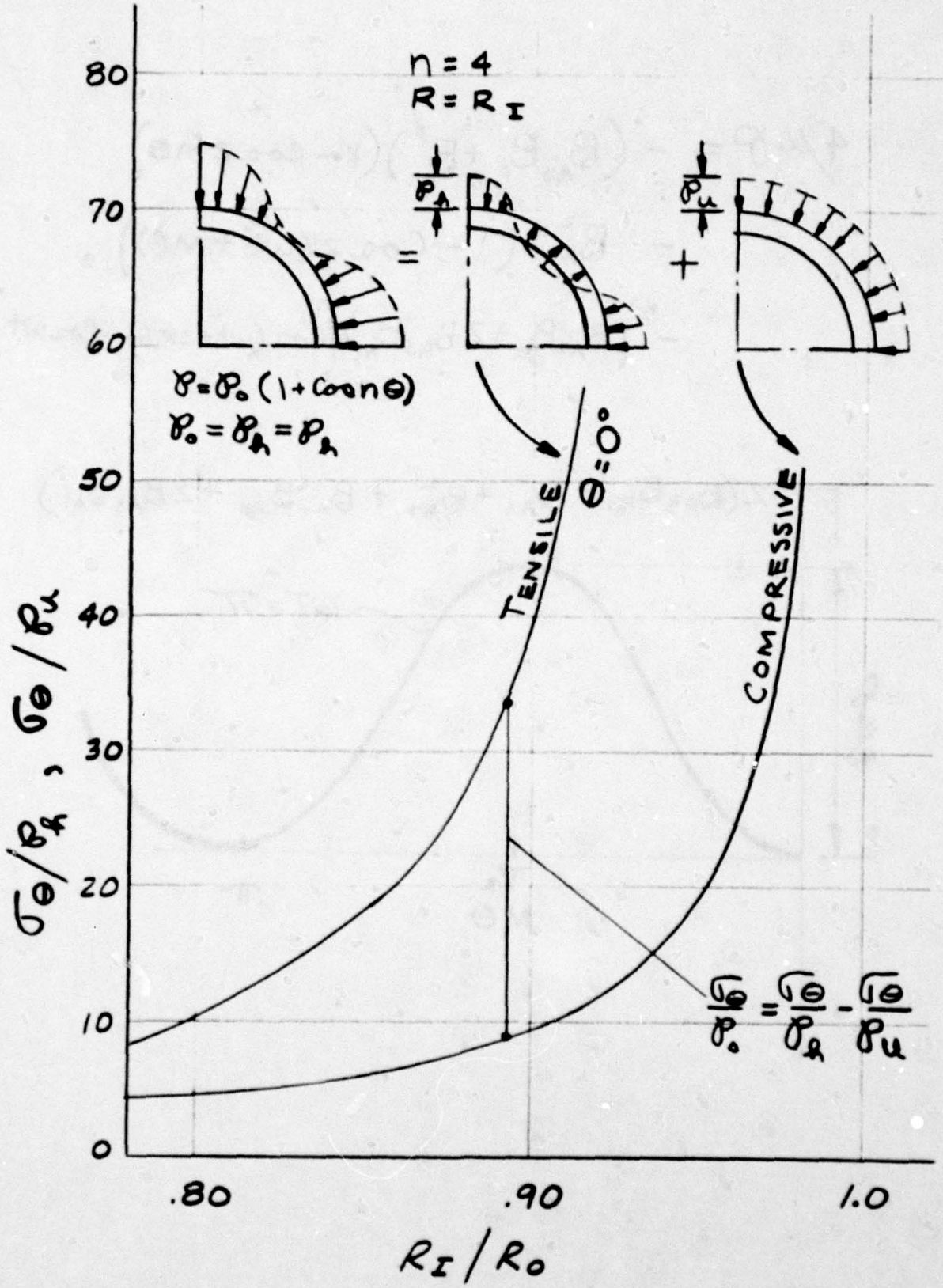
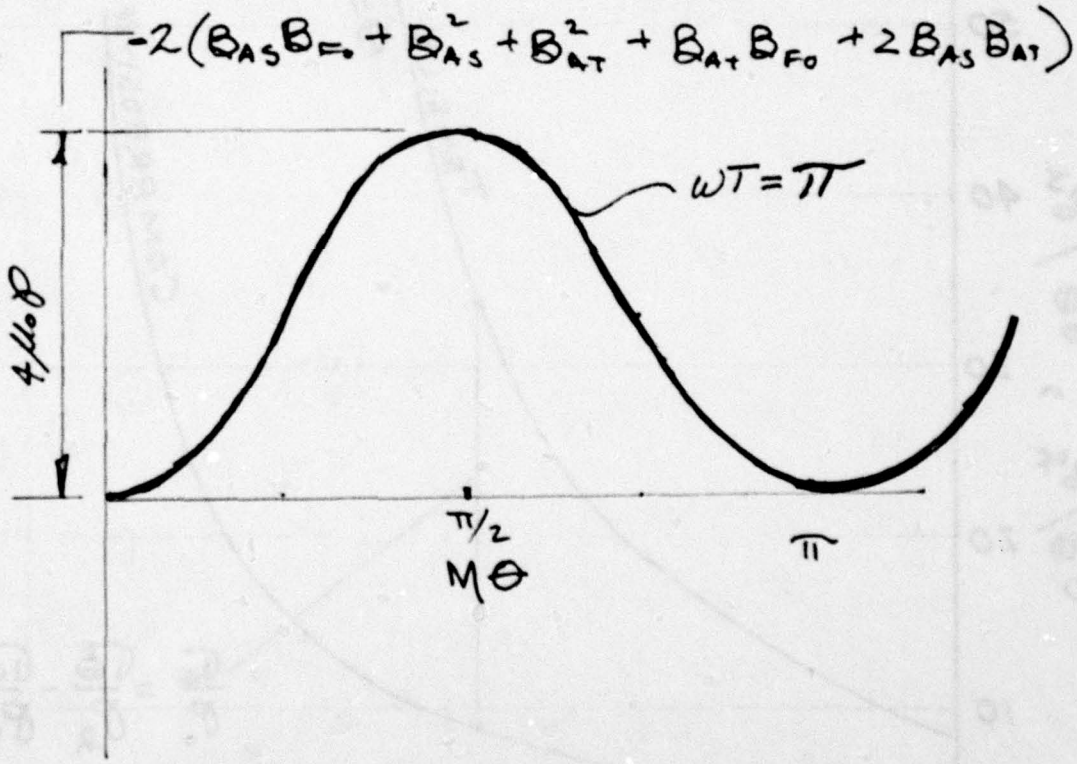

n = 4
R = R_I
p = p_o (1 + cos nθ)
p_o = p_A = p_H
=
+
TENSILE
COMPRESSIVE
θ = 0°
σ_θ / p_A , σ_θ / p_H
σ_θ / p_o = σ_θ / p_A - σ_θ / p_H
80
70
60
50
40
30
20
10
0
.80
.90
1.0
R_I / R_o

Figure (4)

$$4/\mu_0 \rho = -(B_{AS}B_F + B_{AS}^2)(1 - \cos 2M\theta)$$
$$- B_{AT}^2 (1 - \cos 2(\omega t + M\theta))$$
$$- (B_{AT}B_F + 2B_{AS}B_{AT})\{\cos(\omega t + 2M\theta) - \cos\omega t\}$$



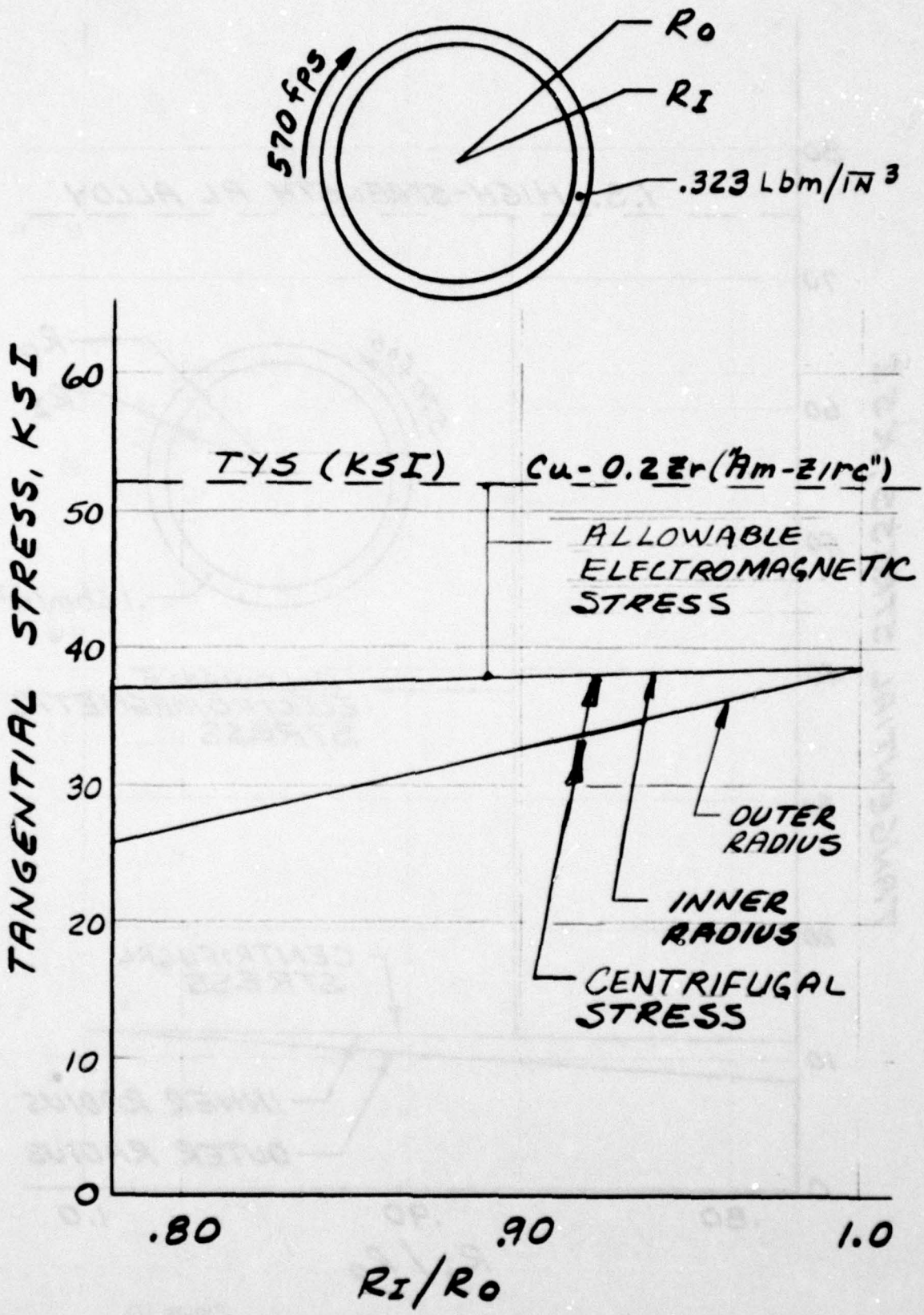

Ro
RI
570 fps
.323 Lbm/IN 3
TANGENTIAL STRESS, KSI
60
50
40
30
20
10
0
TYS (KSI)
Cu-0.2Zr("Am-Zirc")
ALLOWABLE ELECTROMAGNETIC STRESS
OUTER RADIUS
INNER RADIUS
CENTRIFUGAL STRESS
.80
.90
1.0
RI/Ro

Figure (6)

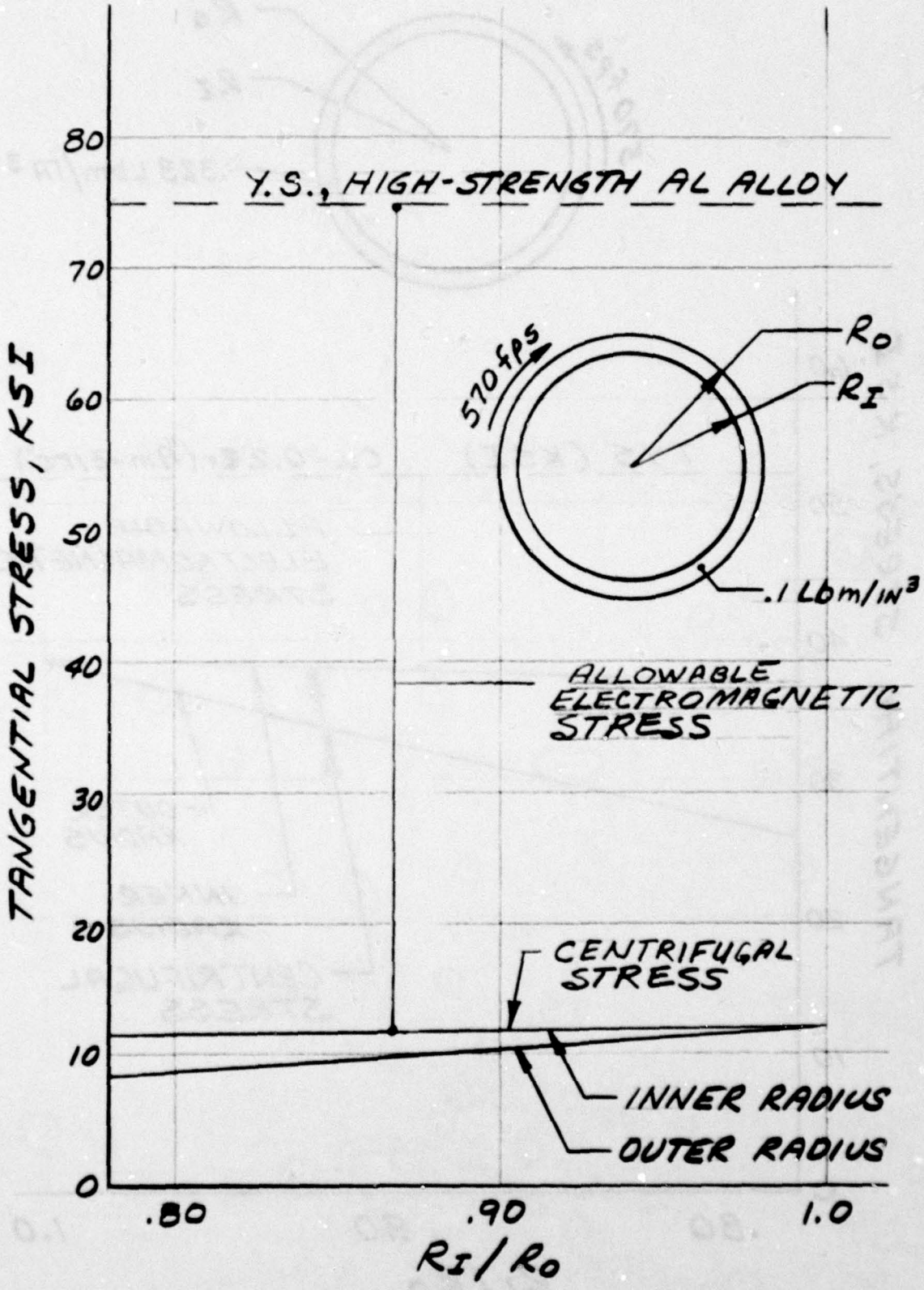

Y.S., HIGH-STRENGTH AL ALLOY
570 fps
R_O
R_I
.1 Lbm/in³
ALLOWABLE ELECTROMAGNETIC STRESS
CENTRIFUGAL STRESS
INNER RADIUS
OUTER RADIUS
TANGENTIAL STRESS, KSI
80
70
60
50
40
30
20
10
0
.80
.90
1.0
R_I/R_O

Figure (7)

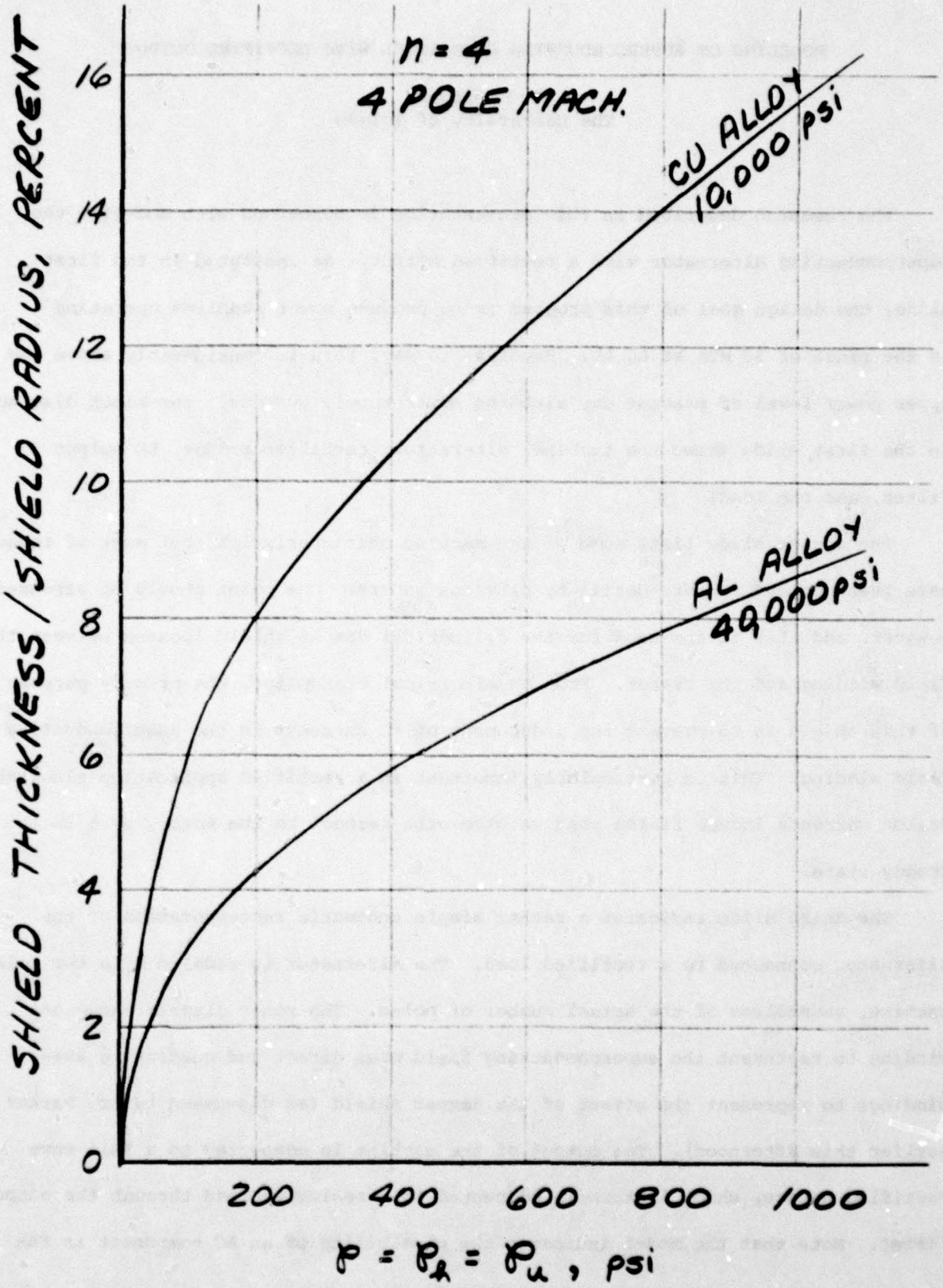

n = 4
4 POLE MACH.
CU ALLOY
10,000 psi
AL ALLOY
49000psi
SHIELD THICKNESS / SHIELD RADIUS, PERCENT
0
2
4
6
8
10
12
14
16
200
400
600
800
1000
P = P_l = P_u , psi

Figure (8)

MODELING OF SUPERCONDUCTING GENERATORS WITH RECTIFIED OUTPUT

T. A. Stuart
The University of Toledo

The research described in this presentation is concerned with modeling the superconducting alternator with a rectified output. As indicated in the first slide, the design goal of this program is to produce power supplies operating in the range of 50 MVA at 60 kV. Needless to say, this is considerably above the upper power level of present day airborne power supply systems. The block diagram in the first slide shows the turbine, alternator, rectifier bridge, LC output filter, and the load.

The second slide lists some of the machine characteristics, but most of these have been covered in more detail by previous papers. One point should be stressed however, and that is the need for the cylindrical damper shield located between the field winding and the stator. From an electrical standpoint, the primary purpose of this shield is to prevent the inducement of AC currents in the superconducting field winding. This is particularly important in a rectified application since the stator currents induce fields that revolve with respect to the rotor, even in the steady state.

The third slide indicates a rather simple schematic representation of the alternator connected to a rectified load. The alternator is modeled by a two pole machine, regardless of the actual number of poles. The rotor diagram shows one winding to represent the superconducting field plus direct and quadrature axes windings to represent the effect of the damper shield (as discussed by Dr. Parker earlier this afternoon). The output of the machine is connected to a full wave rectified bridge, which in turn is connected to a resistive load through the output filter. Note that the model indicates the possibility of an AC component in the

field current (i_f) which I will discuss further in a moment (the DC component of the field current is denoted by I_f). The model predicts a value of i_f which is relatively small; as pointed out in an earlier paper however, i_f may actually be zero if the correct parameters are used.

The standard model for the alternator is to consider the machine as six mutually coupled inductive circuits. The inductance matrix is shown in slide 4. This matrix indicates all of the self and mutual inductances, including those of the damper shield.

The fifth slide indicates the output voltage and current waveforms. There are two intervals that we are concerned with. The first is the 1-2 interval which we refer to as the conduction interval, and the second is the 2-3 interval which is referred to as the commutation interval. The conduction interval refers to the period where only 2 phases conduct. In the commutation interval all 3 phases conduct simultaneously. Since the filter inductor maintains a constant load current, you have a constant current in one phase, one phase is turning on, and the last is turning off during the commutation interval. The commutation angle is indicated by μ, and the angle at which commutation starts is indicated by β. Although the diagram indicates a β of 90°, it will actually be greater than this when the machine is loaded. One other variable of interest is the commutation current, i_k.

A number of aspects were considered in the process of modeling this machine, but today I'd like to concentrate on the determination of the steady state solution. Slide 6 indicates the approach which was used along with some of the approximations.

First of all we assume the average output voltage, the average load current, and the mechanical speed remain constant. One possibility for finding the steady state solution would be to derive a set of nonlinear differential equations from the inductance matrix and use an integration routine to find a numerical solution. A much easier approach, however, would be to use the method indicated by item 3 on the slide. In this approach we first assume that the flux linkage of each rotor

circuit remains constant. This type of formulation actually was proposed several years ago for conventional machines by Dr. Paul Franklin of the University of Missouri. Basically what we have done is taken the same approach as Franklin and applied it to the superconducting machine, while making some changes in the computational process.

Using this approach we come up with a set of five nonlinear simultaneous equations with five variables. The variables and equations are shown in slides 7 and 8, respectively (the coefficients for the equations are shown on slide 9). These five equations can be solved by some numerical technique such as the Newton-Raphson algorithm outlined on slide 10. I haven't given any indication as to how these five equations were derived, but this is shown in another paper which I'll mention at the end of the presentation.

To solve these five equations by the Newton-Raphson method, there is one catch in that we have to find a satisfactory starting point, $\underline{x}_o$. Finding this starting point is somewhat of a problem because it is difficult to physically interpret the W and V variables, which are integral functions of the commutation current. Because of this, it is difficult to estimate just exactly what initial values should be used for these two variables. On the other hand, β, μ and I_f have an obvious physical interpretation, meaning that adequate initial values could be predicted. However, instead of trying to guess any of the initial values, it is much easier to use a version of Franklin's equations to find an approximate starting point. These are shown in slide 11.

This brings up the primary difference between Franklin's analysis and the one used here. Franklin's original paper uses a linear approximation for the commutation current, i_k, that involves a linearization factor, K. It turns out that the value of K is load dependent and varies from 0.5 to 0.9. This means that Franklin's method requires that β, μ, I_f, W, V and K must all be evaluated in order to determine the final solution. In the approach used here, K is set equal to 1.0 simply to find an initial starting point. This value of K is adequate for this purpose, even though it

would not be sufficient for a final solution. Once a starting point is determined from the equation on slide 11, the five equations on slide 8 can be iterated to find the final values of β, μ, I_f, W and V.

Slide 12 indicates some of the other variables of interest that are included in this model. The first of these is an expression for the commutation current, i_k. Next is an expression for the AC component of the field current, i_f. However, it turns out this i_f calculation is very sensitive to slight errors in the inductance parameters. Because of this sensitivity, the accuracy of this equation is highly questionable. This also relates to Dr. Parker's earlier comment regarding a constraint on the values of the machine inductances. If this constraint were met exactly, the K_f term (defined on slide 9) would be equal to zero, indicating $i_f = 0$.

Two other variables that can be calculated are the currents in the equivalent direct and quadrature axes windings which represent the damper shield (i_d and i_q). These expressions are shown on slides 12 and 13.

The last two expressions on slide 13 indicate the instantaneous value of the voltage at the output of the rectifier bridge, v_o. The first expression is for the conduction interval, and the second is for the commutation interval. One of the main problems in this study was to obtain the minimum weight LC filter for a given amount of ripple voltage at the load. Using these last two expressions, it is possible to write a Fourier series to obtain the harmonics of v_o.

Next I would like to comment on a few of the results from our computer simulations. These results are based on the same Westinghouse superconducting alternator that was described in some of the earlier papers presented at this seminar. The inductance values and simulated loading conditions are shown on slide 14. These inductance parameters were calculated by Westinghouse and supplied to us by the Air Force.

Slide 15 shows a plot of the DC field current, I_f, vs. the load current, I_L. Slide 16 shows a plot of β and μ vs. I_L. This indicates that β increases from 90°

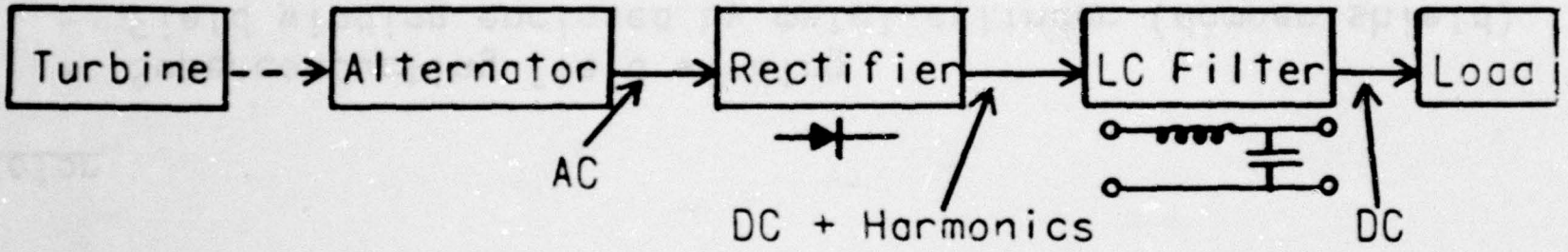
to about 100° as I_L increases from no load to full load (1420 A.D.C.). Likewise μ increases from 0° at no load to about 35° at full load. Slide 17 shows a plot of the first three AC harmonics of v_o vs. I_L.

The last slide (18) indicates some of the references which were used in this study. Reference [1] includes the details of the derivations while [2] describes the original work by Franklin. Reference [3] is one of several papers describing the Westinghouse superconducting machine used in the simulations.

RECTIFIED ALTERNATOR MODELLING

1. Airborne HVDC Power Supplies

   - Design Goal of 50 MVA/60 KV
   - Ultra-low Weight
   - Filtered DC Output



Superconducting Alternator with Rectified Output

II. Machine Characteristics

Stator

- 3 phase windings
- No iron between windings
- More space for insulation
- Higher output voltage

Rotor

- Superconducting field winding
- Field winding enclosed by metal cylinder (damper shield)
- Damper shield protects field winding from AC fields induced by armature currents

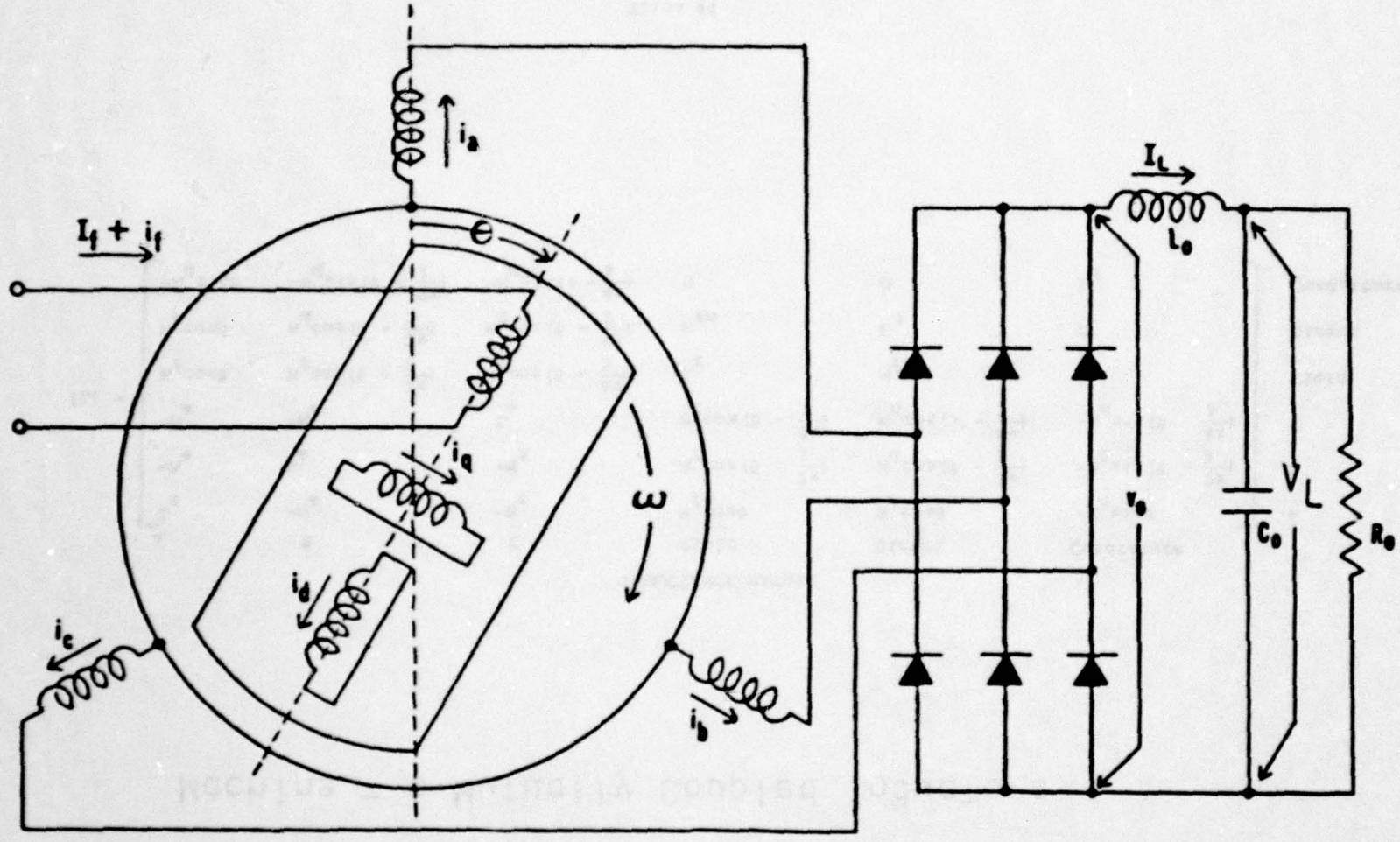
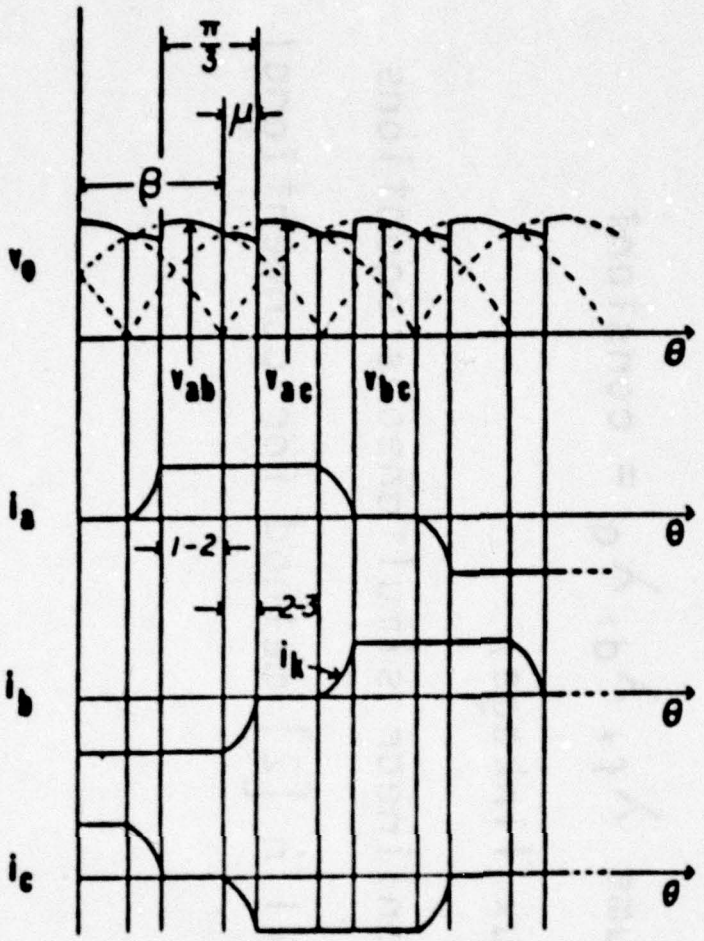


Fig. 1. Alternator-Rectifier Circuit

Machine = 6 Mutually Coupled Inductors

INDUCTANCE MATRIX

$$[L] = \begin{array}{c} \\ \text{A} \\ \text{B} \\ \text{C} \\ \text{Field} \\ \text{Direct} \\ \text{Quadrature} \end{array} \begin{array}{c} \begin{array}{ccccccc} \text{A} & \text{B} & \text{C} & \text{Field} & \text{Direct} & \text{Quadrature} \end{array} \\ \begin{bmatrix} L_a & -M_a & -M_a & M_f\cos\theta & M_d\cos\theta & -M_d\sin\theta \\ -M_a & L_a & -M_a & M_f\cos(\theta - \frac{2\pi}{3}) & M_d\cos(\theta - \frac{2\pi}{3}) & -M_d\sin(\theta - \frac{2\pi}{3}) \\ -M_a & -M_a & L_a & M_f\cos(\theta - \frac{4\pi}{3}) & M_d\cos(\theta - \frac{4\pi}{3}) & -M_d\sin(\theta - \frac{4\pi}{3}) \\ M_f\cos\theta & M_f\cos(\theta - \frac{2\pi}{3}) & M_f\cos(\theta - \frac{4\pi}{3}) & L_f & M_{fd} & 0 \\ M_d\cos\theta & M_d\cos(\theta - \frac{2\pi}{3}) & M_d\cos(\theta - \frac{4\pi}{3}) & M_{fd} & L_d & 0 \\ -M_d\sin\theta & -M_d\sin(\theta - \frac{2\pi}{3}) & -M_d\sin(\theta - \frac{4\pi}{3}) & 0 & 0 & L_d \end{bmatrix} \end{array} \begin{array}{l} \\ \text{A} \\ \text{B} \\ \text{C} \\ \text{Field} \\ \text{Direct} \\ \text{Quadrature} \end{array}$$



1-2 = Conduction interval

2-3 = Commutation interval

Figure 2. Output Voltage and Current Waveforms

III. Want Steady State Solution (details in [1])

1. V_L, I_L, speed = constant

2. Could derive nonlinear differential equations for system and solve numerically - very involved calculations

3. Instead of 2, assume $\lambda_f, \lambda_d, \lambda_q$ = constant

(λ = magnetic flux linkage)

- This yields 5 nonlinear simultaneous equations

- Similar to Franklin [2] method for conventional machines

4. Use these five variables

β = Angle at which commutation starts

μ = Commutation angle

I_f = DC field current

$$W = \int_{\beta}^{\beta+\mu} i_k(\theta) \sin(\theta)\, d\theta$$

$$V = \int_{\beta}^{\beta+\mu} i_k(\theta) \cos(\theta)\, d\theta$$

where, $i_k(\theta)$ = armature commutation current

θ = electrical angle

5. Five steady state equations

$$0 = \Delta_o W + A(\cos(\beta+\mu) - \cos\beta) + \frac{B}{4}(2\mu - \sin(2\beta + 2\mu) + \sin 2\beta)$$
$$+ \frac{C}{2}(\sin^2(\beta+\mu) - \sin^2\beta) \qquad (1)$$

$$0 = \Delta_o V + A(\sin\beta - \sin(\beta+\mu)) + \frac{B}{2}(\sin^2(\beta+\mu) - \sin^2\beta)$$
$$+ \frac{C}{4}(2\mu + \sin(2\beta + 2\mu) - \sin 2\beta) \qquad (2)$$

$$0 = -V_L + \frac{3\omega}{\pi}\left(\frac{3}{4} I_L \Delta_o + \sqrt{3}\, I_f M_f \sin(\beta+\mu)\right)$$
$$+ \frac{9M_o}{\pi}(W\sin(\beta+\mu) + V\cos(\beta+\mu)) \qquad (3)$$

$$0 = \frac{I_f}{\sqrt{3}\, I_L} M_f \cos\beta + \frac{3M_o}{\pi I_L}(W\cos\beta - V\sin\beta) + \frac{3M_o}{\pi}\cos\mu \qquad (4)$$

$$0 = -\Delta_o - \frac{4I_f}{\sqrt{3}\, I_L} M_f \cos(\beta + \tfrac{\mu}{2}) \sin(\tfrac{\mu}{2}) - \frac{6M_o}{\pi}\sin\mu$$
$$+ \frac{6M_o}{\pi I_L}[W(\sin\beta - \sin(\beta+\mu)) + V(\cos\beta - \cos(\beta+\mu))] \qquad (5)$$

(Coefficients defined on next page)

Coefficients:

$$K_q = \frac{M_d}{L_d} \quad , \quad K_f = \frac{M_f L_d - M_d M_{fd}}{L_f L_d - (M_{fd})^2} \quad , \quad K_d = \frac{M_d L_f - M_f M_{fd}}{L_f L_d - (M_{fd})^2}$$

$$M_o = K_f M_f + K_d M_d \quad , \quad \Lambda_f = 2\, M_o \quad , \quad \Delta_o = 4/3\,(L_a + M_a) - \Lambda_f$$

$$A = \frac{2}{\sqrt{3}} I_f M_f \sin\beta + \frac{6M_o}{\pi} (W\sin\beta + V\cos\beta - I_L \sin\mu)$$

$$B = \frac{2}{\sqrt{3}} I_f M_f + \frac{6M_o}{\pi} (W + I_L \cos(\beta+\mu))$$

$$C = \frac{6M_o}{\pi} (V - I_L \sin(\beta+\mu))$$

6. Use Newton-Raphson method to solve (1)-(5)

$$\underline{x} \equiv \begin{bmatrix} \beta \\ \mu \\ I_f \\ V \\ W \end{bmatrix}, \quad \underline{f}(\underline{x}_0) = \text{R.H.S. of } \begin{bmatrix} (1) \\ (2) \\ (3) \\ (4) \\ (5) \end{bmatrix}_{\underline{x}=\underline{x}_0}, F(\underline{x}) = \left.\frac{\partial \underline{f}(\underline{x})}{\partial \underline{x}}\right|_{\underline{x}=\underline{x}}$$

$\underline{x}_0$ = initial starting point

$F(\underline{x}_0)\ (\underline{x}-\underline{x}_0) \simeq \underline{f}(\underline{x}) - \underline{f}(\underline{x}_0)$

Solve for $\underline{x}$ until $|\underline{x}-\underline{x}_0| \leq$ convergence tolerance

7. Use Franklin's equations [2] to find x_o

$$W = -I_L \cos(\beta+\mu) + \frac{2I_L}{\mu} \sin(\mu/2) \cos(\beta+\mu/2) \tag{6}$$

$$V = -I_L \sin(\beta+\mu) - \frac{2I_L}{\mu} \sin(\mu/2) \cos(\beta+\mu/2) \tag{7}$$

$$\mu = \cos^{-1}\left[\frac{4\pi V_L - 9\omega I_L \Delta_o}{4\pi V_L + 9\omega I_L \Delta_o}\right] \tag{8}$$

$$\beta = \tan^{-1}\left[\frac{\pi\Delta_o\mu + 12\, M_o (\sin\frac{\mu}{2})^2\,(1-\cos\mu)}{12\, M_o \sin(\frac{\mu}{2}).\cos(\frac{\mu}{2})\,(1-\cos\mu)}\right] \tag{9}$$

$$I_f = \frac{1}{\sqrt{3}\, M_f \sin(\beta+\mu)}\left[\frac{\pi V_L}{3\omega} - \frac{3}{4} I_L\Delta_o - \frac{18\, I_L M_o}{\pi\mu}(\sin\tfrac{\mu}{2})^2\right] \tag{10}$$

IV. Other variables of interest

1. Commutation current, i_k

$$i_k = \frac{1}{\Delta_o}\left[\left(\frac{2M_f I_f}{\sqrt{3}} + \frac{6M_o W}{\pi}\right)(\sin\beta - \sin\theta) + \frac{6M_o V}{\pi}(\cos\beta - \cos\theta) - \frac{3I_L \Lambda_f}{\pi}(\sin\mu + \sin(\theta - \beta - \mu))\right]$$

2. AC field current, i_f (quite small but very sensitive to errors in machine parameters, accuracy is doubtful).

$$i_f = \sqrt{3}\, K_f \left[\frac{3}{\pi}(W + I_L \cos(\beta+\mu)) - I_L \cos(\theta+\pi/6) - i_k \sin\theta\right]$$

3. Direct axis current, i_d (equivalent current for direct axis of damper shield, cannot be measured)

$$i_d = \sqrt{3}\, K_d \left((3/\pi)[W + I_L \cos(\beta+\mu)] - [I_L \cos(\theta+\pi/6) + i_k \sin(\theta)]\right.$$

4. Quadrature axis current, i_q (equivalent current for quadrature axis of damper shield, cannot be measured)

$$i_q = \sqrt{3}\, K_q \{(3/\pi)[V - I_L \sin(\beta+\mu)] + [I_L \sin(\theta+\pi/6) - i_k \cos(\theta)]\}$$

5. Rectifier output voltage, v_o (used to determine output voltage harmonics).

Conduction interval (1-2)

$$v_{o12} = \omega[\sqrt{3}\, I_f M_f + (9/\pi)\, M_o W] \sin(\theta+\pi/6) + (9\omega/\pi)\, M_o V \cos(\theta+\pi/6) + (9\omega I_L M_o/\pi) \sin(\theta+\pi/6-\beta-\mu)$$

Commutation interval (2-3)

$$v_{o23} = v_{o12} + (\omega/\Delta_o)(3M_o/2-L_a-M_a)[(2M_f I_f/\sqrt{3} + 6M_o W/\pi)\cos\theta - (6M_o V/\pi)\sin\theta + (6I_L M_o/\pi) \cos(\theta-\beta-\mu)]$$

V. Numerical Results

4 pole, 400 Hz., 10 MVA/5 kV superconducting Westinghouse machine [3]

V_L = 6760 V. d.c. I_L = 1420 A. d.c.

L_f = 1.2 H. $M_f = 7.9 \times 10^{-3}$ H.

$L_d = 8.2 \times 10^{-8}$ H. $M_{fd} = 1.9 \times 10^{-4}$ H.

$L_a = 3.0 \times 10^{-4}$ H. $M_d = 3.8 \times 10^{-6}$ H.

$M_a = 1.5 \times 10^{-4}$ H.

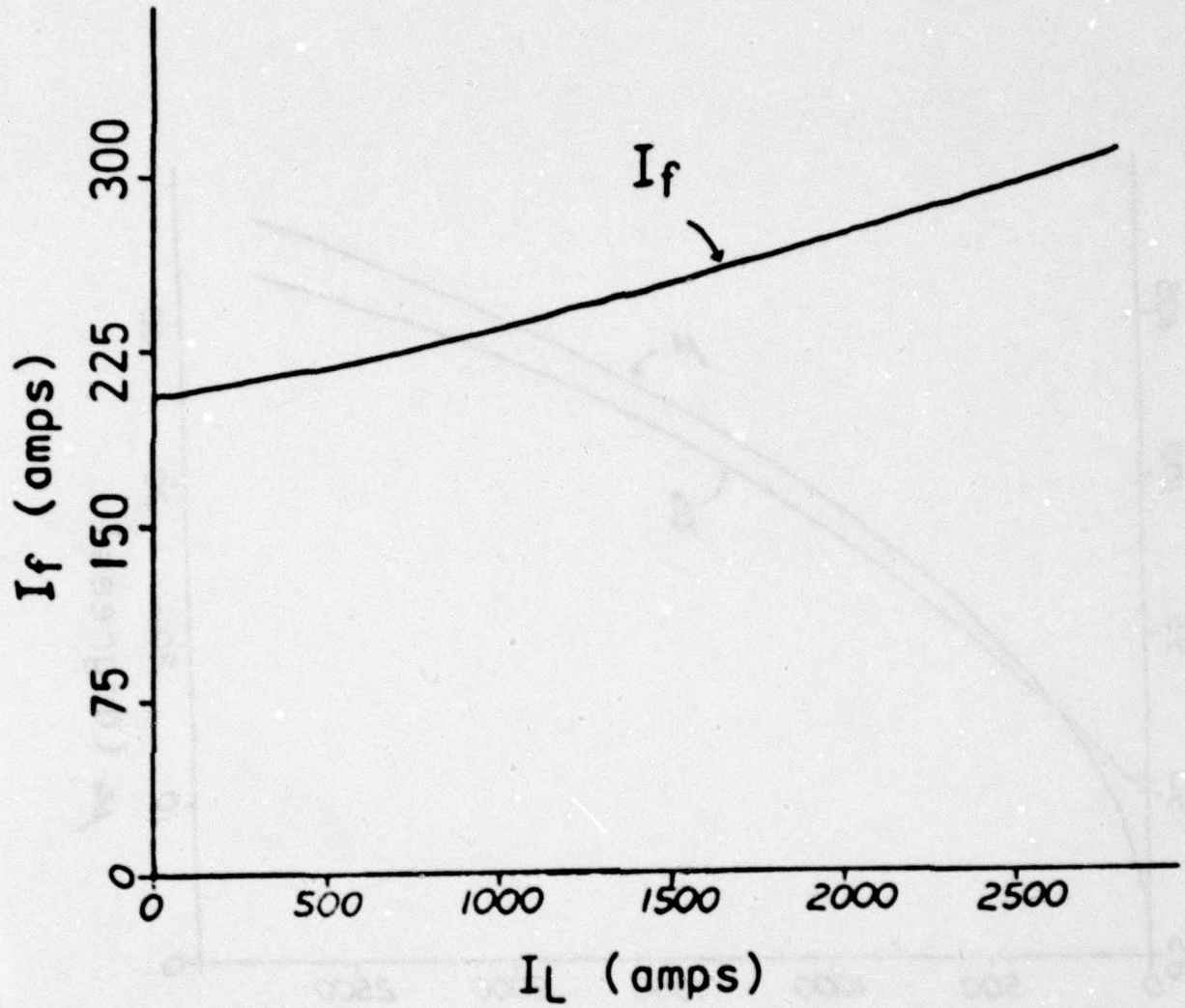


Figure 3. I_f vs. I_L

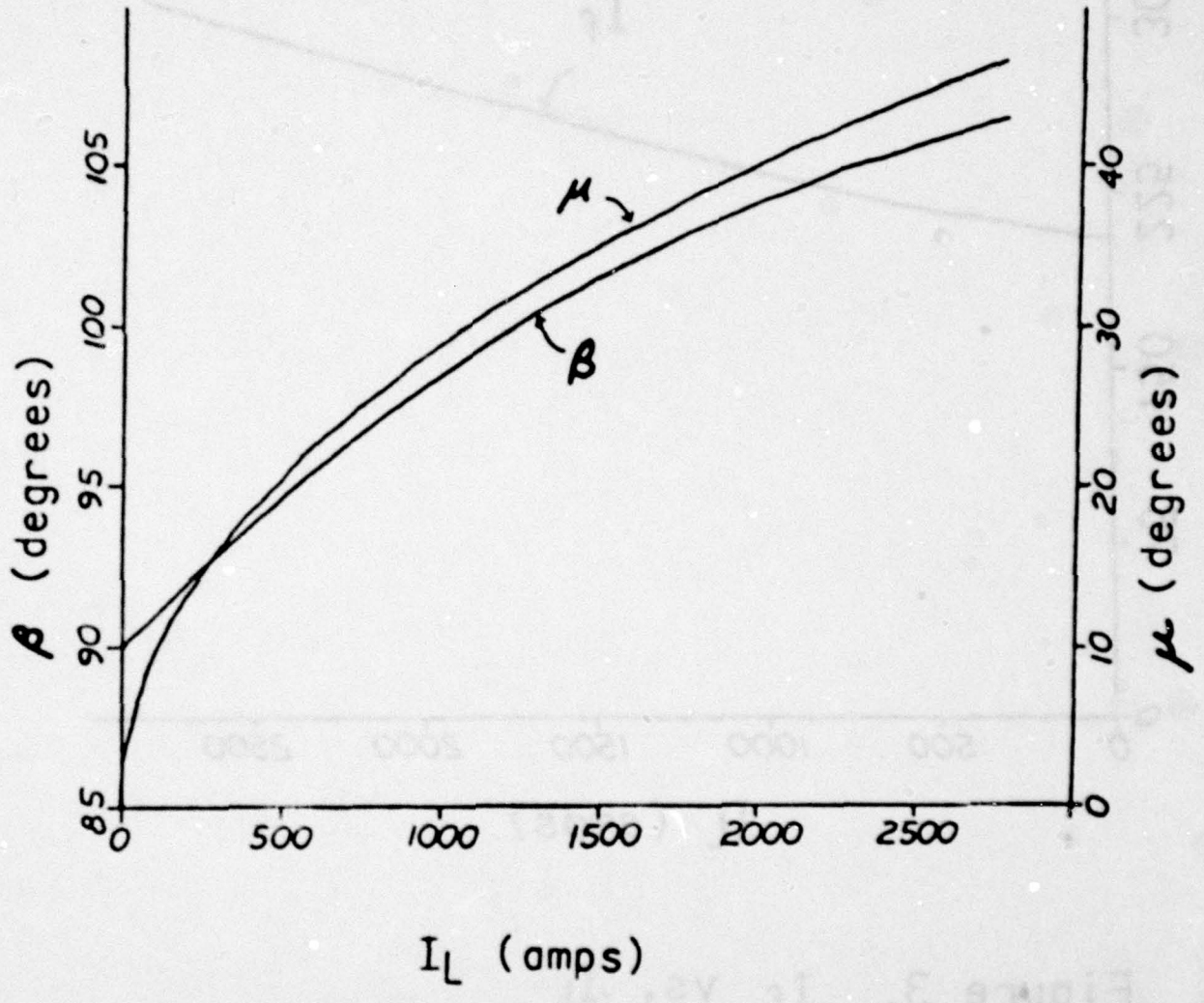


Figure 4. β and μ vs. I_L

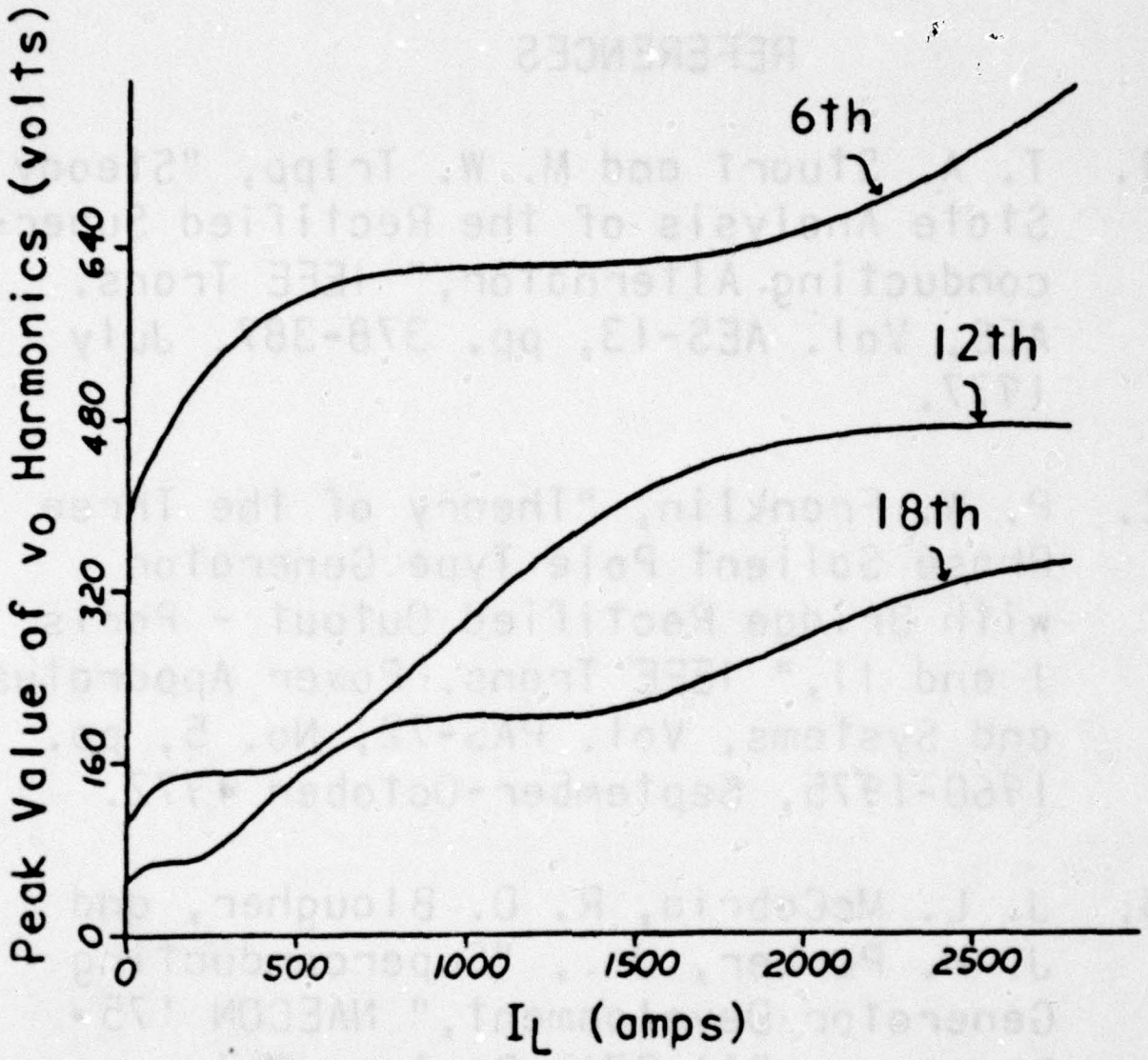


Figure 5. Harmonics of v_o vs. I_L

REFERENCES

1. T. A. Stuart and M. W. Tripp, "Steady State Analysis of the Rectified Superconducting Alternator," IEEE Trans. AES, Vol. AES-13, pp. 378-387, July 1977.

2. P. W. Franklin, "Theory of the Three Phase Salient Pole Type Generator with Bridge Rectified Output - Parts I and II," IEEE Trans. Power Apparatus and Systems, Vol. PAS-72, No. 5, pp. 1960-1975, September-October 1972.

3. J. L. McCabria, R. D. Blaugher, and J. H. Parker, Jr., "Superconducting Generator Development," NAECON '75 Rec., pp. 261-271, Dayton, Ohio, June 1975.

COMPUTER SIMULATION OF A 6-KVA AIRCRAFT ALTERNATOR AND COMPARISON OF TEST RESULTS

C.H. LEE
AiRESEARCH MANUFACTURING CO. OF CALIFORNIA, TORRANCE, CA

Recent generator applications call for accurate predictions of sub-cycle transient responses. The conventional approach of using transient and subtransient reactances and time constants is no longer adequate for this kind of transient analysis. The U.S. Air Force, in 1975, awarded a contract to the AiResearch Manufacturing Company of California, to test and to model in a digital computer a 6 KVA aircraft generator under transient load conditions.

The primary objective of this work was to demonstrate and to verify the alternator analytical methods and techniques utilized to attain the full-scale, larger-rating, lightweight alternator designs previously conducted by AiResearch for the Air Force. A secondary objective of this work was to demonstrate the ac resonant loading concept.

The alternator model adopted by AiResearch is the coupled-circuit configuration with lumped constants approach. The stator of the alternator is modeled by the actual three phase windings rather than its equivalent d-, q-, and 0-component circuits. This is because the actual phase quantities are more convenient to use. Also in case of severe non-linearity, the transformation and inverse transformation between phases a, b, c, and d, q, Q quantities can be very difficult. The damper winding is resolved into direct and quadrature components because of the saliency of the rotor. Only one direct and one quadrature damper circuits are used. This is one source of error in the simulation. The alternator model is shown in Figure 1.

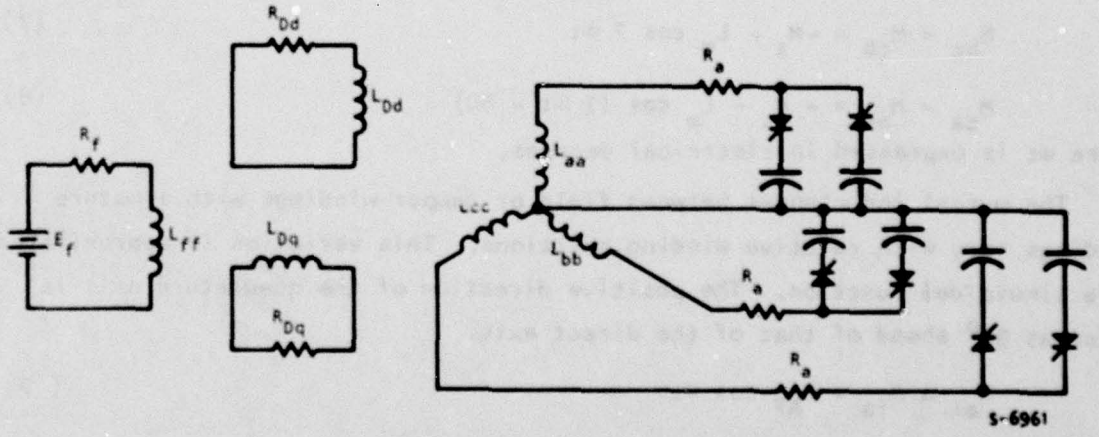


FIGURE 1. Alternator Model

The matrix equation for the six-circuit model is given by:

$$\frac{d}{dt}(\tilde{M}I) + \tilde{R}I + V = E \qquad (1)$$

Since inductances are affected by saturation, Equation 1 can be written as

$$\frac{d}{dt}\left[(\tilde{L}_1 + f\tilde{M}_s)I\right] + \tilde{R}I + V = E \qquad (2)$$

Definitions of the symbols and matrixes can be found in Appendix I.

Accuracy of the performance prediction depends on the accuracy of the alternator constants used in the above differential equations. AiResearch Mfg. Co., through years of experience, has developed a computer program to calculate alternator constants that can produce good steady state performance predictions. These constants were also used in this model analysis.

The alternator under consideration has a round, solid rotor. Uneven slotting gives a slight saliency to the machine. Damping effect comes from eddy currents induced in the solid rotor structure.

The self and mutual inductances of the armature windings can be approximated by the following expressions (the saliency is approximated by a double-frequency sinusoidal term.)

$$L_{aa} = L_s + L_m \cos 2\omega t \tag{3}$$

$$L_{bb} = L_s + L_m \cos (2\omega t + 120) \tag{4}$$

$$L_{cc} = L_s + L_m \cos (2\omega t - 120) \tag{5}$$

$$M_{ab} = M_{ba} = -M_s - L_m \cos (2\omega t + 60) \tag{6}$$

$$M_{bc} = M_{cb} = -M_s + L_m \cos 2\omega t \tag{7}$$

$$M_{ca} = M_{ac} = -M_s - L_m \cos (2\omega t - 60) \tag{8}$$

where ωt is expressed in electrical degrees.

The mutual inductances between field or damper windings with armature windings vary with relative winding positions. This variation is approximated by a sinusoidal function. The positive direction of the quadrature axis is taken as 90° ahead of that of the direct axis.

$$M_{af} = M_{fa} = M_{AF} \cos \omega t \tag{9}$$

$$M_{bf} = M_{fb} = M_{AF} \cos (\omega t - 120) \tag{10}$$

$$M_{cf} = M_{fc} = M_{AF} \cos (\omega t + 120) \tag{11}$$

$$M_{aDd} = M_{Dda} = M_{ADD} \cos \omega t \tag{12}$$

$$M_{bDd} = M_{Ddb} = M_{ADD} \cos (\omega t - 120) \tag{13}$$

$$M_{cDd} = M_{Ddc} = M_{ADD} \cos(\omega t + 120) \tag{14}$$

$$M_{aDq} = M_{Dqa} = M_{ADQ} \cos(\omega t + 90) \tag{15}$$

$$M_{bDq} = M_{Dqb} + M_{ADQ} \cos(\omega t - 30) \tag{16}$$

$$M_{cDq} = M_{Dqc} = M_{ADQ} \cos(\omega t + 210) \tag{17}$$

Other mutual inductances are

$$M_{fDd} = M_{Ddf} = \text{a constant } M_{FDD} \tag{18}$$

$$M_{fDq} = M_{Dqf} = 0 \tag{19}$$

$$M_{DdDq} = M_{DqDd} = 0 \tag{20}$$

Calculations of the self and mutual inductances as well as the saturation effects are given in Appendix II.

Two approaches were used to solve the set of differential equations describing the six-circuit model: (1) the SCEPTRE program and (2) an AiResearch program.

Equation (2) can be written as:

$$(\tilde{L}_1 + f\tilde{M}_s)\frac{dI}{dt} + f\frac{d\tilde{M}_s}{dt}I + \frac{df}{dt}\tilde{M}_s I + \tilde{R}I + V = E \tag{21}$$

where

$$\frac{df}{dt} = \frac{df}{d(MMF)} \cdot \frac{d(MMF)}{dt} \tag{22}$$

$$\frac{d(MMF)}{dt} = \frac{MMF_d}{MMF} \cdot \frac{d(MMF_d)}{dt} + \frac{MMFq}{MMF} \cdot \frac{d(MMFq)}{dt} \tag{23}$$

and

$$\frac{d(MMF_d)}{dt} = \frac{di_f}{dt} + k_{af}\frac{di_{Dd}}{dt} + \frac{k_{af}}{2}\left[\frac{di_a}{dt}\cos\omega t + \frac{di_b}{dt}\cos(\omega t - 120) + \frac{di_c}{dt}\cos(\omega t + 120)\right] - \omega\frac{k_{af}}{2}\left[i_a \sin\omega t + i_b \sin(\omega t - 120) + i_c \sin(\omega t + 120)\right] \tag{24}$$

$$\frac{d(MMFq)}{dt} = k_{af}\frac{di_{Dq}}{dt} - \frac{k_{af}}{2}\left[\frac{di_a}{dt}\sin\omega t + \frac{di_b}{dt}\sin(\omega t - 120) + \frac{di_c}{dt}\sin(\omega t + 120)\right] - \omega\frac{k_{af}}{2}\left[i_a\cos\omega t + i_b\cos(\omega t - 120) + i_c\cos(\omega t+120)\right] \quad (25)$$

Substituting equations (48) through (50) into equation (47)

$$\frac{df}{dt} = C_a\frac{di_a}{dt} + C_b\frac{di_b}{dt} + C_c\frac{di_c}{dt} + C_f\frac{di_f}{dt} + C_{Dd}\frac{di_{Dd}}{dt} + C_{Dq}\frac{di_{Dq}}{dt} + C_x \quad (26)$$

Let $$\frac{df}{d(MMF)} = f' \quad (27)$$

$$\frac{MMF_d}{MMF} = P_d \qquad \frac{MMF_q}{MMF} = P_q \quad (28)$$

then

$$C_a = f'\frac{k_{af}}{2}(P_d\cos\omega t - P_q\sin\omega t) \quad (29)$$

$$C_b = f'\frac{k_{af}}{2}\left[P_d\cos(\omega t - 120) - P_q\sin(\omega t - 120)\right] \quad (30)$$

$$C_c = f'\frac{k_{af}}{2}\left[P_d\cos(\omega t + 120) - P_q\sin(\omega t + 120)\right] \quad (31)$$

$$C_f = f'P_d \quad (32)$$

$$C_{Dd} = f'P_d k_{af} \quad (33)$$

$$C_{Dq} = f'P_q k_{af} \quad (34)$$

$$C_x = -f'\omega\frac{k_{af}}{2}\left\{P_d\left[i_a\sin\omega t + i_b\sin(\omega t - 120) + i_c\sin(\omega t + 120)\right] + P_q\left[i_a\cos\omega t + i_b\cos(\omega t-120) + i_c\cos(\omega t + 120)\right]\right. \quad (35)$$

SCEPTRE PROGRAM APPROACH

Since $\frac{df}{dt}$ contains derivatives of state variables (i.e., $\frac{di_a}{dt}$, etc.) the term $\frac{df}{dt}\tilde{M}_s I$ must be included in SCEPTRE as a fictitious voltage:

$$(\tilde{L}_1 + f\tilde{M}_s)\frac{dI}{dt} + \tilde{R}I = (E - f\frac{d\tilde{M}s}{dt}i - \tilde{M}s\frac{df}{dt}I - V) \quad (36)$$

Iteration and numerical integration can then be carried out like an ordinary SCEPTRE problem.

AIRESEARCH PROGRAM APPROACH

Let

$$\tilde{M}_s I = \begin{bmatrix} Y_1 \\ Y_2 \\ Y_3 \\ Y_4 \\ Y_5 \\ Y_6 \end{bmatrix} \tag{37}$$

then

$$\frac{df}{dt} \tilde{M}_s I = \tilde{C} \frac{dI}{dt} + C_X \tilde{M}_s I \tag{38}$$

where

$$\tilde{C} = \begin{bmatrix} C_a Y_1 & C_b Y_1 & C_c Y_1 & C_f Y_1 & C_{Dd} Y_1 & C_{Dq} Y_1 \\ C_a Y_2 & C_b Y_2 & C_c Y_2 & C_f Y_2 & C_{Dd} Y_2 & C_{Dq} Y_2 \\ C_a Y_3 & C_b Y_3 & C_c Y_3 & C_f Y_3 & C_{Dd} Y_3 & C_{Dq} Y_3 \\ C_a Y_4 & C_b Y_4 & C_c Y_4 & C_f Y_4 & C_{Dd} Y_4 & C_{Dq} Y_4 \\ C_a Y_5 & C_b Y_5 & C_c Y_5 & C_f Y_5 & C_{Dd} Y_5 & C_{Dq} Y_5 \\ C_a Y_6 & C_b Y_6 & C_c Y_6 & C_f Y_6 & C_{Dd} Y_6 & C_{Dq} Y_6 \end{bmatrix} \tag{39}$$

and C_x is given in Equation (60)

Equation (46) then becomes

$$(\tilde{L}_1 + f\tilde{M}_s + \tilde{C}) \frac{dI}{dt} = E - V - (\tilde{R} + f \frac{d\tilde{M}_s}{dt} + C_x \tilde{M}_s) I \tag{40}$$

A modified Euler technique can now be used to integrate and solve this set of differential equations. The matrix $\tilde{C}$ is in general nonsymmetrical, and is added to the symmetrical inductance matrix $(\tilde{L}_1 + f\tilde{M}_s)$. The resultant matrix is therefore also nonsymmetrical. This is the basic reason the SCEPTRE program cannot solve Equation (40).

Since no circuit change is allowed in SCEPTRE, the thyristor switches are simulated by resistors that change in value depending on the direction of current flow. This requires extra computer time to iterate into current values. It also results in leakage currents through resistors that do not actually exist. This current leakage decreases the accuracy of the solution.

The AiResearch program needs no iteration. It actually simulates the switching phenomena and also uses much less computer time than the SCEPTRE program.

Figures 2, 3, and 4 are computer plots of transient response for cases of suddenly applied load, single line to ground fault and one line open respectively. The dotted lines show the envelopes of the test results. As can be seen from the figures, the transient performance predicted by the model is in reasonable agreement with the test results.

It is therefore concluded that the above described model can be used to predict the sub-cycle transient performances of a 3-phase alternator. The formulas for calculating machine inductances are also adequate for transient analysis purposes.

To design an alternator for a specific transient application, the modeling technique described in the paper should be used as a tool in addition to the traditional procedures.

The SCEPTRE program developed by the Air Force is capable of solving the alternator/load model cases and can do so with good accuracy; but the computer time requirement is somewhat excessive. The AiResearch program is shorter and faster.

More detailed discussion can be found in the report, Number AFWL-TR-75-66, Addendum 2, "Subsystem Design Analysis Report for Lightweight Alternator (Model Alternator Test and Computer Simulation)", June 30, 1976, prepared for Air Force Special Weapons Center, Kirkland AFB, New Mexico 87117, Contract No. F29601-74-C-0055.

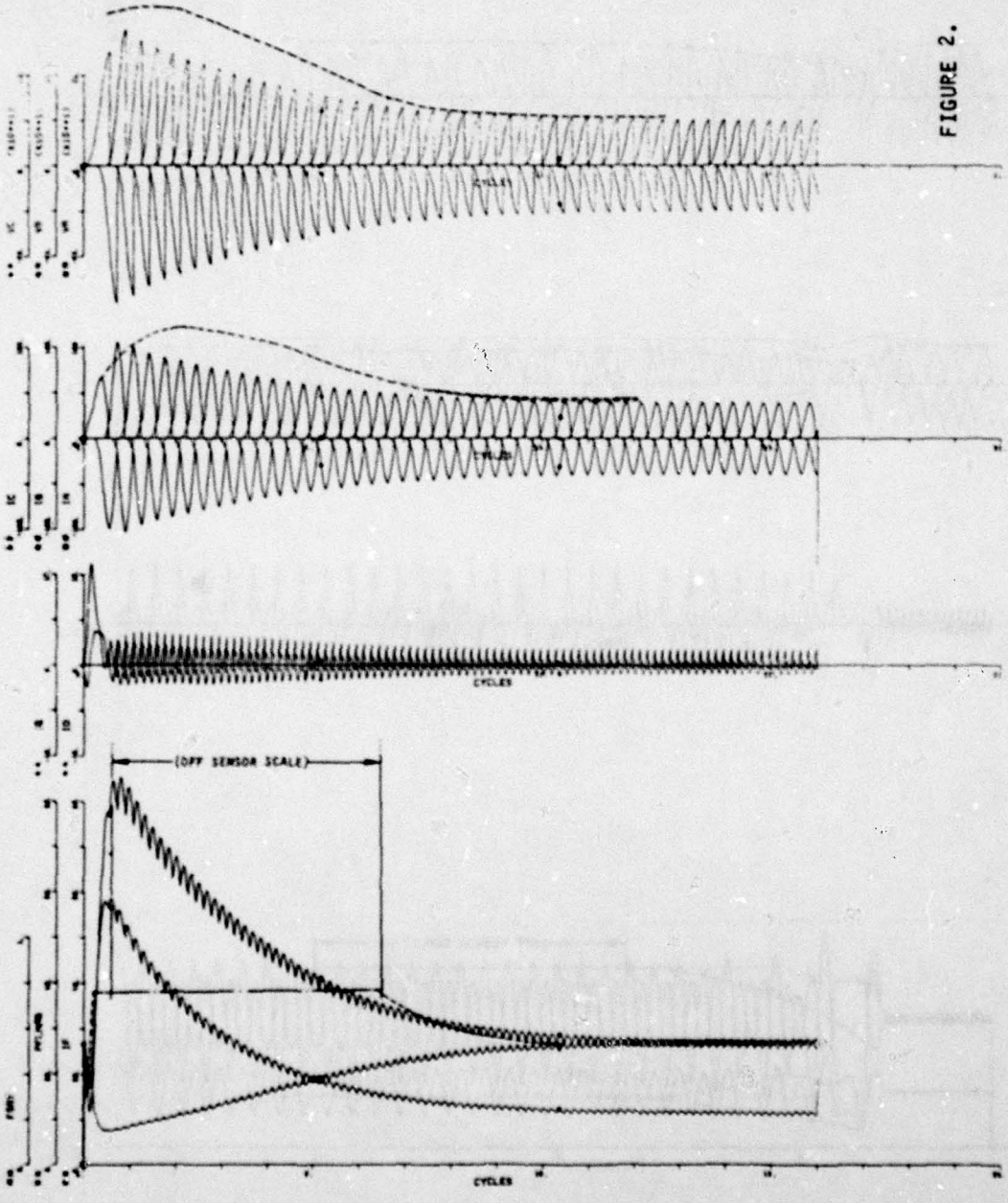


FIGURE 2. Transient Response - Suddenly Applied Load

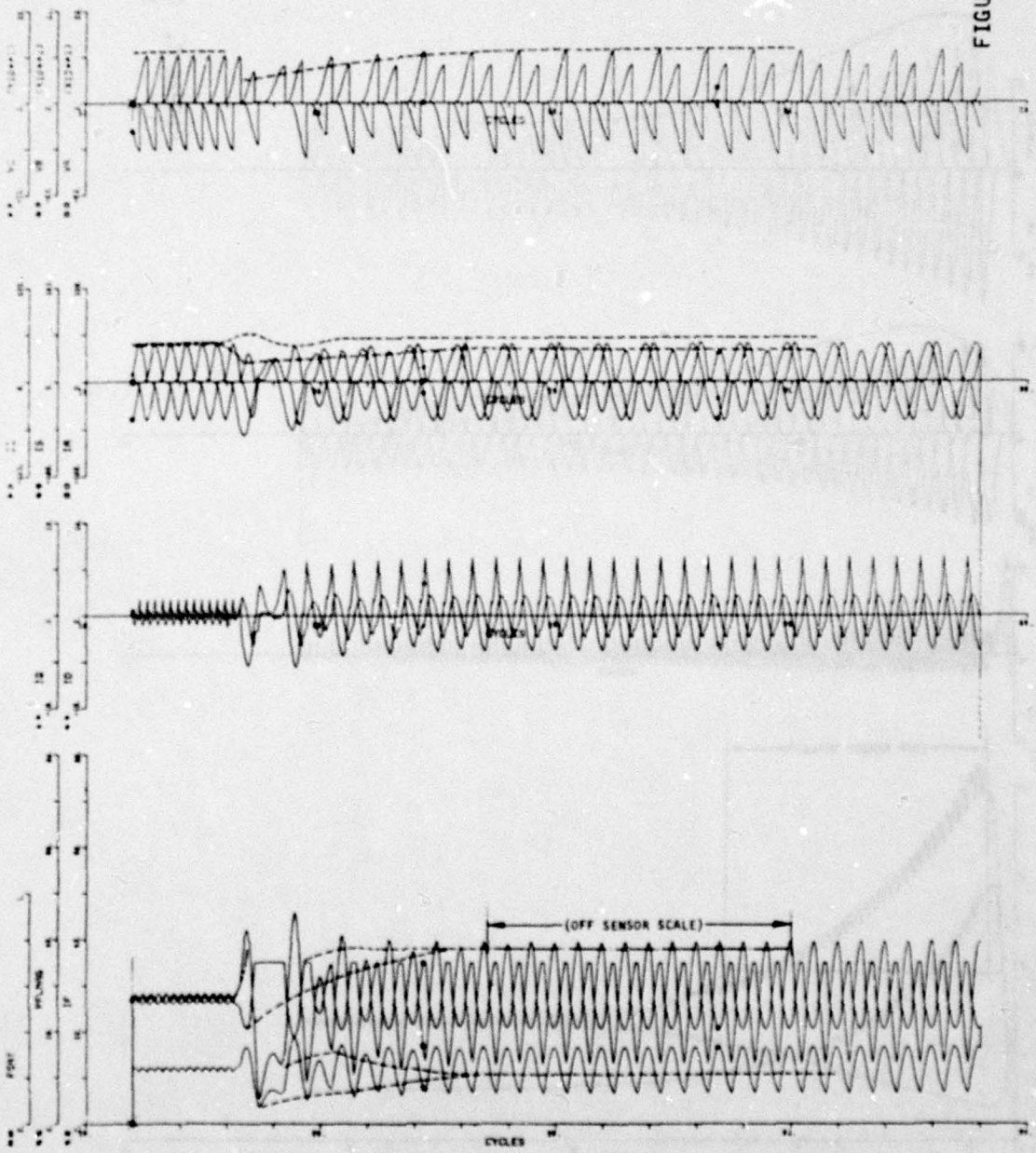


FIGURE 3. Single Line to Ground Short

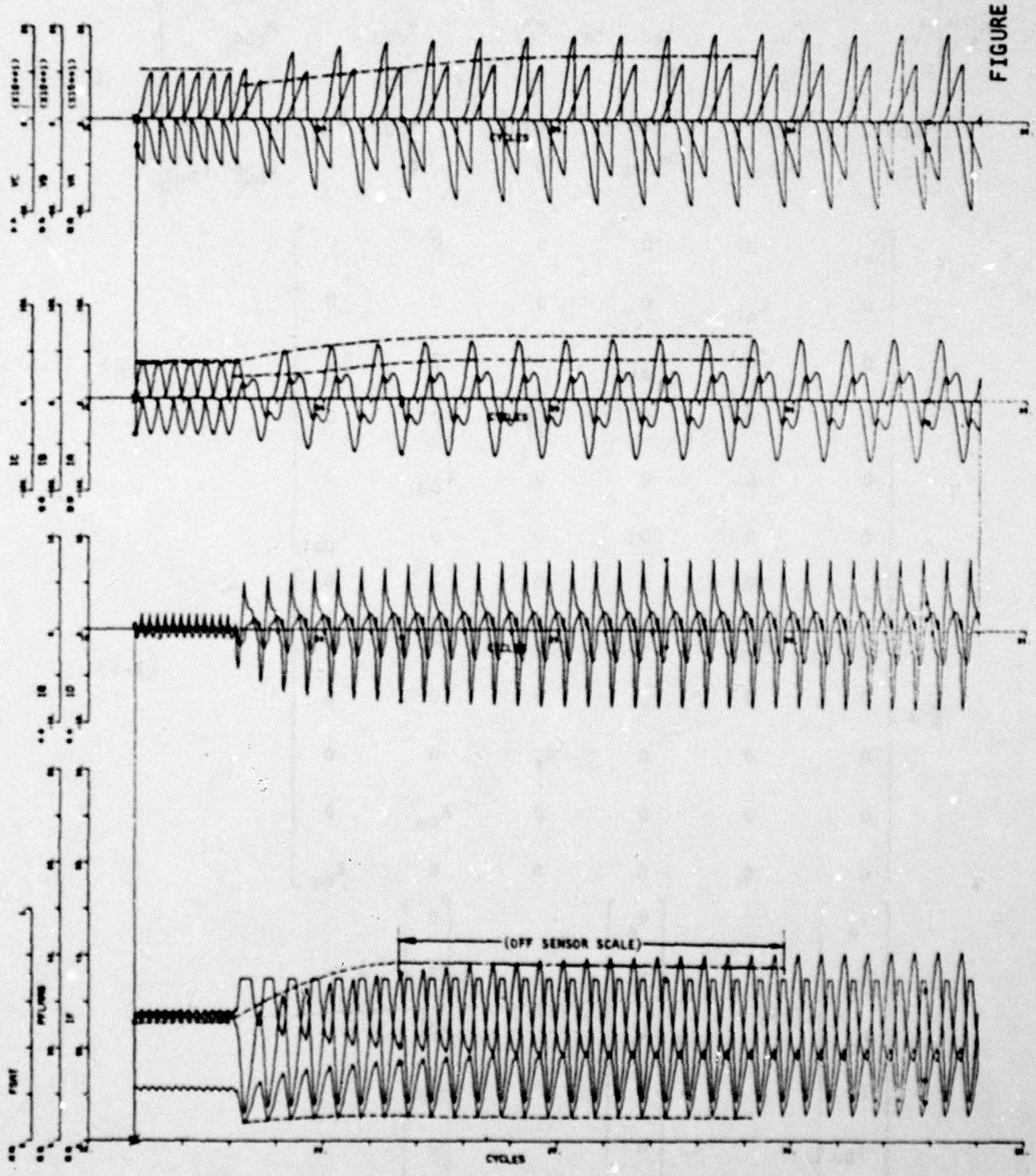


FIGURE 4. One Line Open

APPENDIX I
NOMENCLATURES AND MATRIXES

The matrixes in Equation (2) of the main paper are as follows:

$$\tilde{M}_s = \begin{bmatrix} L_{aa} - L_{al} & M_{ab} & M_{ac} & M_{af} & M_{aDd} & M_{aDq} \\ M_{ab} & L_{bb} - L_{al} & M_{bc} & M_{bf} & M_{bDd} & M_{bDq} \\ M_{ac} & M_{bc} & L_{cc} - L_{al} & M_{cf} & M_{cDd} & M_{cDq} \\ M_{af} & M_{bf} & M_{cf} & L_{ff} - L_{fl} & M_{fDd} & 0 \\ M_{aDd} & M_{bDd} & M_{cDd} & M_{fDd} & L_{Dd} - L_{Ddl} & 0 \\ M_{aDq} & M_{bDq} & M_{cDq} & 0 & 0 & L_{Dq} - L_{Dql} \end{bmatrix} \quad \text{(I-1)}$$

$$\tilde{L}_l = \begin{bmatrix} L_{al} & 0 & 0 & 0 & 0 & 0 \\ 0 & L_{al} & 0 & 0 & 0 & 0 \\ 0 & 0 & L_{al} & 0 & 0 & 0 \\ 0 & 0 & 0 & L_{fl} & 0 & 0 \\ 0 & 0 & 0 & 0 & L_{Ddl} & 0 \\ 0 & 0 & 0 & 0 & 0 & L_{Dql} \end{bmatrix} \quad \text{(I-2)}$$

$$\tilde{R} = \begin{bmatrix} R_a & 0 & 0 & 0 & 0 & 0 \\ 0 & R_a & 0 & 0 & 0 & 0 \\ 0 & 0 & R_a & 0 & 0 & 0 \\ 0 & 0 & 0 & R_f & 0 & 0 \\ 0 & 0 & 0 & 0 & R_{Dd} & 0 \\ 0 & 0 & 0 & 0 & 0 & R_{Dq} \end{bmatrix} \quad \text{(I-3)}$$

$$I = \begin{bmatrix} i_a \\ i_b \\ i_c \\ i_f \\ i_{Dd} \\ i_{Dq} \end{bmatrix} \quad \text{(I-4)} \qquad V = \begin{bmatrix} V_a \\ V_b \\ V_c \\ 0 \\ 0 \\ 0 \end{bmatrix} \quad \text{(I-5)} \qquad E = \begin{bmatrix} 0 \\ 0 \\ 0 \\ E_f \\ 0 \\ 0 \end{bmatrix} \quad \text{(I-6)}$$

also $\frac{dV_a}{dt} = \frac{i_a}{C}$ (I-7)

$\frac{dV_b}{dt} = \frac{i_b}{C}$ (I-8)

$\frac{dV_c}{dt} = \frac{i_c}{C}$ (I-9)

Conventional alternator design programs calculate the direct and quadrature machine constants such as X_d, X_q, X_{al}, X'_d, X''_d, X'_q, X_{Dd}, X_{Dq}, X_{Ddl}, X_{Dql}, X_2, X_0, X_{fl} and L_{ff},

as well as a predicted no-load saturation curve. From these values, the following unsaturated machine inductances can be obtained:

L_d	Direct axis inductance, H
L_q	Quadrature axis inductance, H
L_{al}	Armature leakage inductance per phase, H
L'_d	Direct axis transient inductance, H
L''_d	Direct axis subtransient inductance, H
L''_q	Quadrature axis subtransient inductance, H
L_{Dd}	Direct axis damper winding inductance, H
L_{Dq}	Quadrature axis damper winding inductance, H
L_{Ddl}	Direct axis damper winding leakage inductance, H
L_{Dql}	Quadrature axis damper winding leakage inductance, H
L_2	Negative sequence inductance, H
L_o	Zero sequence inductance, H
L'_{fl}	Field winding leakage inductance, in terms of armature, H
L_{ff}	Field winding self-inductance (in its own term), H

The inductances and resistance of the alternator model are as follows. (These inductances can be derived from the direct and quadrature axes inductances listed above).

L_{aa}	Self inductance of armature winding phase A, H
L_{bb}	Self inductance of armature winding phase B, H
L_{cc}	Self inductance of armature winding phase C, H

M_{ab}, M_{ba}	Mutual inductance between armature windings A and B, H
M_{bc}, M_{cb}	Mutual inductance between armature windings B and C, H
M_{ca}, M_{ac}	Mutual inductance between armature windings C and A, H
L_{ff}	Self inductance of field winding, in its own term, H
L_{Dd}	Self inductance of direct damper winding, in armature terms, H
L_{Dq}	Self inductance of quadrature damper winding, in armature terms, H
M_{af}, M_{fa}	Mutual inductance between field and armature winding Phase A, H
M_{bf}, M_{fb}	Mutual inductance between field and armature winding Phase B, H
M_{cf}, M_{fc}	Mutual inductance between field and armature winding Phase C, H
M_{aDd}, M_{Dda}	Mutual inductance between direct damper and armature winding Phase A, H
M_{bDd}, M_{Ddb}	Mutual inductance between direct damper and armature winding Phase B, H
M_{cDd}, M_{Ddc}	Mutual inductance between direct damper and armature winding Phase C, H
M_{aDq}, M_{Dqa}	Mutual inductance between quadrature damper and armature winding Phase A, H
M_{bDq}, M_{Dqb}	Mutual inductance between quadrature damper and armature winding Phase B, H
M_{cDq}, M_{Dqc}	Mutual inductance between quadrature damper and armature winding Phase C, H
M_{fDd}, M_{Ddf}	Mutual inductance between field and direct damper windings, H
L_{al}	Armature winding leakage inductance, same for all three phases, H (portion of the armature inductance not subject to saturation)
L_{fl}	Field winding leakage inductance (in its own term), H
L_{Ddl}	Direct damper winding leakage inductance, H
L_{Dql}	Quadrature damper winding leakage inductance, H
R_a	Armature winding resistance per phase, ohms
R_f	Field winding resistance, ohms

R_{Dd} Direct damper winding resistance, ohms

R_{Dq} Quadrature damper winding resistance, ohms

The mutual inductances between the field and the quadrature damper as well as between the direct and the quadrature damper windings are assumed to be zero even though the saturation effect would cause some slight coupling between them.

APPENDIX II

The machine constants in Equations (3) through (18) can be obtained from the direct and quadrature axes inductances as follows:

$$L_s = 1/3\ (L_d + L_q + L_o) \tag{II-1}$$

$$M_s = 1/2\ (L_s - L_o) \tag{II-2}$$

$$L_m = 2/3\ (L_d - L_s - M_s) \tag{II-3}$$

$$M_{AF} = \sqrt{\frac{2}{3} L_{ff}\ (L_d - L'_d)} \tag{II-4}$$

(L_{ff} is in field terms, not in terms of the armature)

Let k_{af} = effective turns ratio, armature (one phase only, not three-phase equivalent) to field.

$$M_{ADD} = k_{af} M_{AF} \tag{II-5}$$

$$M_{ADQ} = \sqrt{\frac{2}{3} L_{Dq} (L_q - L''_q)} \tag{II-6}$$

The value of M_{FDD} can be obtained by solving the following quadratic equation.

$$M_{FDD}^2 - \frac{3M_{ADD}M_{AF}}{Ld - Ld''} M_{FDD} + \left[\frac{3}{2} \frac{L_{Dd}M_{AF}^2 + L_{ff}M_{ADD}^2}{Ld - Ld''} - L_{Dd}L_{ff}\right] = 0 \tag{II-7}$$

The smaller root is used, which is the physical solution. This quadratic equation comes from the relation:

$$L_d - L_d'' = \frac{3}{2} \frac{L_{Dd}M_{AF}^2 - 2M_{FDD}M_{ADD}M_{AF} + L_{ff}M_{ADD}^2}{L_{Dd}L_{ff} - M_{FDD}^2} \qquad \text{(II-8)}$$

In a solid rotor alternator without pole face type damper winding, the subtransient component decays very rapidly. Using one damping winding on each direct and quadrature axis, a good compromised open-circuit subtransient time constant is 1/3 cycle. In a 400-Hz machine,

$$T_{do}'' = T_{qo}'' \cong 0.00083 \text{ sec}$$

and

$$R_{Dd} = \frac{L_{Dd}}{T_{do}''} \qquad \text{(II-9)}$$

$$R_{Dq} = \frac{L_{Dq}}{T_{qo}''} \qquad \text{(II-10)}$$

In this experimental alternator with round rotor construction it is considered reasonable to use one saturation factor for all inductances. The saturation factor is determined by the resultant MMF (field ampere-turns plus the armature reaction).

The resultant MMF can be resolved into two components, MMF_d along the direct axis and MMF_q along the quadrature axis. Armature, field, and direct damper currents contribute to MMF_d. Armature and quadrature damper currents contribute to MMF_q. The MMF produce by any armature phase current is pulsating in magnitude and stationary in space. This MMF can be resolved into two opposite-revolving MMF's, each with one half the magnitude of the pulsating MMF. The forward revolving component, which is stationary with respect to the rotating field, is the armature reaction component. The three backward revolving components of the three phases will cancel each other in the case of a balanced load. In case of unbalanced load, the resultant MMF will revolve with double speed relative to the field structure. The contribution of this double-speed MMF to saturation of inductances is ignored in the analysis.

If the MMF's are expressed in terms of equivalent field amperes, and at time zero, the field axis coincides with the axis of armature winding phase A, the instantaneous values of MMF_d and MMF_q can be expressed in terms of the instantaneous currents as follows:

$$MMF_d = i_f + k_{af} i_{Dq} + \frac{1}{2} K_{af} \left[i_a \cos \omega t + i_b \cos (\omega t - 120^\circ) + i_c \cos (\omega t + 120^\circ) \right] \quad \text{(II-11)}$$

$$MMF_q = k_{af} i_{Dq} - \frac{1}{2} k_{af} \left[i_a \sin \omega t + i_b \sin (\omega t - 120^\circ) + i_c \sin (\omega t + 120^\circ) \right] \quad \text{(II-12)}$$

As mentioned previously, the positive direction of this quadrature axis is assumed to be 90 deg ahead of that of the direct axis. The resultant MMF can then be obtained:

$$MMF = \sqrt{MMF_d^2 + MMF_q^2} \quad \text{(II-13)}$$

With unbalanced load and during transient, these MMF's vary with time. From the no-load saturation curve and the air gap line, a saturation factor can be defined from Figure II-1 such that at a certain resultant MMF of I_{f1},

$$F_{sat} = \frac{AB}{AC}$$

Since in general, MMF is a function of time, the saturation factor is also a function of time.

The saturated inductances are obtained by multiplying the unsaturated inductance by the saturation factor. For instance, the saturated self-inductance of armature winding phase A is:

$$L_{aa,sat} = L_{al} + F_{sat} (L_{aa} - L_{al}) \quad \text{(II-14)}$$

where L_{al} is leakage inductance and is for practical purposes not subject to saturation.

PARAMETER IDENTIFICATION OF A SYNCHRONOUS MACHINE

Owen T. Tan
Electrical Engineering Department
Louisiana State University
Baton Rouge, LA 70803

In predicting armature transients of a synchronous generator connected to an isolated load through solid state devices, a higher-order model of the generator is to be employed where it is customary to use standard parameter values obtained from established field tests[1]. The accuracy of some parameter values, however, is generally far from satisfactory, particularly due to inherent errors of the graphical method applied in the parameter calculation and the effects of measurement noise. This parameter inaccuracy is likely to cause large discrepancies between simulation and field test results.

The extent to which the output variables of interest are affected by parameter inaccuracy was investigated by a sensitivity analysis study[2,3], where the output sensitivity with respect to parameter variations is evaluated. The numerical results of the sensitivity analysis applied to a salient-pole aircraft generator showed that the output sensitivity to parameter changes is greater for a capacitive than an inductive load, and such that it increases with a more leading load power-factor. Furthermore, for a capacitive load, X'_d, X''_d and X''_q are the dominant parameters greatly affecting the output behavior. Since the accuracy of these parameter values obtained by conventional tests is not satisfactory, a method is needed to determine these parameters much more accurately.

The method presented here utilizes the parameter estimation technique as known in modern control theory and which is based on the following principle. Applying the same input signal, the response of a real system is compared with that of the system model of a given structure. The model parameters are iteratively determined such that the difference between the output behaviors of real system and model reference is a minimum.

In applying the parameter estimation method to the synchronous generator[4,5], the input signal is chosen to correspond with the sudden short-circuit test of the real synchronous generator. Furthermore, the armature short-circuit currents and the field current are assumed to be the only ob-

servable output variables. The coefficients of the generator state-space model are expressed in the standard machine parameters X_d, X'_d, X''_d, X_ℓ, X_q, X''_q, R_a, T'_{do}, T''_{do} and T''_{qo}. These parameters, ten in total, will be determined simultaneously.

The procedure in estimating the parameters is pictured in block-diagram form shown in Fig.1. The synchronous generator is excited by a constant field voltage v_f^o and the generator is then subjected to a sudden short-circuit test. The observed (generally noise-corrupted) armature current i^r_{abc}(A) is first divided by its base value i_B (since the model is expressed in the per-unit values), after which transformed into its d,q,o components. The observed (also generally noise-corrupted) field current i^r_f(A) is first subtracted by its value i^{or}_f(A) before short-circuit, then divided by its base value i_{fB}. The iterative computation of the parameters is started by chosing a set of initial estimates in the model equations, which are then excited by an input signal equal to minus the known no-load voltage E of the real generator before short-circuit. Then, using the state and output response data ψ, i_{dq} and i^*_f of the model together with the processed output data i^r_{dq} and i^{*r}_f of the real generator, the machine parameter estimator computes off-line a new set of parameter values which is fed back to the model equations. The model response to the same input signal is then recorded again and with the same string of processed output data of the real machine, i^r_{dq} and i^{*r}_f, the parameter estimator computes another new set of parameter values. This computation procedure is repeated again and again until no significant change occurs in any of the parameters.

The estimator based on the W(eighted)-L(east)-S(quares) method[4] was implemented to the same aircraft generator used in the output sensitivity analysis study. Here, the generator was simulated by a model of the same structure as that of the model reference with parameter values as given by its manufacturer. Thus, in this case, the true parameter values are known. The numerical results showed that for initial estimates of the parameters between 40% and 200% of their true values, all parameters converged to their true values within a few iterations. A typical sample of the convergence behavior for initial estimates chosen at random is visualized in graph form in Fig.2, where the ratios of estimates to true values are plotted versus the number of iterations. It is observed that all parameter estimates nicely converge to their true values within 1%.

The effect of output noise on the WLS estimation was also investigated[5] since in practice the measurement can be noise-corrupted. Noise was added to the simulated generator output with standard deviations of 5% of the magnitude of the steady-state short-circuit currents and field current. The accuracy of the WLS estimation is indeed affected as shown in Fig.3 where a maximum error of 13% was found. However, by applying the M(aximum)-L(ikelihood) method[5] using apriori knowledge of the noise statistics, the estimation accuracy is significantly improved as shown in Fig.4 where the maximum error is only 2.5%.

From this study, the following conclusions can be summarized. (1) In the numerical example, no convergence problems have been encountered, at least not with initial estimates within the interval from 40% to 200% of the true values. Similar results were obtained for different sets of parameter values typical for large machines. For initial estimates outside the above-mentioned interval, the algorithm may diverge, in which case a different gain matrix in the estimator equations can be attempted. (2) The estimator proved to be accurate and effective, recalling that the complete set of parameters is simultaneously obtained from the data of a single short-circuit test, where it is not even necessary to reach the steady-state condition. (3) The test procedure was properly chosen. Another test may not be satisfactory, e.g., one with short-circuited armature winding and then applying a step-function field voltage was found to be no good since the subtransient behavior of the armature currents is practically not noticeable so that a much larger estimation error, slower convergence rate or even divergence can occur as indeed has been observed.

REFERENCES

1. Test Procedures for Synchronous Machines, *IEEE Publ.*, No.115, March 1965.
2. Owen T. Tan & F. Shokooh, "Synchronous Machine Analysis Using State Equations with Simple and Relevant Coefficients", *Proc. IEEE Southeast Conf.* (Charlotte, NC., Apr. 1975), Vol.2, pp.4B41-4B44.
3. Owen T. Tan & C. C. Lee, "Output Sensitivity Analysis of a Synchronous Generator", *Proc. Eighteenth Mid-West Symposium on Circuits & Systems* (Montreal, Canada, Aug. 1975), pp.563-567.
4. C. C. Lee & Owen T. Tan, "A Weighted-Least-Squares Parameter Estimator for Synchronous Machines", *IEEE Trans. Power App. & Systems*, Vol.PAS-96, Jan./Feb. 1977, pp.97-101.
5. Owen T. Tan & C. C. Lee, "Synchronous Machine Modeling by Parameter Estimation", *Proc. IFAC International Symposium on Aut. Control & Protection of Electric Power Systems* (Melbourne, Australia, Feb. 1977), pp.475-479.

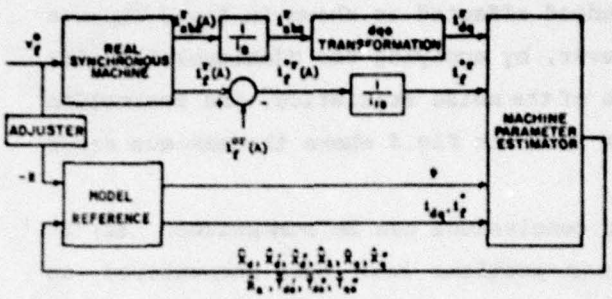


Fig.1 Machine Parameter Estimation

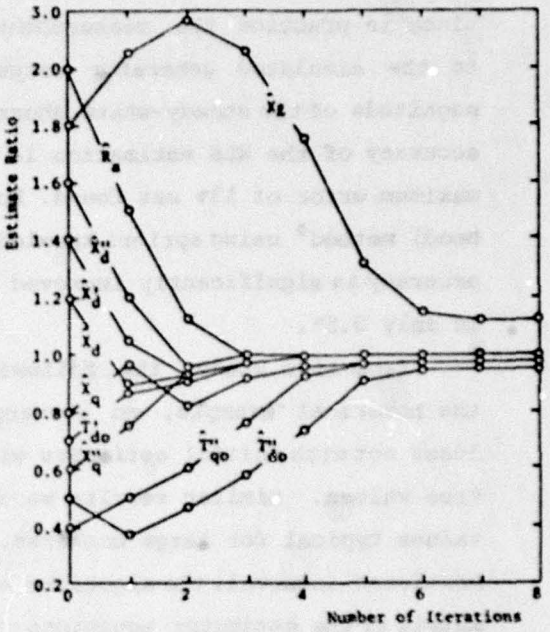


Fig.3 Ratio of WLS Estimate to True Value: Output Noise Effect

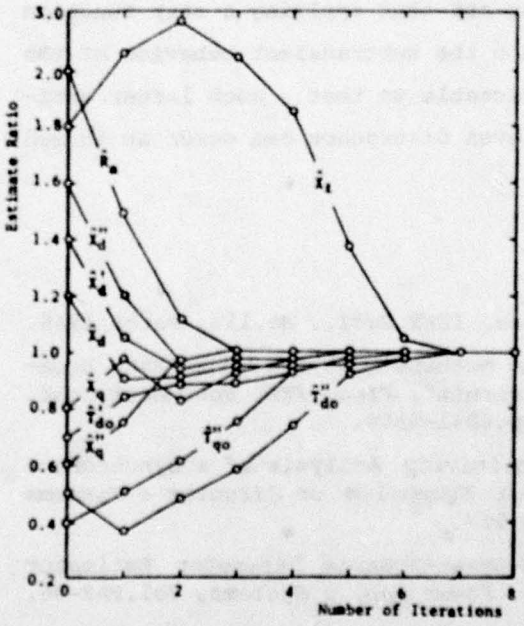


Fig.2 Ratio of WLS Estimate to True Value for Random Initial Estimates

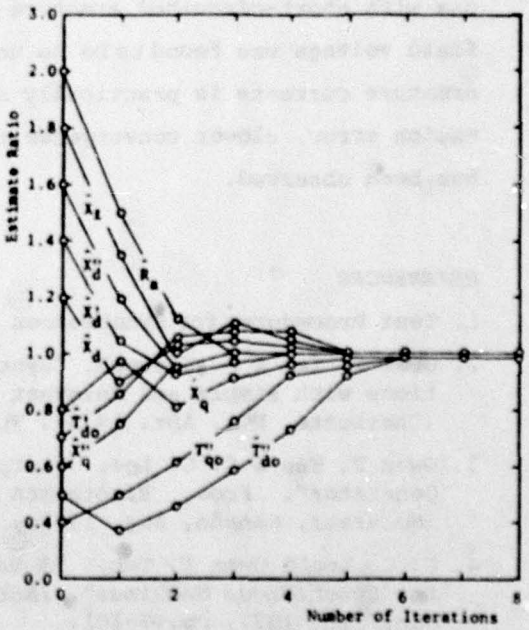


Fig.4 Ratio of ML Estimate to True Value for Random Initial Estimates

DISCUSSION

Q: In the graphs showing the convergence behavior of the algorithm, the ratios of estimates to true values are plotted versus the number of iterations. How were the true parameter values found?

A: In the case considered here, the generator was simulated by a model having the same structure as that of the model reference and parameter values as given by the manufacturer. Thus, these values are functioning as the true parameter values of the real machine.

Q: What values for the initial parameter estimates should generally be used in the practical implementation of this method?

A: The parameter values provided by the machine manufacturer or obtained by conventional tests can be used as initial parameter estimates.

Q: Will the estimation method be successful if the initial estimates are much different from their true values?

A: For initial estimates sufficiently far from their true values, e.g., outside the interval from 40% to 200% of their true values, the algorithm converges slower and may even diverge. However, by taking initial estimates equal to the parameter values obtained from reference tables, design data or/and conventional tests, convergence problems are not likely to occur.

HIGHER ORDER MODELLING OF SOLID IRON ROTOR TURBOGENERATORS

D.R. Brown P.C. Krause
Energy Systems Simulation Laboratory
School of Electrical Engineering
Purdue University
West Lafayette, Indiana 47907

Detailed models of large solid iron rotor turbogenerators which include the effects of eddy currents in the solid iron, machine saturation and unequal mutual coupling tend to become quite complex. The so-called Jackson Winchester Model (Ref. 1) is an example of the amount of detail possible. This model is difficult if not impossible to incorporate in time domain simulations and is used primarily as a machine design tool. The systems analyst must generally resort to simpler models for which machine data is readily available. Typically, this implies use of a model with one damper winding represented in the direct axis and one or two damper windings represented in the quadrature axis. ANSI Standard C42.10 time constants and reactances do not provide the necessary information to specify the parameters of models more detailed than these. Nevertheless, there is evidence that these standard models do not perform adequately in certain instances where models only slightly more complex do. For example, it has been shown (Ref. 2) that a simple modification which takes into account the difference in mutual coupling between rotor to rotor circuits and rotor to stator circuits can significantly improve computational accuracy when field circuit variables are of interest. Use of the so-called standard models can lead to errors (factor of ten) in these variables.

Perhaps the most detailed model in use for time domain simulations is the one described in Ref. 3. This model is shown in Fig. 1. It is derived

from frequency response data generated by the Jackson Winchester model. It therefore approximates the square root of slip frequency response characteristic produced by the eddy currents in the solid iron rotor body. A method for including the effects of saturation is described in Ref. 3 and the model does take into account the effects of unequal mutual inductances. This model is currently being studied at the Energy Systems Simulation Laboratory at Purdue University. A detailed hybrid simulation has been established which permits the correlation of significant effects with different portions of the model. Because data for the model is not generally made available a key objective in this research is to determine what types of studies require all of the detail provided by the model and whether in fact a simpler model with appropriate data might not perform as well. A study involving transient electromagnetic torque calculation is a typical example.

The computation of the complete transient electromagnetic torque waveforms is quite sensitive to the model used and, in particular, depends heavily on the quadrature axis damper winding representation. This is easily demonstrated with low order models. ANSI Standard C42.10 data shown below was assumed for a two pole machine:

$$H = 3.12 \text{ sec}$$

$$r_a = .0037$$

$x_d = 1.75$	$x_q = 1.68$
$x'_d = .260$	$x'_q = .47$
$x''_d = .205$	$x''_q = .205$
$T'_{do} = 4.0$	$T'_{qo} = .54$
$T''_{do} = .029$	$T''_{qo} = .053$

Three possible machine representations were studied in some detail:

1. A model with two quadrature axis damper windings denoted the MC model.
2. A model with one quadrature axis damper winding determined from transient characteristics (x_q' and T_{qo}') denoted the C' model.
3. A model with one quadrature axis damper winding determined from subtransient characteristics (x_q'' and T_{qo}'') denoted the C'' model.

The electromagnetic torque calculated by each of the above models was compared for out-of-phase synchronization, three phase faults and a fast reclosing sequence.

Figure 2 shows a typical result on out-of-phase synchronization. The machine in this case was synchronized directly to an infinite bus with the machine voltage leading the bus voltage by +120°. Note that the maximum and minimum electromagnetic torque values during the first cycle following breaker closing are 13 pu and -2 pu respectively. These first cycle maximum and minimum values of electromagnetic torque are shown for all three models compared and for a range of positive and negative synchronization angles in Fig. 3. The C' and C'' models differ considerably from the MC model particularly at synchronization angles near $\pm$ 120°. A significant torque waveform distortion also occurs with the C' and C'' models. In order to assess the impact of these discrepancies both in torque magnitude and waveform shape a mechanical system consisting of a high pressure, intermediate pressure and two low pressure turbines was added to the simulation. Inertia constants and shaft stiffness factors were chosen to be in the same ratio as those of the IEEE benchmark model of Ref. 4. Figure 4 shows the electromagnetic torque and shaft torque for the shaft section between the low pressure turbine and

the generator for all three models on an out-of-phase synchronization at +120°. The shaft torque predicted by the C'' model is approximately 50% higher than that predicted by the MC model. Similar discrepancies occur in the other shaft sections. When synchronization at -120° was compared the C' model displayed significant errors. Thus neither the C' or the C'' model produced shaft torque results consistent with the MC model.

Comparison of torque waveforms on application of a symmetrical three phase fault revealed waveform distortion predicted by the C' and C'' models where none was predicted by the MC model. In the case of the C' model, $x''_q \neq x''_d$ implies a subtransient saliency which can yield a significant second harmonic component (Refs. 5 and 6).

Fast reclosing studies were made comparing the three models using the system shown in Fig. 5. The fault was applied at the point shown for 3 cycles then the faulted line was opened. Thirty cycles from the time of fault initiation the transmission line was reclosed with the fault still present. The errors in electromagnetic torque magnitudes and waveform shapes caused significant errors in the instantaneous shaft torques particularly on reclosing. For example the C'' model predicted a first cycle peak-to-peak shaft torque between the low pressure turbine and the generator of 2.7 pu on reclosing versus 4.3 pu for the MC model.

The above examples show that models with a single quadrature axis damper winding based solely on either subtransient or transient characteristics do not compare well with the more detailed model. They also show the critical nature of the quadrature axis damper winding representation. In order to investigate these and other effects in greater detail, further investigation is planned using the SIRM described earlier as a suitably detailed benchmark model. Specifically, it is hoped that it will be possible to identify those

aspects of the model critical to the accurate calculation of transient electromagnetic torque.

REFERENCES

1. W.B. Jackson and R.L. Winchester, "Direct and Quadrature Axis Equivalent Circuits for Solid Rotor Turbine Generators," IEEE Trans. on Power Apparatus and Systems, Vol. 88, July 1969, pp. 1121-1136.

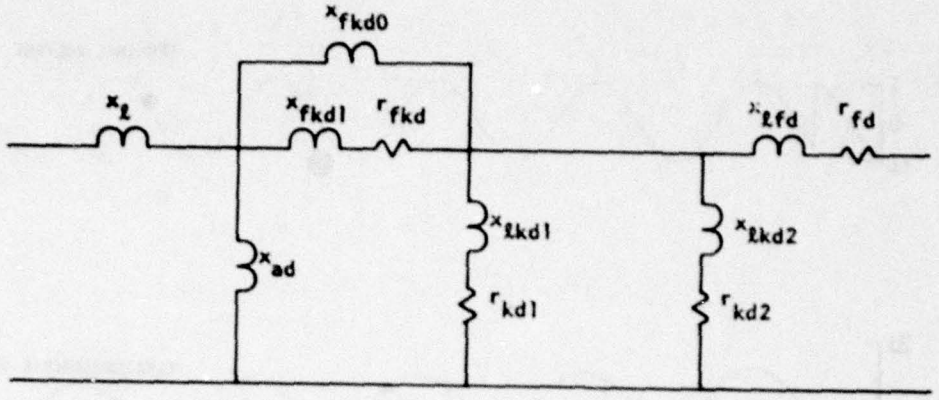
2. I.M. Canay, "Extended Synchronous Machine Model for the Calculation of Transient Processes and Stability," Electric Machines and Electromechanics, Vol. 1, No. 2, Jan./March 1977, pp. 137-150.

3. R.P. Schulz, W.D. Jones and D.N. Ewart, "Dynamic Models of Turbine Generators Derived from Solid Rotor Equivalent Circuits," IEEE Trans. on Power Apparatus and Systems, Vol. 92, May/June 1973, pp. 926-933.

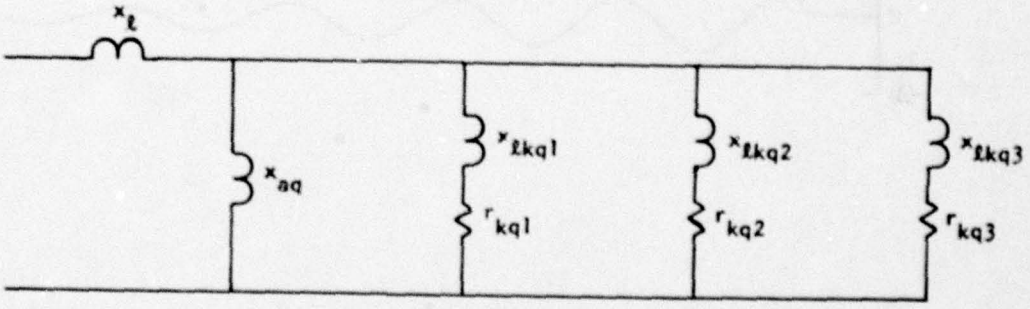
4. IEEE Committee Report, "First Benchmark Model for Computer Simulation of Subsynchronous Resonance," IEEE Trans. on Power Apparatus and Systems, Vol. 96, Sept./Oct. 1977, pp. 1565-1572.

5. I.M. Canay and L. Werren, "Interrupting Sudden Assymetric Short Circuit Currents Without Zero Transition," Brown Boveri Review, Vol. 56, 1969(10), pp. 484-493.

6. B. Adkins and R.G. Harley, The General Theory of Alternating Current Machines: Application to Practical Problems, London, Chapman and Hall, 1975.



direct axis



quadrature axis

Figure 1 The solid iron rotor model (SIRM).

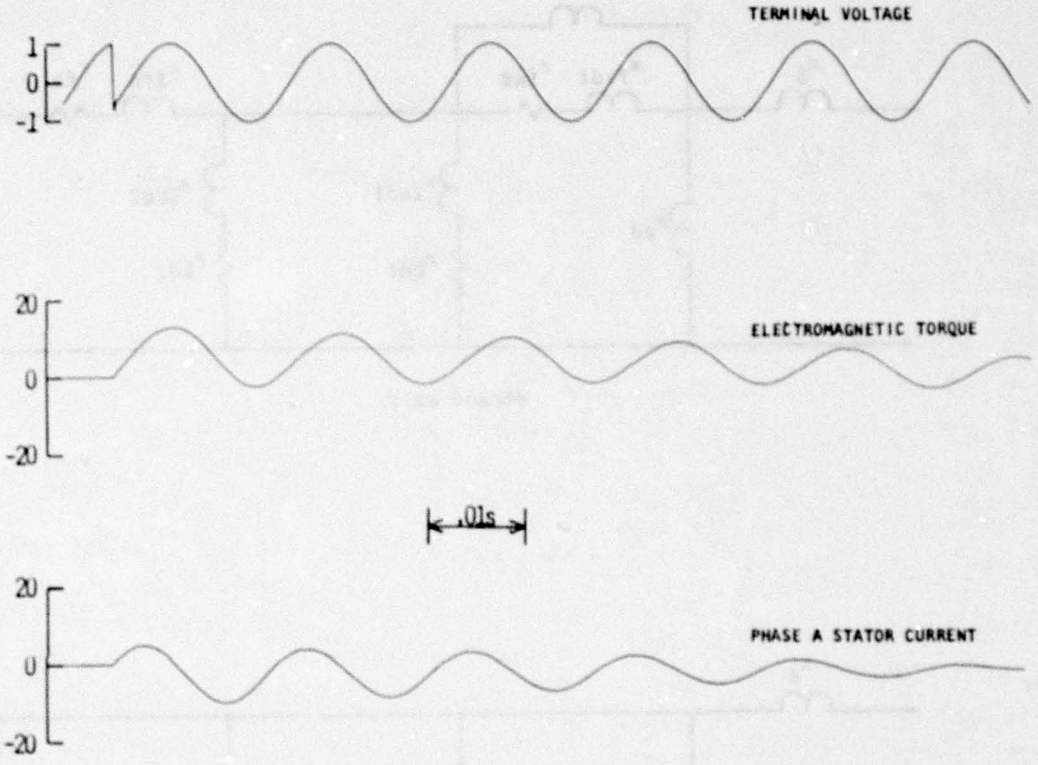


Figure 2 Out-of-phase synchronization at +120°, MC model.

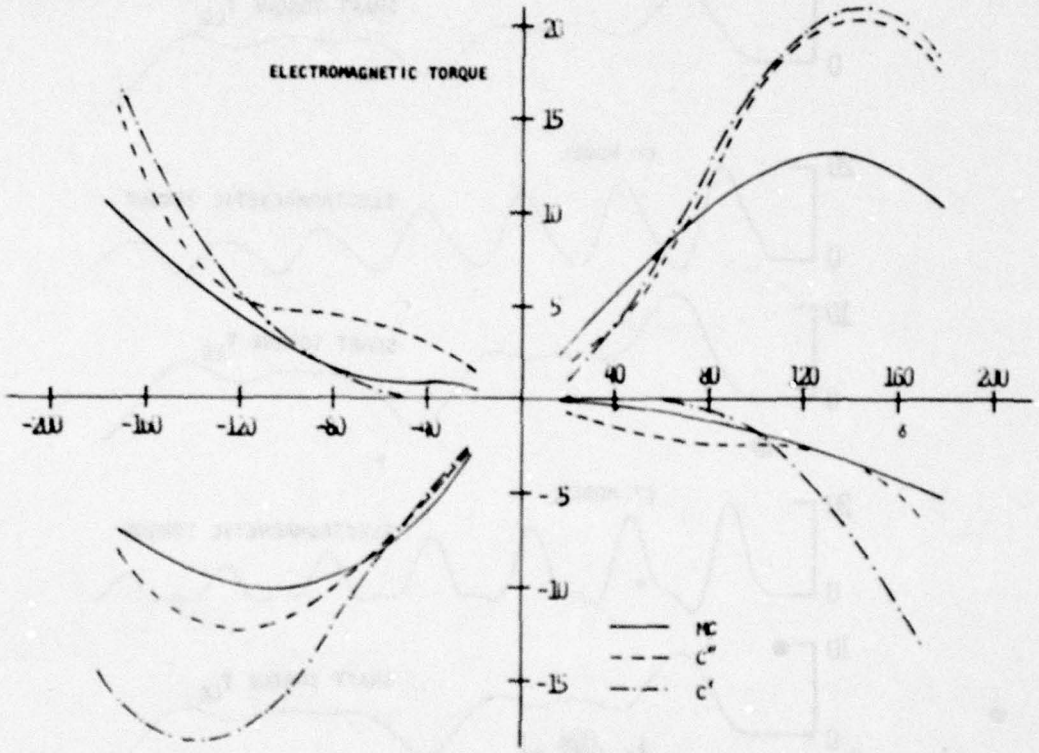


Figure 3 Maximum and minimum first cycle torques on out-of-phase synchronization for the three models.

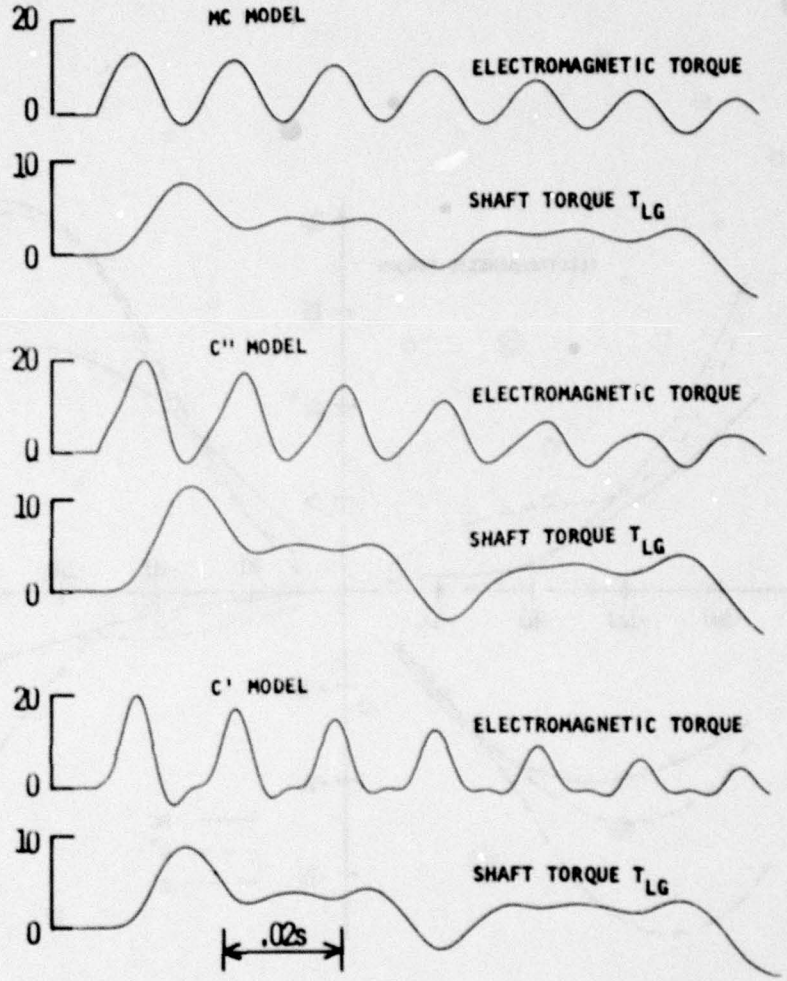


Figure 4 Out-of-phase synchronization at +120° with mechanical system.

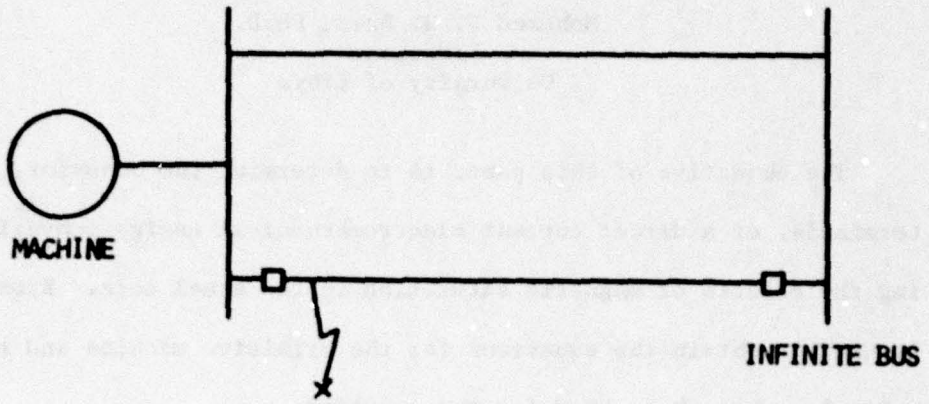


Figure 5 System studied for fast reclosing.

MATHEMATICAL MODEL OF DIRECT CURRENT MACHINES INCLUDING THE EFFECTS OF MAGNETIC SATURATION

D. D. Wier, M. S.
Associate Professor
Mississippi State University

Mohamed F. H. Bara, Ph.D.
Professor
University of Libya

The objective of this paper is to determine the behavior, at its terminals, of a direct current electromechanical energy converter including the effects of magnetic saturation in the steel core. Kron's method is used to obtain the equations for the primitive machine and the state variable approach is used for the solution.

The Primitive Machine Equations

The primitive machine model is shown in figure 1. It is an ideal, smooth rotor, salient pole machine with two stationary axes; the direct axis (d) along the axis of the salient poles and the quadrature axis (q) along the axis of interpolar space. Each coil on either axis represents a circuit or part of a circuit of the actual machine. The rotor coils are designated as d_r and q_r. The stator coils are designated as d_s and q_s. The sign convention and the direction of rotation are as given in figure 1.

The magnetic circuit saturation is neglected in this model and will be handled separately.

The instantaneous voltage equations using Kron's primitive machine are given as:

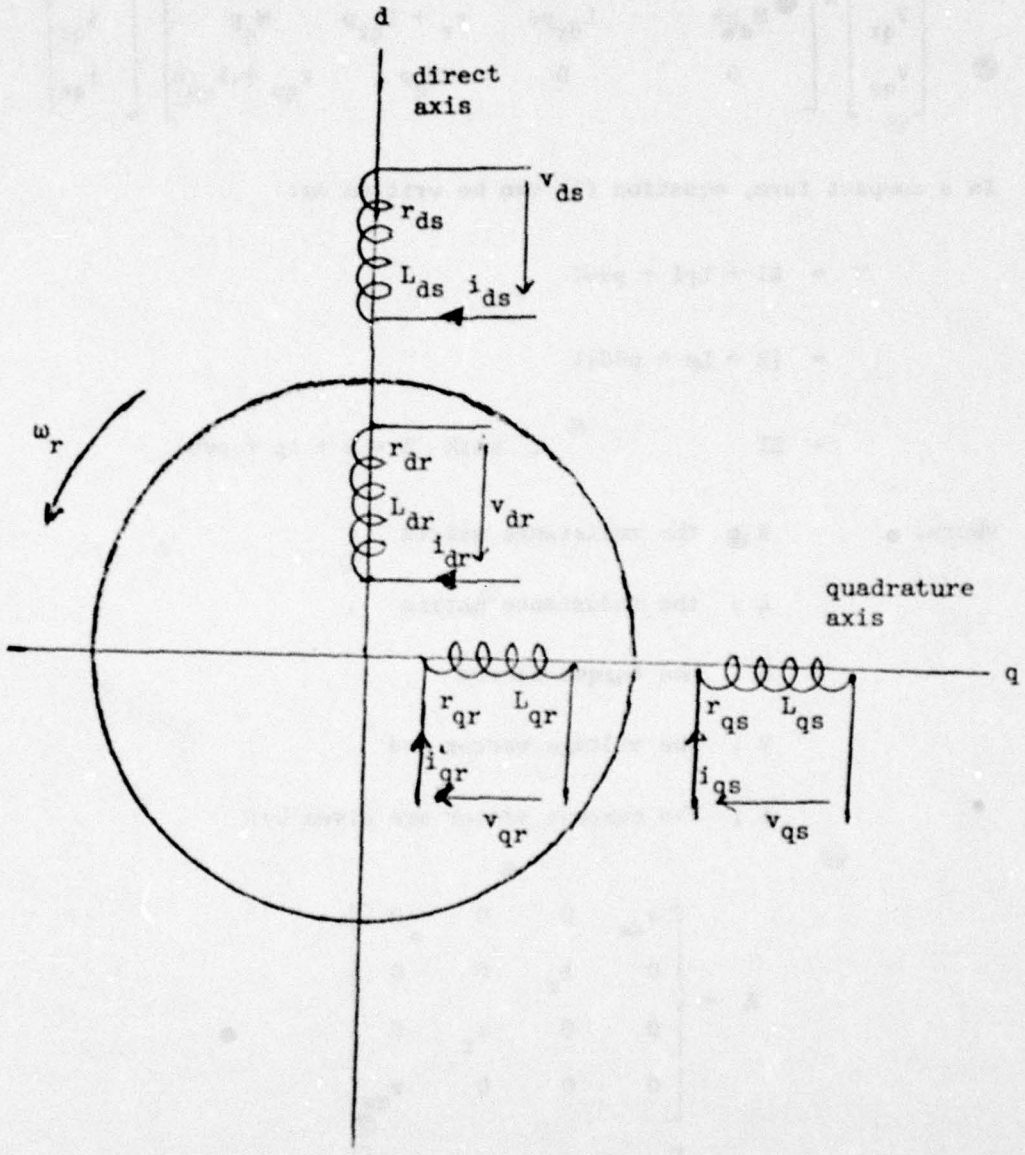


Figure 1. The Primitive Machine Circuit Model.

$$\begin{bmatrix} V_{ds} \\ V_{dr} \\ V_{qr} \\ V_{qs} \end{bmatrix} = \begin{bmatrix} r_{ds} + L_{ds}p & M_d p & 0 & 0 \\ M_d p & r_r + L_{dr}p & -l_{qr}p\theta & -M_q p\theta \\ M_d p\theta & L_{dr}p\theta & r_r + L_{qr}p & M_q p \\ 0 & 0 & M_q p & r_{qs} + L_{qs}o \end{bmatrix} \begin{bmatrix} i_{ds} \\ i_{dr} \\ i_{qr} \\ i_{qs} \end{bmatrix} \quad (1)$$

In a compact form, equation (1) can be written as:

$$\begin{aligned} V &= RI + LpI + p\theta GI \\ &= [R + Lp + p\theta G]I \\ &= ZI \qquad , \text{ with } Z = R + Lp + p\theta G \end{aligned} \quad (2)$$

where, R ; the resistance matrix ,

L ; the inductance matrix ,

G ; the torque matrix ,

V ; the voltage vector and

I ; the current vector are given by:

$$R = \begin{bmatrix} r_{ds} & 0 & 0 & 0 \\ 0 & r_r & 0 & 0 \\ 0 & 0 & r_r & 0 \\ 0 & 0 & 0 & r_{qs} \end{bmatrix}$$

$$L = \begin{bmatrix} L_{ds} & M_d & 0 & 0 \\ M_d & L_{dr} & 0 & 0 \\ 0 & 0 & L_{qr} & M_q \\ 0 & 0 & M_q & L_{qs} \end{bmatrix}$$

$$G = \begin{bmatrix} 0 & 0 & 0 & 0 \\ 0 & 0 & -L_{qr} & -M_q \\ M_d & L_{dr} & 0 & 0 \\ 0 & 0 & 0 & 0 \end{bmatrix}$$

$$V = \begin{bmatrix} v_{ds} \\ v_{dr} \\ v_{qr} \\ v_{qs} \end{bmatrix} \qquad I = \begin{bmatrix} i_{ds} \\ i_{dr} \\ i_{qr} \\ i_{qs} \end{bmatrix}$$

In equation (2), the impressed voltages are equated to the sum of the resistance drops RI, the inductance drops LpI and the voltages induced by rotation $p\theta GI$. They apply to the general machine model of Figure (1) with the sign conventions and the direction of rotation shown and for the motor mode of operation. If the machine is a generator, the impressed voltage signs are reversed; that is

$$(-V) = ZI$$

or

$$V = (-Z)I \quad .$$

To determine the values of the voltages and circuit parameters to be used in equation (1), the power is assumed to be invariant. The values are then given by equations (3) and (4), where the primed quantities represent the actual machine and unprimed represent the primitive model. The matrix C is the transformation matrix.

$$V' = C^t V \tag{3}$$

$$Z' = C^t Z C \tag{4}$$

The actual currents are related to the primitive machine currents by the equation

$$I = CI' \tag{5}$$

The impressed voltages of the primitive machine are shown to be related to the coil currents through a set of simultaneous ordinary differential equations. If these voltages are considered as the inputs to the machine and the currents as the outputs, the equations need to be solved for the coil currents. The actual currents may then be found by the use of equation (5).

The electromagnetic torque, T_{em}, may be found by the use of equation (6)

$$T_{em} = I'^t G I' \tag{6}$$

The State Variable Equation

The form of the machine equations suggests the use of the state variables technique (a powerful analysis tool) to handle these equations and analyze the machine behavior.

In the state variables analysis, the state of the system is completely described by the state vector, whose elements are the state variables. The solution of the state equation gives the state vector at any time (t) in terms of the system initial conditions and the present input vectors.

From the state and the input vectors, the outputs at any time (t) can be easily evaluated using the output equation.

The state equation derived from an n^{th} order ordinary differential equation or n simultaneous first-order ordinary differential equations takes the standard form:

$$\dot{x} = A\,x + B\,u \tag{7}$$

where:

- x is the (nx1) state vector x(t).
- $\dot{x}$ is a vector whose elements are the derivatives of the corresponding elements of x, with respect to the independent variable (t).
- A is an (nxn) coefficient matrix.
- B is an (nxr) coefficient matrix.
- u is the (rx1) input vector u(t), where r is the number of inputs to the system.

The output vector y(t) is given by the output equation:

$$y = C\,s + D\,u \tag{8}$$

Multiplying equation (2) by C^t gives

$$C^tV = C^tRI + C^tLpI + C^tp\theta GI$$

which in terms of the actual machine quantities yields

$$V' = C^tRCI' + C^tLCpI' + C^tGGp\theta I' \quad .$$

that is,

$$V' = R'I' + L'pI' + G'p\theta I' \tag{9}$$

where,

$$R' = C^t RC$$

$$L' = C^t Lc$$

$$G' = C^t GC \ .$$

In the state variable from equation (9) can be written as

$$pI' = (-L'^{-1})(R' + p\theta G')\ I' + (L'^{-1})\ V' \tag{10}$$

It is noted here that the elements of the inductance matrix of an electrical machine represent actual quantities and its inverse exists for all practical machines. Comparing equation (10) with (7) gives the coefficient matrices:

$$A = (-L'^{-1})(R' + p\theta G') \tag{11a}$$

and

$$B = L'^{-1} \tag{11b}$$

The torque equation of an electrical machine is given by:

$$T = Jp^2\theta + Bp\theta \pm K\theta \pm T_l - T_{em} \tag{12}$$

where

J is the polar moment of inertia

B is the constant of viscious friction

K a constant of the machine

T_1 is the load torque

T_{em} is the electromagnetic torque

T is the applied torque

θ is the angular displacement of the rotor

This can be placed in the state variables form by letting

$$\theta_1 = \theta \tag{13}$$

$$\theta_2 = p\theta_1 \tag{14}$$

and hence

$$p^2\theta = p\theta_2$$

Equation (12) may be rewritten as

$$p\theta_2 = -\frac{K}{J}\theta_1 - \frac{B}{J}\theta_2 - \frac{1}{J}(T_L - T_{em}) \tag{15}$$

where $T_L = \pm T_1 - T$.

By use of equation (13), (14), and (15) the matrix equation (16) can be obtained

$$\begin{bmatrix} \theta_1 \\ \dot{\theta}_2 \end{bmatrix} = \begin{bmatrix} 0 & 1 \\ -k/J & -B/J \end{bmatrix} \begin{bmatrix} \theta_1 \\ \theta_2 \end{bmatrix} + \begin{bmatrix} 0 \\ -1/J \end{bmatrix} (T_L - T_{em}) \tag{16}$$

This is in the same form as equation (7) with ,

$$A = \begin{bmatrix} 0 & 1 \\ -k/J & -B/J \end{bmatrix} \qquad B = \begin{bmatrix} 0 \\ -1/J \end{bmatrix}$$

and θ_1 and θ_2 are the state variables.

The primitive machine model of a simple separately excited direct current machine is shown in Figure 2. It has only two coils; ds to represent the field circuit and qr for the armature windings.

The voltage equations of this model can be developed by using the transformation technique relating the actual machine model to its primitive with, C, the connection matrix here being a unit matrix or directly by eliminating the rows and columns of the coils qs and dr from Equation (1).

The same result will be obtained if the equations are formed by inspection from Figure 1.

By any of these methods, the motor voltage equations, with the primes eliminated, are,

$$\begin{bmatrix} V_{ds} \\ V_{qr} \end{bmatrix} = \begin{bmatrix} r_{ds} & 0 \\ 0 & r_{qr} \end{bmatrix} \begin{bmatrix} i_{ds} \\ i_{qr} \end{bmatrix} + \begin{bmatrix} L_{ds} & 0 \\ 0 & L_{qr} \end{bmatrix} \frac{d}{dt} \begin{bmatrix} i_{ds} \\ i_{qr} \end{bmatrix}$$

$$+ \omega_r \begin{bmatrix} 0 & 0 \\ M_{grds} & 0 \end{bmatrix} \begin{bmatrix} i_{ds} \\ i_{qr} \end{bmatrix} \qquad (17)$$

In the state variable form this can be written as:

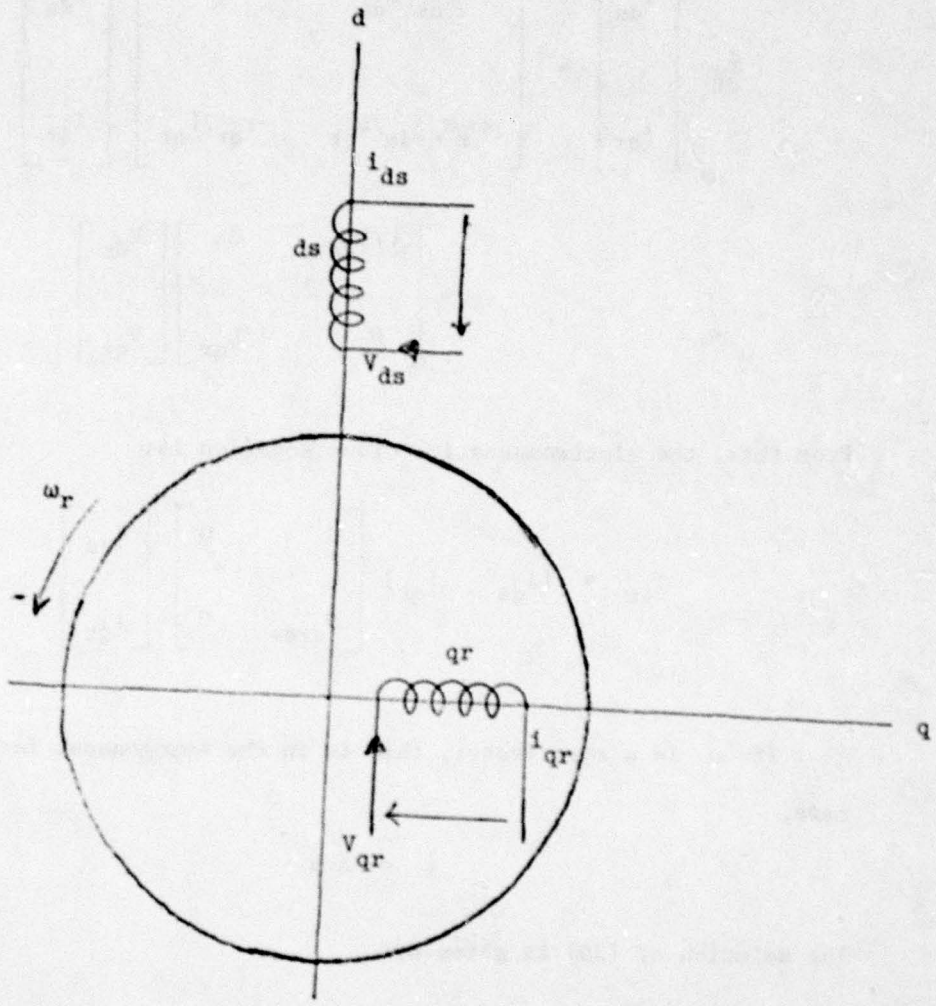


Figure 2. Separately Excited DC Machine Circuit Model

$$\frac{d}{dt}\begin{bmatrix} i_{ds} \\ \\ i_{qr} \end{bmatrix} = \begin{bmatrix} -r_{ds}/L_{ds} & 0 \\ \\ -\omega_r M_{qrds}/L_{qr} & -r_{qr}/L_{qr} \end{bmatrix}\begin{bmatrix} i_{ds} \\ \\ i_{qr} \end{bmatrix} + \begin{bmatrix} 1/L_{ds} & 0 \\ \\ 0 & 1/L_{qr} \end{bmatrix}\begin{bmatrix} V_{ds} \\ \\ V_{qr} \end{bmatrix} \tag{18}$$

From this, the electromagnetic torque equation is:

$$T_{em} = [i_{ds} \quad i_{qr}]\begin{bmatrix} 0 & 0 \\ \\ M_{qrds} & 0 \end{bmatrix}\begin{bmatrix} i_{ds} \\ \\ i_{qr} \end{bmatrix} \tag{19}$$

If u is a zero vector, that is in the homogeneous force free case,

$$\dot{x} = A\,x \tag{20}$$

The solution of (20) is given by:

$$x(t) = e^{At}\,x(0) \tag{21}$$

where

$x(0)$ = the initial value vector of x

e^{At} = the state transition matrix.

The solution of (7) can be written as

$$x(t) = e^{A(t-t_o)}\,x(t_o) + \int_{t_o}^{t} e^{A(t-\tau)}\,B\,u(\tau)d\tau \tag{22}$$

Effect of Saturation

In the general theory machine equations, the induced voltages are considered proportional to the currents producing them. This is an approximation of the actual conditions in practical machines where this voltage-current relation is a nonlinear one characterized by the familiar open circuit curve with its first part as a linear portion coinciding approximately with the air-gap line. The magnetic circuit saturation causes the curve to deviate forming a knee and then an almost flat portion.

Saturation effects are different for different constants and types of machines. It results in reducing the machine inductances from their unsaturated values and decreases the generated voltage.

The reduction in the field inductance and induced voltage, may become considerable for DC machines operating on heavy currents.

Several means have been used to handle the saturation effects by introducing adjusted, equivalent or saturated reactances in the machine equations.

In the steady state analysis, suitably chosen values of the reactances may be used. For transient conditions, the continuous change of the inductance due to saturation, has to be taken into account for better results.

Graphical methods were studied to evaluate the saturation effect. Saturation factors were defined from the open circuit characteristics and applied to the unsaturated reactances to get the saturated ones.

Empirical functional relations have been considered to represent the B - H curve, such as;

$$B = a H^n \tag{24}$$

and

$$H = a_0 + a_1 B + a_n B^n + a_m B^m \tag{25}$$

where the coefficients and the powers can be obtained using graphical constructions or curve fitting methods.

Another empirical formula that has shown a good fit is Froelich's equation given by

$$B = \frac{H}{a + b H} \quad . \tag{26}$$

When used to express the changes of the voltage induced by rotation, or in effect, give the proper value of the rotational mutual inductance coefficient M, Froelich's equation can be used to obtain equation (27).

$$e_j = \frac{\alpha}{\alpha + i_k} M_{jk} \omega_r i_k \quad ; \quad j \neq k \tag{27}$$

where

e_j = the voltage induced in coil j

α = a chosen constant

i_k = the current in coil k that induces e_j .

M_{jk} = the mutual inductance between coils j and k with saturation neglected.

Example Using DC Separately Excited Generator

The DC separately excited generator is a simple case which will be used to illustrate the effect of saturation in the steel core. The behavior of the armature and field currents and the electromagnetic torque as functions of time will be studied. The generator will be assumed to be operating at a constant speed with a resistive load following the sudden application of the field voltage. The values of the machine parameters, load resistance, speed, and field voltage are given in Table 1.

Table 1. DC separately Excited Machine Data

r_{ds}	40	Ohm
r_{qr}	0.1	Ohm
r_L	1.5	Ohm
L_{ds}	20	Henry
L_{qr}	0.05	Henry
M	0.2	Henry
ω_r	200	Radians/s
V_{ds}	220	volts

With these values the state equations are obtained as

$$p\begin{bmatrix} i_{ds} \\ i_{qr} \end{bmatrix} = \begin{bmatrix} -2 & 0 \\ 800 & -32 \end{bmatrix}\begin{bmatrix} i_{ds} \\ i_{qr} \end{bmatrix} + \begin{bmatrix} 0.05 & 0 \\ 0 & -20 \end{bmatrix}\begin{bmatrix} 220 \\ 0 \end{bmatrix}$$

where

$$A = \begin{bmatrix} -2 & 0 \\ 800 & -32 \end{bmatrix}, \qquad B = \begin{bmatrix} 0.05 & 0 \\ 0 & 20 \end{bmatrix}$$

$$G = \begin{bmatrix} 0 & 0 \\ 0.2 & 0 \end{bmatrix}$$

$$XO = \begin{bmatrix} 0 \\ 0 \end{bmatrix} \qquad \text{and} \qquad U = \begin{bmatrix} 220 \\ 0 \end{bmatrix},$$

The steady state field and armature currents and the electromagnetic torque are obtained respectively with:

$$r_{qr} = -(1.5 + 0.1) = -1.6 \text{ ohms}$$

$$i_{ds} = 5.5 \text{ Amperes}$$

$$i_{qr} = 137.5 \text{ Amperes}$$

$$T_{em} = 151.25 \text{ Newton-Meter}$$

The complete response is as shown in figures 3, 4, and 5.

Conclusion

Although the only machine considered here is the d.c. machine, the method and computer program described can be used on most electro-mechanical machines.

The state equations are easily obtainable in forms that can be directly applied to solve machine problems in the steady-state, transient, and dynamic conditions. The solution of the state equations using the state transition matrix evaluated by series expansion is easily programable on the digital computer. The limitations are those which arise from neglecting the effects of such things as space harmonics, flux leakages, and magnetic saturation. These can be partially included as specific refinements as was done here with the consideration of the effect of magnetic saturation.

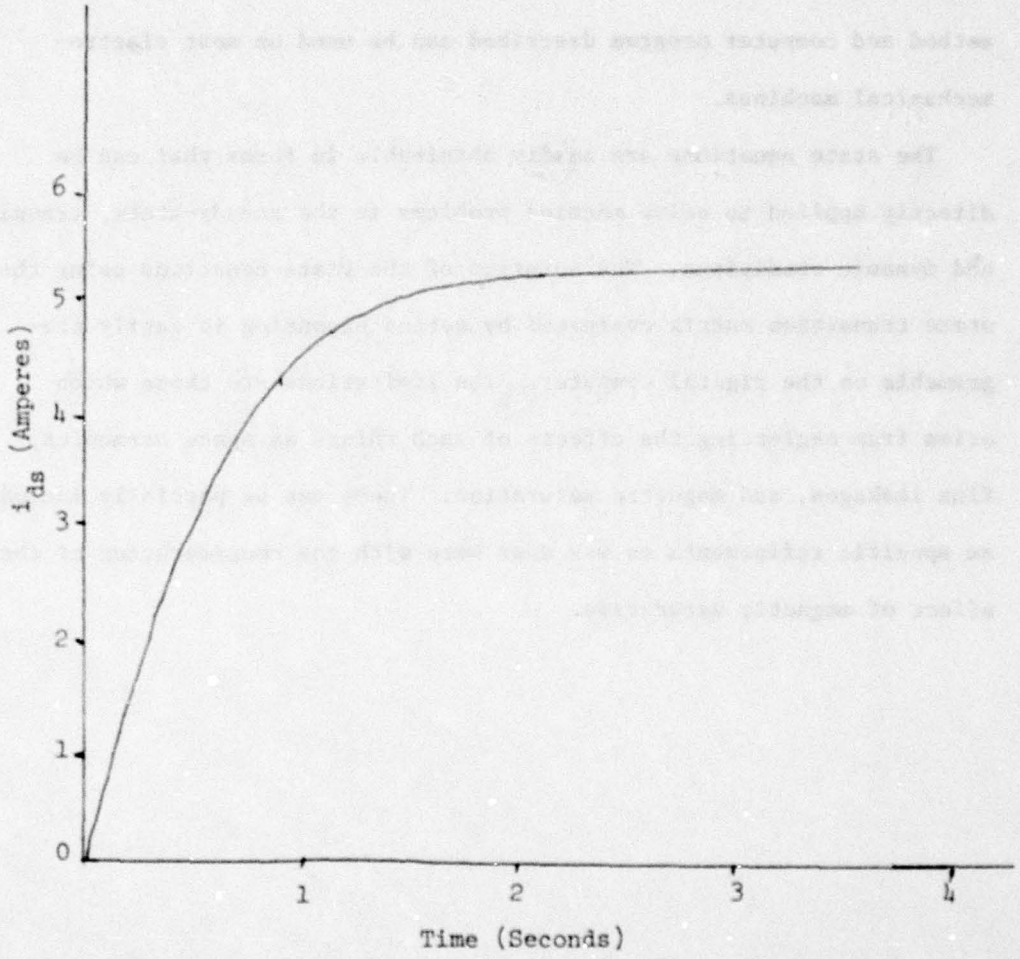


Figure 3. DC Machine Field Current (i_{ds}).

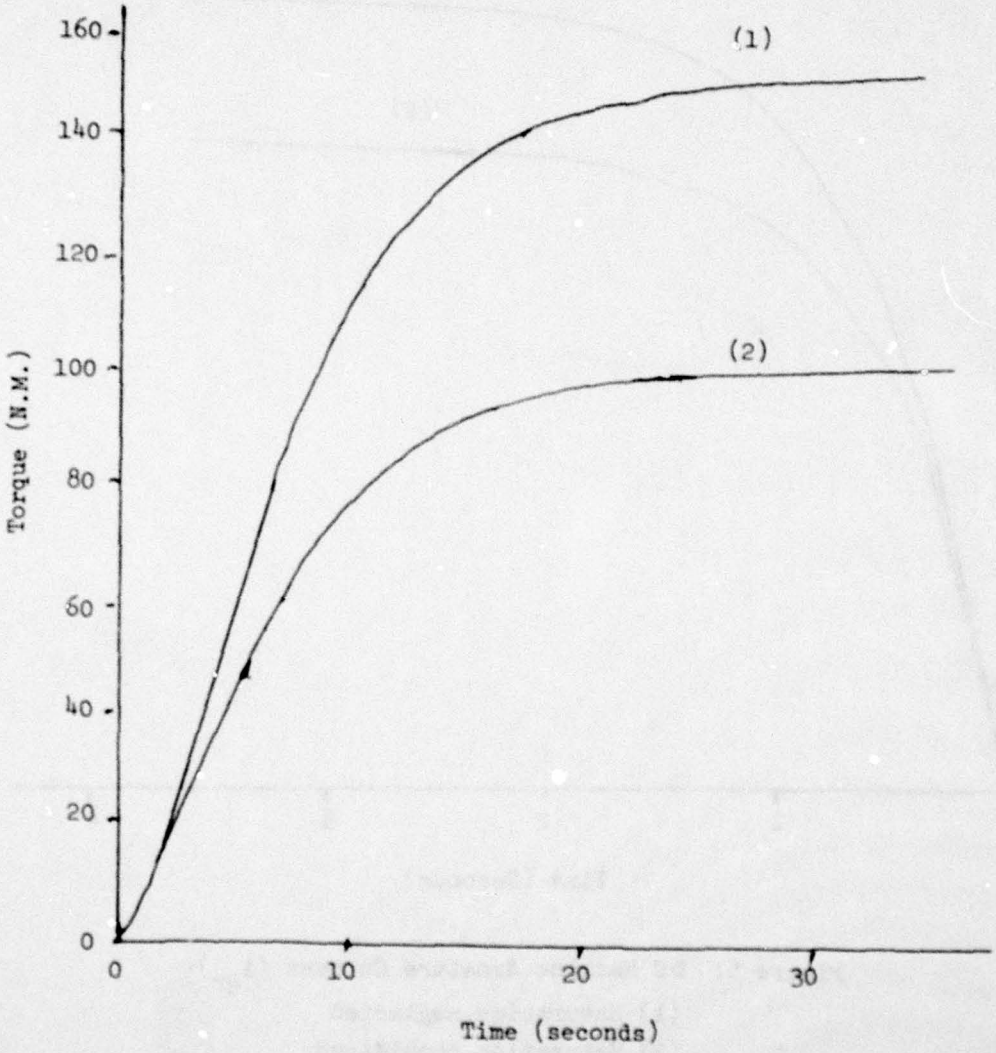


Figure 4. DC Machine--Electromagnetic Torque.
(1) Saturation neglected
(2) Saturation considered

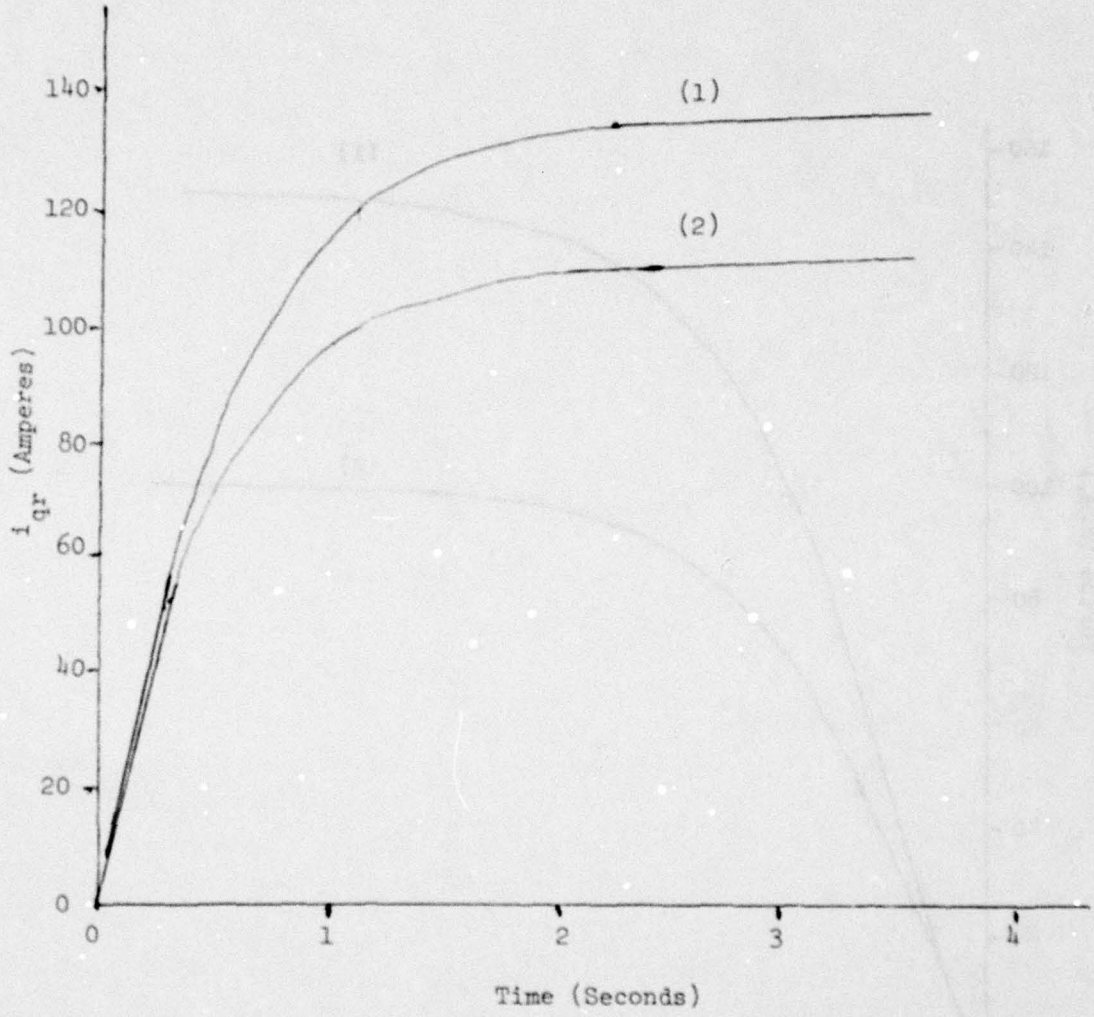


Figure 5: DC Machine Armature Current (i_{qr}).
(1) Saturation neglected
(2) Saturation considered

BIBLIOGRAPHY

Adkins, Bernard, Generalized Theory of Electrical Machines, Chapman & Hall, London, 1957.

Attanasio-D'Atri, M. L., "A Note on the State Variables in Generalized Electric Machine Theory," Proceedings of the IEEE, Vol. 56, pp. 341-343, March 1968.

Bewely, L. V., Tensor Analysis of Electric Circuits and Machines, The Ronald Press, New York, 1961.

Concordia, Charles, Synchronous Machines Theory and Performance, John Wiley & Sons, Inc., New York, 1951.

Derusso, Rob J. Roy and Charles M. Close, State Variables for Engineers, John Wiley & Sons, New York, 1965.

De Sarkar, Asish K., and Gunnar J. Berg, "Digital Simulation of Three Phase Induction Motors," IEEE Trans. Power Apparatus and Systems, Vol. PAS-89, pp. 1031-1037, July/August 1970.

Garg, V. K., "A Digital Method for Transient Analysis of Saturated Salient Pole Synchronous Machines," Electrical Machines and Electromechanics: An International Quarterly, Vol. 1, pp. 267-279, 1977.

Kron, Gabriel, "Classification of the Reference Frame of a Synchronous Machine," Transactions of the American Institute of Electrical Engineers, Vol. 69, pp. 720-727, 1950.

Kron, Gabriel, Tensors for Circuits, Dover Publications, Inc., New York, 1959.

Lewis, W. A., The Principles of Synchronous Machines, Illinois Institute of Technology, Chicago, Illinois, 1959.

Mablekos, Van E. and Ahmad H. El-Abiad, "A Unified Approach for Dynamic Simulation of D C and Single-Phase A C Energy Converters," Proceedings of the IEEE PAS Summer Meeting of Energy Resources Conference, Anaheim, Cal, Paper No. C74393-5, July 1974.

Meisel, Jerome, Principles of Electromechanical Energy Conversion, McGraw Hill Book Company, New York, 1966.

O'Kelly, D. and S. Simmons, Introduction to Generalized Electrical Machine Theory, McGraw Hill Publishing Company, London, 1968.

AD-A078 341 AIR FORCE AERO PROPULSION LAB WRIGHT-PATTERSON AFB OH F/G 10/2
PROCEEDINGS OF THE AFAPL GENERATOR AND MOTORS SEMINAR (1ST), HE--ETC(U)
AUG 79 H L SOUTHALL , J L MCCABRIA

UNCLASSIFIED AFAPL-TR-79-2090 NL

3 OF 3
AD-
A078341





END
DATE
FILMED
1-80
DDC

POWER RESEARCH AT THE UNIVERSITY OF MISSOURI-COLUMBIA

Dr. Charles Slivinsky
Professor of Electrical Engineering
University of Missouri-Columbia

Introduction

Electric power engineering education at both the undergraduate and graduate level is a major interest of the Department of Electrical Engineering at UMC. Research programs on power electronics, rotating machinery, hybrid simulation of large power systems and new modelling techniques provide unique educational opportunities for interested students. Three of the major research efforts presently underway are summarized in the following remarks.

Solid State Power Control Program

The principal objective of this Program is to motivate talented students to do applied research in this field. In general, the work performed involves the analysis, design, construction and/or evaluation of breadboard model power control circuits involving thyristors, power transistors and related semiconductor devices. Experience on real engineering problems suggested by one or more sponsors is provided for both undergraduate and graduate students. The central thrust of the program is M.S. level research. A very important additional objective is to provide useful technical results that are disseminated to the sponsors in annual technical reports and project review seminars.

At present, research is being done on each of the following:

Optimal Control of Variable Frequency Induction motors

Microcomputer controlled Transistor Inverter Induction Motor Drives

Power Electronic Circuit Analysis Techniques

Microcomputer Control of Cycloconverters

Two Cylinder Switching Regulator for 250V to 12V DC Converter

The goals of this work are to improve the understanding of power electronic circuits and to devise new and improved circuits for electric power conversion and control using modern power semiconductor devices.

The SSPC Program is jointly sponsored by several industries. During 1976-1977, the sponsors were Delco Electronics, Garrett-Airesearch, General Electric, Gould, International Rectifier and Reliance Electric. Dr. Richard G. Hoft is the project director and Dr. James E. Rathke is the associate project director for this program.

In support of the program, a two semester sequence of courses in power electronics is offered. These are complemented by a number of undergraduate and graduate level courses in rotating machinery and automatic control.

Thyristor System Simulator

The simulator is being designed and constructed on an NSF Research Equipment Grant ENG77-17185. Dr. Richard G. Hoft is the principal investigator and Dr. Robert W. McLaren and Dr. Charles Slivinsky are co-principal investigators.

The goal of this work is to develop a Thyristor System Simulator for studying the dynamic performance of solid-state power electronic systems of the type now in use for a wide range of applications, including electric vehicles, ac motor drives, and high-voltage direct current transmission. The proposed Simulator is to consist of a digital control section based on a standard real-time microcomputer development facility and

modular assemblies of actual thyristor equipment with their associated gating amplifiers, buffers, and sensing circuits.

The Simulator will allow

(1) verification of analysis techniques for practical thyristor systems

(2) investigation of aspects of system performance that are impractical to model analytically

(3) evaluation of new approaches for system control

(4) feasibility studies on the use of microcomputer controls.

A DECLAB PDP 11/03 microcomputer system provides the digital control capability. Several commercial thyristor equipments including a 50HP full reversing dc motor drive and a variable frequency thyristor inverter will provide the thyristor hardware section of the simulator. In addition, work is now underway to develop the electronic interface which will permit the computer logic level signals to control the thyristor power equipment. The Thyristor System Simulator will provide a most valuable research tool for research on power electronic circuit analysis, control of rotating machines, adaptive control techniques, digital signal processing and microprocessor applications.

Hybrid Simulation of Large Power Systems

This work is being carried on by the digital power research group within the Department of Electrical Engineering. It involves a combined effort of faculty and students interested in power and digital systems working under the direction of Dr. Lewis N. Walker and Dr. James R. Tudor. The work is currently sponsored by EPRI, several electric utilities and NSF.

One of the most interesting projects in this area has been the development of a faster-than-real-time hybrid simulator for study of long term power system dynamics. The power systems are simulated in analog fashion. Approximately 4000 operational

amplifiers, 3000 additional IC components and a large amount of associated special purpose electronics, all controlled from a powerful minicomputer, are included in the simulator. It permits the simulation of a system with 16 machines and 68 busses. The simulator operates three times faster than real time and it has been operated for twenty minutes.

This simulator provides a powerful facility for dynamic studies of large power systems. The availability of low cost operational amplifiers, a wide range of digital IC components and powerful minicomputers made it possible to produce this extremely flexible and powerful hybrid simulator.

APPENDIX A

LIST OF ATTENDEES

"TOPICAL MEETING ON GENERATORS AND MOTORS"

PAUL AGARWAL
General Motors Copr.
Research Laboratories
Warren MI 48090

DONALD S. BEARD
DOE
Div. of Magnetic Fusion Energy
M.S. G-234
Wash DC 20545

B. BENTSEN
FTD/ETDP
Wright-Patterson AFB OH 45433

PAUL R. BERTHEAUD
AF Aero Propulsion Laboratory
ATTN: AFAPL/POP-2
Wright-Patterson AFB OH 45433

EDMUND BEYMA
DOE
Wash DC 20545

J. C. BETTS
Hitachi Magnetics Corp.
Edmore MI 48829

DANIEL K. BIRD
AFFDL/FGL
Wright-Patterson AFB OH 45433

HAROLD J. BLAKNEY
Naval Ship Engineering Center
Code 6158C
Wash DC 20362

WILLIAM BORGER
AF Aero Propulsion Laboratory
ATTN: AFAPL/POP-2
Wright-Patterson AFB OH 45433

Col P. O. BOUCHARD
AF Aero Propulsion Laboratory
ATTN: AFAPL/CC
Wright-Patterson AFB OH 45433

JOHN R. BRAUER
A. O. Smith Corp.
8651 N. Fort Washington Rd.
Milwaukee WI 53217

H. J. BRAUN
Westinghouse Electric Corp.
Aerospace Electrical Div.
P.O. Box 989
Lima OH 45802

Capt FREDERICK C. BROCKHURST
AF Aero Propulsion Laboratory
ATTN: AFAPL/POD-1
Wright-Patterson AFB OH 45433

DAVID BROWN
Purdue University
Dept. of Electrical Engineering
West Lafayette IN 47907

ARTHUR CHAIKIN
Naval Sea Systems Command
Code SEA-0331H
Wash DC 20362

M. V. K. CHARI
General Electric Co. Corp. R&D Center
Bldg 37, Rm 355
P.O. Box 43
Schenectady NY 12301

DAVID COWGER
David W. Taylor Naval Ship R&D Center
Annapolis MD 21402

ATIF DEBS
Georgia Institute of Technology
Dept. of Electrical Engineering
Atlanta GA 30332

N. A. DEMERDASH
Virginia Polytechnic Institute and State University
Dept. of Electrical Engineering
Blacksburg VA 24061

MICHAEL P. DOUGHERTY
AF Aero Propulsion Laboratory
ATTN: AFAPL/POD-1
Wright-Patterson AFB OH 45433

TIMOTHY J. DOYLE
David W. Taylor Naval Ship R&D Center
Code 2722
Annapolis MD 21402

WILLIAM J. DUFFY
University City Science Center
Power Information Center
3624 Science Center
Philadelphia PA 19104

WILLIAM DUNBAR
1065 149th Place, S.E.
Bellevue WA 98007

E. F. ECHOLDS
AiResearch Manufacturing Company of California
2525 West 190th St.
Torrance CA 90509

JAMES S. EDMONDS
DOE
Division of Electric Energy Systems
Wash DC 20545

JOHN EWING
Reliance Electric Co.
24701 Euclid Avenue
Cleveland OH 44117

ROBERT J. FLAHERTY, JR.
David W. Taylor Naval Ship R&D Center
Code 2771
Annapolis MD 21402

JERROLD FOUTZ
Naval Ocean Systems Center
Code 9234
271 Catalina Blvd.
San Diego CA 92152

THOMAS L. FRANCAVILLA
U.S. Naval Research Labs.
4555 Overlook Ave.
Wash DC

BRUCE B. GAMBLE
General Electric Co.
Bldg 37, Rm 355
P.O. Box 43
Schenectady NY 12301

HAROLD J. GARRETT
Air Force Materials Laboratory
ATTN: AFML/LTE
Wright-Patterson AFB OH 45433

ANGELO GATTOZZI
Reliance Electric Co.
Euclid OH 44117

RICHARD GEYER
Philips Laboratories
345 Scarborough Rd.
Briarcliff Manor NY 10510

D. R. GORDON
ASD/ENACD
Wright-Patterson AFB OH 45433

F. GOURASH
NASA Lewis Research Center
Cleveland OH 44135

RON GRIPSHOVER
Naval Surface Weapons Center
Dahlgren VA 22448

THEODORE R. HALLER
General Electric Co.
Bldg 37, Rm 355
P.O. Box 355
Schenectady NY 12301

HOWARD B. HAMILTON
University of Pittsburgh
Dept. of Electrical Engineering
Pittsburgh PA 15260

FREDERICK R. HENRIKSON
Naval Ship Engineering Center
Wash DC 20362

PHILIP C. HERREN JR.
AF Aero Propulsion Laboratory
ATTN: AFAPL/POD-1
Wright-Patterson AFB OH 45433

HOWARD IRELAND
Naval Air Development Center
Warminster PA 18974

MILTON S. ISAACKSON
Nu-Tech Industries, Inc.
5885 Wolf Creek Pike
Dayton OH 45424

JOSEPH JACKSON
Electric Power Research Institute
3412 Hillview Ave.
Palo Alto CA 94304

LEOPOLD J. JOHNSON
Naval Ocean Systems Center
Code 7211
271 Catalina Blvd.
San Diego CA 92152

A. L. JOKL
USA Mobility Equipment R&D Command
ATTN: DRDME-EA
Ft Belvoir VA 22060

KENNETH KENNERUD
Boeing Aerospace Co.
P.O. Box 3999
M.S. 13-85
Seattle WA 91241

ALAN KING
Westinghouse Electric Corp.
Aerospace Electrical Division
P.O. Box 989
Lima OH 45802

JAMES KIRTLEY
Massachusetts Institute of Technology
Room 10-093
Cambridge MA 02139

C. C. KOUBA
Westinghouse Electric Corp.
Aerospace Electrical Division
P.O. Box 989
Lima OH 45802

PAUL C. KRAUSE
Purdue University
Dept. of Electrical Engineering
West Lafayette IN 47907

MICHAEL J. KUHLMANN
Naval Ship Engineering Center
Code 6156D
Wash DC 20362

C. H. LEE
AiResearch Manufacturing Co. of California
2525 West 190th St.
Torrance CA 90509

PATRICK LEONG
Boeing Aerospace Co.
Mechanical Electronic Technology
Boeing Military Airplace Development
P.O. Box 3999
Seattle WA 98124

WILLIAM J. LEVEDAHL
David W. Taylor Naval Ship R&D Center
Code 2703
Annapolis MD 21402

M. LIPO
General Electric Co.
Bldg 37, Rm 355
P.O. Box 43
Schenectady NY 12301

WILLIAM LORD
Colorado State University
Dept. of Electrical Engineering
Fort Collins CO 80523

ISAQUE S. MEHDI
Boeing Aerospace Co.
Military Airplane Development
P.O. Box 3999
Seattle WA 98124

HERB MILDRUN
University of Dayton
Dayton OH 45410

FRANK J. MOLLURA
Rome Air Development Center
ATTN: RBEG
Griffiss AFB NY 13441

L/C KARL H. MULLER
AF Aero Propulsion Laboratory
ATTN: AFAPL/PO
Wright-Patterson AFB OH 45433

E. F. McBRIEN
NASA Lewis Research Center
Cleveland OH 44135

J. L. McCABRIA
Westinghouse Electric Corp.
Aerospace Electrical Division
P.O. Box 989
Lima OH 45802

THOMAS W. NEHL
Virginia Polytechnic Institute and State University
Blacksburg VA 24061

ALFRED P. NICKLEY
Naval Ship Engineering Center
Code 2158C
Wash DC 20362

SAMUAL NOODLEMAN
Kollmargen Corp.
Inland Motor Division
Radford VA 24141

CHARLES E. OBERLY
AF Aero Propulsion Laboratory
ATTN: AFAPL/POD-1
Wright-Patterson AFB OH 45433

WALTER F. O'BRIEN
Virginia Polytechnic Institute and State University
Mechanical Engineering Dept.
Randolph Hall
Rm 101
Blacksburg VA 24061

STEPHEN O'DEA
Charles Stark Draper Laboratories
555 Technology Square
Cambridge MA 02139

HENRY B. ODON
Naval Surface Weapons Center
Dahlgren VA 22448

J. H. PARKER
Westinghouse Electric Corp.
Aerospace Electrical Division
P.O. Box 989
Lima OH 45802

R. J. PARKER
Hitachi Magnetics Corp.
Edmore MI 48829

A. L. PARRILLO
ASD/ENACD
Wright-Patterson AFB OH 45433

JOHN J. PEIRSON
University City Science Center
Power Information Center
3624 Science Center
Philadelphia PA 19104

CAL PUSATERI
A. O. Smith Corp.
1 Erie View Plaza
Suite 816
Cleveland OH 44101

MARIO RABINOWITZ
Electric Power Research Institute
3412 Hillview Ave.
Palo Alto CA 94304

EIKE RICHTER
General Electric Co.
Corporate R&D Center
Bldg 37
Rm 355, P.O. Box 43
Schenectady NY 12301

HENRY N. ROBEY JR.
USN: David Taylor Naval Ship R&D Center
Annapolis MD 21402

HOWARD E. RUSKIE
Naval Intelligence Support Center
(NISC-36)
4301 Suitland Road
Wash DC 20390

JOSEPH B. SALAY
Naval Ship Engineering Center
Code 6157C
Wash DC 20362

JOSEPH D. SEGREST
Naval Air Development Center
ATTN: AVTD; Code 3043
Warminster PA 18974

JOHN SCHWAB
NASA Lewis Research Center
Cleveland OH 44135

RICHARD R. SECUNDE
NASA Lewis Research Center
M.S. 500-215
21000 Brookpark Road
Cleveland OH 44135

LCDR. W. R. SENG
Office of Naval Research
Code 473
800 N. Quincy St.
Arlington VA 22217

W. J. SHILLING
Westinghouse Electric Corp.
Aerospace Electrical Division
P.O. Box 989
Lima OH 45802

Capt TIM SKAVARENINA
3630 Brandywine Ct., Apt. F
Lafayette IN 47905

CHARLES SLIVINSKY
AFFDL/FG
Wright-Patterson AFB OH 45433

Capt HUGH L. SOUTHALL
AF Aero Propulsion Laboratory
ATTN: AFAPL/POD-1
Wright-Patterson AFB OH 45433

JAMES SPIETH
ASD/YXEF
Wright-Patterson AFB OH 45433

HOWARD O. STEVENS, JR.
David W. Taylor Naval Ship R&D Center
Code 2722
Annapolis MD 21402

JOHN STONE
Franklin Institute Research Labs.
The Benjamin Franklin Parkway
Philadelphia PA 19103

PHILIP E. STOVER
AF Aero Propulsion Laboratory
ATTN: AFAPL/POD
Wright-Patterson AFB OH 45433

T. A. STUART
University of Toledo
Dept. of Electrical Engineering
2801 West Bancroft
Toledo OH 43606

OWEN TAN
Louisiana State University
Dept. of Electrical Engineering
University Station
Baton Rouge LA 70803

PIERRE A. THOLLOT
NASA Lewis Research Center
M.S. 500-201
21000 Brookpark Rd.
Cleveland OH 44135

PHILIP THULLEN
Los Alamos Scientific Laboratory
M.S. 464
Los Alamos NM 87545

DOMINIC S. TOFFOLO
Naval Ship Engineering Center
Code 6157C
Wash DC 20362

LAWRENCE TURNER
220 7th St. N.E.
Charlottesville VA 22901

RICHARD L. VERGA
AF Aero Propulsion Laboratory
ATTN: AFAPL/POD-1
Wright-Patterson AFB OH 45433

WAYNE VOGEN
University of California
Department of Materials Science and Engineering
Hearst Mining Building
Berkeley CA 94720

WILLIAM WELDON
The University of Texas
Center for Electromechanics
167 Taylor Hall
Austin TX 78712

D. D. WIER
Mississippi State University
Drawer EE
Mississippi State MS 39762

W. W. YATES
Westinghouse Electric Corp.
Aerospace Electrical Division
P.O. Box 989
Lima OH 45802

DID NOT ATTEND BUT TO RECEIVE LITERATURE:

RICHARD HOFT
Department of Electrical Engineering
University of Missouri-Columbia
Columbia MO 65201

*U.S.Government Printing Office: 1979 — 657-084/262